

Monitoring land restoration projects
of Justdiggit in Kenya, using
downscaled passive microwave
remote sensing products of VanderSat

Martijn G.J. Mulder



Monitoring land restoration projects of JustdiggIt in Kenya, using downscaled passive microwave remote sensing products of VanderSat

by

Martijn G.J. Mulder

to obtain the degree of Master of Science
at the Delft University of Technology,
to be defended publicly on Tuesday November 27, 2018 at 15:00.

Student number:	4517962	
Project duration:	January, 2018 – November, 2018	
Thesis committee:	Prof. dr. ir. S. C. Steele-Dunne,	TU Delft, supervisor
	Dr. ir. T. A. Bogaard,	TU Delft
	Dr. ir. A. G. van Turnhout,	TU Delft
	Dr. ir. R. A. M. de Jeu,	VanderSat B.V.

An electronic version of this thesis is available at <http://repository.tudelft.nl/>.

Preface

This thesis is the result of several months of research as part of the final stage of my Master Water Management at Delft University of Technology. During my master, I was mainly interested in (geo-)hydrology and water resources management, with special interest in the applications within agriculture and ecology. A question that often ran through my mind was how we can adapt our water usage to the growing world population and increasing demand in agriculture due to the growing food production, without further harming the Earth's ecosystems and biodiversity. After working on the land restoration projects of JustdiggIt, I'm glad I have contributed in this field and got to learn about all the work that's already being done. And, although I probably didn't even come across half the remote sensing techniques that are currently being developed in Earth sciences, I'm already greatly inspired by how remote sensing can contribute to water resources management.

I'm thankful to all of those who supported me during my research. First of all, I want to thank Richard de Jeu and Thijs van Leeuwen for giving me the opportunity to work on this project at VanderSat. I've had a great experience at VanderSat and definitely have become a fan of your passive microwave remote sensing products! I want to thank my colleagues as well for their help and making me feel welcome. A special thank you to Richard for providing me feedback during my research and thank you Céline for supporting me during my internship.

Furthermore, I want to thank JustdiggIt, and especially Sander de Haas, for his guidance throughout my thesis and preparing me for my fieldwork in Kenya. I'm impressed by the work that JustdiggIt has done so far and I'm still amazed by how a fairly simple concept can have such a big impact on land restoration. I'm incredibly grateful for the opportunity I got to travel to Kenya and carry out a small fieldwork. Although the extreme rainfall did not make my work easy, I'll always remember the experiences from the field. I also owe a big thank you to the people of Maasai Wilderness Conservation Trust in the Kuku group ranch in Kenya, for having me in March. A special thank you to George Kingola for still keeping track of the in-situ stations in the field and regularly sending me new data. And, I wouldn't have felt safe during my fieldwork on the African Savanna, without help of my friend William Sarijore. Luckily we didn't run into any lions in the field!

I want to thank Susan Steele-Dunne for her work as my daily supervisor and chair of my committee. Susan, without your guidance and feedback this Thesis wouldn't be the same. Thank you as well, for being straightforward and keeping me on track, by letting me focus on what's important! Furthermore, I would also like to thank the other members of my committee, Thom Bogaard and André van Turnhout, for their feedback and help during my thesis. Thom, thank you as well for your tips regarding my fieldwork.

In addition, I also would like to thank my fellow students from Water Management and especially my roomies from room 4.84, aka 'Hokje 1' for the enjoyable time, nice discussions and great atmosphere! Without you, I wouldn't have survived the unbearable hot days in summer and the walks to the coffee machine would have been a whole lot more boring. I'm not going to miss beating up that coffee machine though!

Finally, to my family, friends and especially my parents, thank you for supporting me during my study, motivating me and keeping me distracted during the weekends. Thank you for always being there for me!

*Martijn G.J. Mulder
Delft, November 2018*

Abstract

The growing world population and climate change have resulted in increasing stress on the Earth's ecosystems. Especially the overexploitation of agricultural land, overgrazing and extreme droughts have resulted in land degradation, often called desertification. This leads to the disappearing of natural vegetation, the loss of soil quality, lower production capacity in agriculture and increased water scarcity, which is most severe on drylands like the African continent. Globally, organizations such as the United Nations Convention to Combat Desertification (UNCCD) are fighting land degradation by implementing sustainable farming practices and supporting re-vegetation projects such as the Green Wall Initiative in Africa, often using ancient water harvesting techniques. Justdiggitt, a Dutch NGO, is currently working on land restoration projects and dug over 72,000 water-retaining semi-circular bumps, or 'bunds', in Kenya. By retaining rainwater in these bunds, water is given the time to infiltrate into the soil, erosion rates by overland flow are reduced, while vegetation recovers and on the long term can take over the function of the bunds. Although the first results of the bunds at small scale are promising, the impact of the projects of Justdiggitt has never been quantified on a large scale in terms of the amount of water that's retained, increase of vegetation and decrease of surface temperature.

As dense in-situ networks are expensive and have difficulties in capturing the large spatial variability of parameters such as soil moisture and temperature, often remote sensing (satellite observation) is used, which does well in measuring spatial variability on large scales. However, as optical remote sensing is often affected by cloud cover, data availability is limited. Furthermore, it is difficult to translate optical vegetation parameters such as the Normalized Difference Vegetation Index (NDVI) to vegetation biomass, as these only observe the surface of the canopy. Passive microwave remote sensing, which is measured in the microwave part of the electromagnetic spectrum, has proven to be very accurate in determining parameters such as soil moisture content, surface temperature and vegetation optical depth (VOD, related to vegetation thickness and water content). The advantage of using microwaves is that it can 'see' through clouds and can therefore be used under almost all atmospheric circumstances. However, due to the low intensity of passive microwaves, resolutions are low ($\approx 50 \times 30 \text{ km}$). VanderSat, a Dutch remote sensing company, downscales the low-resolution passive microwave observations to $100 \times 100 \text{ m}$ field-scale resolution. The goal of this research is therefore to test if the project areas of Justdiggitt can be monitored using these downscaled passive microwave remote sensing soil moisture, surface temperature (night-time) and vegetation optical depth products of VanderSat.

Using in-situ data from sensors that were installed inside and outside the bunds during a fieldwork in Kenya in March 2018, the hydrological behaviour of the bunds was investigated. Furthermore, a cross-validation was carried out to compare the downscaled passive microwave soil moisture, surface temperature (night-time) and VOD products to the in-situ sensors, thermal derived surface temperatures (day- and night-time) from MODIS and NDVI from Sentinel-2 and MODIS. After these cross-comparisons, the differences between the project areas of Justdiggitt and the reference area were analysed using the downscaled passive microwave products. Finally, using the Tau-Omega model, the passive microwave signal from the bunds was simulated.

All in all, the analysis of the results have shown that the bunds have a significant effect on the soil moisture content, especially at the deeper soil layers, based on the in-situ sensors, while results of NDVI have shown a clear contrast in vegetation 'greenness' between the project areas and the reference area. Due to the short measuring period, the correlations between the in-situ sensors and the downscaled soil moisture and surface temperature products were still low. Furthermore, highest correlations were found between the downscaled surface temperature product and the night-time surface temperatures of MODIS. As it turned out, no significant differences were found between the project areas and the reference area based on the downscaled passive microwave products. This, in spite of the fact that the soil moisture, surface temperature and VOD products have shown to be consistent. Finally, modelling of the microwave signal of the project areas, has shown that the effect of the bunds is still too small in terms of emissivity and is therefore not being measured yet. Increasing the current percentage of bunds from 10 to roughly 20%, or waiting five years after implementation of the bunds in 2016, should give significant differences in terms of soil moisture, surface temperature and vegetation optical depth, as a result of vegetation development and land restoration in the project areas.

Contents

Preface	iii
Abstract	vi
List of Figures	ix
List of Tables	xi
1 Introduction	1
1.1 Fighting land degradation using water harvesting techniques.	1
1.2 Land restoration projects of Justdiggit	1
1.3 Monitoring land restoration using remote sensing	3
1.4 Aim of this research	4
1.5 Thesis outline	4
2 Project area Justdiggit	5
2.1 Topography and climate	6
2.2 Extreme wet and dry conditions in 2017 and 2018.	7
2.3 Land cover and soil texture	8
3 Microwave remote sensing	9
3.1 Microwave remote sensing	9
3.2 Passive microwave obtained brightness temperatures	10
3.3 Land Parameter Retrieval Model	10
3.4 VanderSat downscaling method.	12
4 Materials and methods	13
4.1 Fieldwork Kenya: Installation of in-situ sensors.	13
4.1.1 Volumetric water content	13
4.1.2 Set-up of soil moisture stations	13
4.1.3 Calibration of in-situ sensors	14
4.2 Remote sensing data	14
4.2.1 Raw brightness temperatures from AMSR	15
4.2.2 VanderSat soil moisture, temperature and vegetation optical depth data	15
4.2.3 MODIS thermal derived land surface temperature.	16
4.2.4 Sentinel-2 & MODIS Normalized Difference Vegetation Index	16
4.3 Temporal smoothing of downscaled soil moisture, temperature and vegetation optical depth products	16
4.4 Data analysis	18
4.4.1 Analysis of raw brightness temperature data.	18
4.4.2 Time series and differences between plots	18
4.4.3 Climatology and anomalies	19
4.4.4 Histograms and cumulative distribution functions	19
4.4.5 Temporal averaging during wet season.	19
4.4.6 Spearman correlation coefficient	19
4.5 Modelling of brightness temperature signal using tau-omega model	20
4.5.1 Brightness temperature modelling.	20
4.5.2 Modelling scenarios	21

5	Discussion of results	23
5.1	Measurements from in-situ sensors	23
5.2	Cross-validation between remote sensing products and in-situ data	25
5.3	Analysis of project areas, using soil moisture, surface temperature and vegetation optical depth data	27
5.3.1	Time series of downscaled soil moisture, temperature and vegetation optical depth	27
5.3.2	Differences between plots of JustdiggIt and reference area	28
5.3.3	Climatologies and anomalies	28
5.3.4	Histograms and cumulative distribution functions	31
5.3.5	Temporal averages during wet season	32
5.3.6	MODIS land surface temperature and NDVI	34
5.4	Modelling brightness temperatures using tau-omega model	36
5.4.1	Sensitivity analysis of brightness temperature	36
5.4.2	Brightness temperature signal from bunds.	37
5.5	Synthesis	39
6	Conclusions and recommendations	43
	Bibliography	45
A	Sentinel-2 NDVI results 2018	49
B	Validation of soil moisture product using cosmic-ray in-situ data	51
C	Calibration of in-situ sensors	53
C.1	Calibration curves & linearly fitted functions	53
C.2	Bulk density & porosity	54
C.2.1	Bulk densities	54
C.2.2	Porosities	54
D	Epanechnikov and Gaussian smoothing filters	55
E	Results of raw brightness temperature data	57
E.1	Raw brightness temperature time series	57
E.2	Raw brightness temperature anomalies.	58
E.3	Raw brightness temperature error plots.	58
E.4	Microwave Polarization Difference Index	59

List of Figures

1.1	Bund filled with water in Kuku, Kenya	2
1.2	Bunds at Plot D, near Kuku, captured by drone	2
1.3	Bunds at Plot D, near Kuku, during the wet season between October and December, 2017 (Photos from Justdiggitt (2018)).	2
2.1	Location of the project sites (plot B and plot D) of Justdiggitt in the Kuku Group Ranch in between Mount Kilimanjaro, the Chyulu hills and the national parks Amboseli and Tsavo West, in Kajiado County, southern Kenya.	5
2.2	Elevation map of the Kuku Group Ranch area around the Justdiggitt sites, with elevations roughly between 800 and 1200m.	6
2.3	Daily accumulated precipitation for 2016, 2017 and 2018 (until July 1) and monthly averaged precipitation between 2000 and 2018, based on the Tropical Rainfall Measuring Mission (NASA Goddard Earth Sciences Data And Information Services Center, 2018)	7
2.4	Most of the area has turned green as a result of intense rainfall in March at April 12, 2018.	8
2.5	Broken bridge at C103 road, nearby Kuku	8
2.6	ESA-CCI Land Cover map, showing that most of the area around the Justdiggitt project sites is covered by shrubs.	8
3.1	Electromagnetic spectrum with band designations within the microwave spectrum (ESA, 2018)	9
3.2	Soil moisture maps of the Netherlands, based on SMAP level 3 data with a resolution of 36x36km (left), and based on the downscaling algorithm of VanderSat, resulting in a resolution of 100x100m (right).	12
4.1	In-situ station, installed at Plot D in Kenya.	14
4.2	5TM and EC5 sensors installed at the soil surface.	14
4.3	Time series of soil moisture, surface temperature and VOD for the reference area	17
4.4	Spatial plots (50x50km) of soil moisture, surface temperature and VOD, showing the 36.5GHz temperature grid artefacts.	17
5.1	Time series of in-situ sensors installed inside and outside the bunds at plot D, with 5TM temperature at 5cm depth (A), 5TM soil moisture content at 5cm depth (B) and EC5 soil moisture content at depths of 5cm (C), 10cm (D), 20cm (E) and 40cm (F). Blue lines represent four periods, P1: March 23 - April 9, P2: April 9 - April 27, P3: April 27 - May 16, P4: May 16 - June 13 and P5: June 13 - August 6.	23
5.2	Time series of VanderSat soil moisture vs. In-situ sensors soil moisture inside and outside the bunds	25
5.3	Time series of VanderSat night-time temperature vs. In-situ sensors temperature inside and outside the bunds & MODIS LST	26
5.4	Time series of VanderSat vegetation optical depth vs. MODIS & Sentinel-2 NDVI	26
5.5	Time series of VanderSat Soil Moisture, Surface Temperature and Vegetation Optical Depth data, for the daily spatial means of plot B (red), plot D (blue) and the 10x10km reference area called Justdiggitt Area (black).	27
5.6	Time series of the differences between Plot B (red) and Plot D (blue) with the reference area, for VanderSat Soil Moisture, Surface Temperature and Vegetation Optical Depth data for the AMSR2 time period.	28
5.7	Climatology of VanderSat Soil Moisture, Surface Temperature and Vegetation Optical Depth 2012-2018	29
5.8	Anomalies of VanderSat soil moisture data for AMSR2 period, for all study areas.	29
5.9	Anomalies of VanderSat surface temperature data for AMSR2 period, for all study areas.	30

5.10	Anomalies of VanderSat vegetation optical depth data for AMSR2 period, for all study areas. . .	30
5.11	Histograms of Normalized data	31
5.12	Histograms of differences between plots and reference area	31
5.13	Cumulative Distribution Functions of individual years between 2013 and 2017, for soil moisture, temperature and vegetation optical depth.	32
5.14	Temporal average between DOY50 and DOY150 for years 2013, 2014, 2015	33
5.15	Temporal average between DOY50 and DOY150 for years 2016, 2017, 2018	34
5.16	Time series of MODIS LST daytime and night-time (1000x1000m) and MODIS NDVI (250x250m)	35
5.17	Time series the differences between plot B, plot D and the reference Justdiggitt area of MODIS LST daytime and night-time (1000x1000m) and MODIS NDVI (250x250m)	35
5.18	MODIS NDVI (250x250m) at June 2, 2018	36
5.19	MODIS NDVI (250x250m) at June 18, 2018	36
5.20	Brightness temperature sensitivity to increasing soil moisture content and vegetation optical depth.	36
5.21	Brightness temperature (horizontal and vertical polarization) sensitivity to soil moisture content and vegetation optical depth.	37
5.22	Results of Scenario 1: Vertical polarized brightness temperature decreases with increasing percentage of bunds.	38
5.23	Results of Scenario 2: Vertical polarized brightness temperature decreases over time.	38
5.24	Development of vegetation (increasing VOD) and increased area with bunds over time.	38
A.1	NDVI images in 2018, showing impact of Justdiggitt projects and cloud cover	49
B.1	Validation of downscaled soil moisture product using a Cosmic-ray in-situ station in Kenya (University of Arizona, 2018).	51
C.1	Calibration of 5TM and EC5 in-situ sensors, installed around the bunds at plot B near Kuku and at the head office of the MWCT, Nyati Camp.	53
D.1	Gaussian and Epanechnikov smoothing of soil moisture, for 6 days, 8 days and 10 days.	55
D.2	Gaussian and Epanechnikov smoothing of surface temperature, for 6 days, 8 days and 10 days.	55
D.3	Gaussian and Epanechnikov smoothing of vegetation optical depth, for 6 days, 8 days and 10 days.	56
D.4	Epanechnikov smoothing of soil moisture for a smoothing window of 0, 6, 8 and 10 days.	56
D.5	Epanechnikov smoothing of surface temperature for a smoothing window of 0, 6, 8 and 10 days.	56
D.6	Epanechnikov smoothing of soil moisture for a smoothing window of 0, 13, 15 and 17 days.	56
E.1	Time series of Raw Brightness Temperatures at 36GHz, for Justdiggitt Area, Plot B and Plot D	57
E.2	Anomalies of Raw Brightness Temperatures for Justdiggitt Area, Plot B and Plot D. The red line indicates the start of the 2016, in when the Justdiggitt projects were implemented.	58
E.3	Error plots of Raw Brightness Temperatures for Justdiggitt Area, Plot B and Plot D, with individual years 2016 and 2017. In terms of rainfall, 2016 represents a regular year, while 2017 was an exceptional dry year according to TRMM data of NASA.	58
E.4	MPDI for Justdiggitt Area and Plot B, for 36.5GHz, 23.7GHz, 18.7GHz and 10.65GHz. As shown, the AMSRE-period shows a larger variability in MPDI than the AMSR2-period, for all frequencies.	59

List of Tables

4.1	Specifications of Advanced Microwave Scanning Radiometers AMSR-E and AMSR-2	15
5.1	Results of a simple T-test between in-situ data inside and outside the bunds	24
C.1	Bulk density values based on 5TM and EC5 sensors	54
C.2	Porosity values based on 5TM and EC5 sensors	54



Introduction

The growing world population and economy have an increasing impact on the Earth's ecosystems, which has resulted in a global warming trend, rising sea levels, shrinking ice sheets and an increase of extreme events (both droughts and floods) (Anderegg et al., 2010; NASA, 2018; Seto et al., 2012; Vitousek et al., 1997). As the world population is projected to reach over 9.8 billion people in 2050, the world food production will need to be increased by 70 percent, while production in Africa alone needs to be doubled, which results in the expand and overexploitation of agricultural land (Foley et al., 2005; Rees, 1992; Scherr, 2000; UN, 2017). The combination of these climatic- and human induced stresses often results in land degradation, which is most severe on the African continent (UNCCD, 2017).

Land degradation, or 'desertification', often occurs in arid, semi-arid and dry sub-humid areas. Especially extensive use of agricultural land and overgrazing by livestock, in combination with extreme dry circumstances lead to the diminishing of vegetation and the loss of soil quality. But also deforestation, intensive use of groundwater and irrigation are big issues. As a result, land degradation leads to lower production capacity for agriculture, a loss of grazing grounds for livestock, higher erosion rates and a loss of drainage- and water storage capacity (FAO, 2011; Tilman et al., 2002).

1.1. Fighting land degradation using water harvesting techniques

As land degradation is a serious problem for agriculture and the Earth's ecosystems, and it affects our climate by contributing to the global greenhouse gas emissions, the question is what can be done to stop these problems. As it turns out, many so-called 'water harvesting' techniques have already been developed and proven successfully to stop desertification by improving water availability for agricultural use, often using ancient techniques (Fleskens et al., 2005; Lasage and Verburg, 2015; Schiettecatte et al., 2005). Examples are triangular Negarim microcatchments, contour bunds for trees, contour ridges for crops, stone lines and several terrace systems (Critchley and Siegert, 1991). All of these techniques can store up to a couple of cubic meters of water, depending on size and placement. Furthermore, these can already be applied in semi-arid climates with a minimum annual precipitation of only 150mm and are most successful on sloping land (0-5%).

Globally, many of these soil restoration projects have been applied on large scale to stop desertification and re-vegetate degraded land. Examples are the Great Green Wall initiative in the Sahel region and Horn of Africa and the implementation of sustainable farming practices on the Löss Plateau in China (UNCCD, 2018; World Bank, 2017). Both aimed to protect the natural resources and revitalize the degraded environment, but also resulted in increased food production and doubled the population's income over the past 30 years.

1.2. Land restoration projects of Justdiggit

Currently Justdiggit, a Dutch NGO, is developing land restoration projects in Africa. Justdiggit dug over 72,000 semi-circular bumps, so-called 'bunds', at two project sites in the range lands around Kuku, Kenya. Using these bunds, Justdiggit is trying to retain rainwater (figure 1.1), giving it time to infiltrate in the soil and stop overland flow and erosion. This gives vegetation the chance to recover (figure 1.2) and on the long term let it take over the function of the bunds by retaining the fertile soils and locally cooling down the surface.



Figure 1.1: Bund filled with water in Kuku, Kenya



Figure 1.2: Bunds at Plot D, near Kuku, captured by drone

In figure 1.3, the development of vegetation inside a bund is presented during the end of the dry season and the beginning of the wet season (October - December) in 2017. At the end of the dry season (October 17), most of the area has turned into bare land. Only a few trees, shrubs and grasses remain in the area. As the bunds are constructed on sloping land, they can easily retain rainwater (also shown in figure 1.1), that would otherwise be lost via overland flow. By retention inside the bunds, water is now given the time to infiltrate into the soil (November 8). Due to seeds that are still present in the soil and because of rainwater that has now infiltrated along the rootzone, the first grasses start to come back inside the bunds (November 17). After two weeks (December 5), all bunds are filled with vegetation, while the surrounding area is still mainly bare land, as no water has infiltrated there.

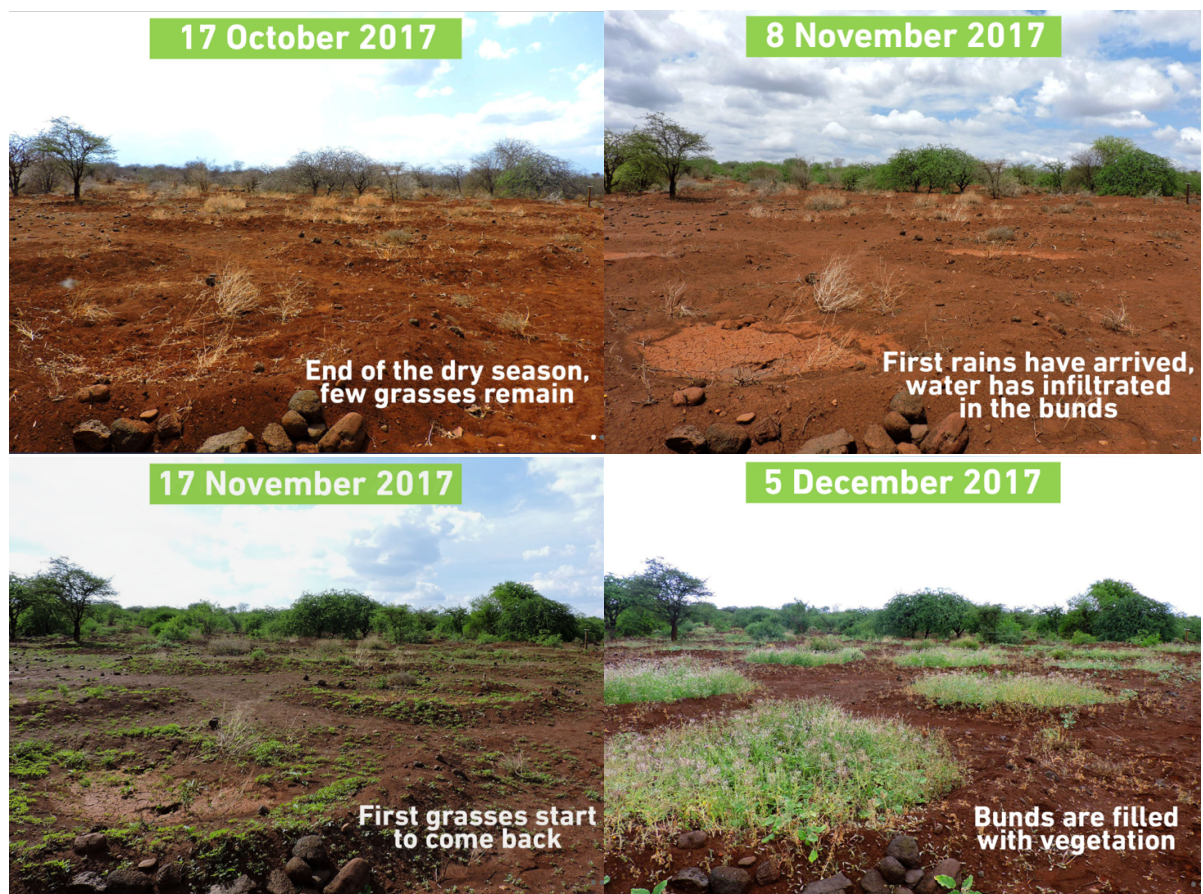


Figure 1.3: Bunds at Plot D, near Kuku, during the wet season between October and December, 2017 (Photos from Justdiggit (2018)).

Parameters such as soil moisture, surface temperature, vegetation cover and evaporation, which are affected by the Justdiggit projects, are all strongly related. As shown by Margulis (2017), changes in land surface characteristics will affect the surface energy balance. The short wave upwelling radiation depends on the albedo, which is determined by the type of land cover, while the long wave upwelling radiation is affected by lower emissivities and surface temperatures, due to changed surface characteristics like increased soil moisture, evaporation and vegetation cover. And, these land-atmosphere interactions in one region, might affect precipitation in another due to moisture recycling (van der Ent et al., 2010). By applying their projects on a large enough scale, Justdiggit hopes to positively affect the regional climate by bringing more moisture in the air, which helps to create clouds and restores the water cycle and forms a 'Hydrologic Corridor' (Justdiggit, 2018).

All in all, the first results of the interventions implemented in 2016 around the Kuku group ranch in Kenya are promising and show interesting insights. However, although quite some research has been done on these type of water harvesting techniques to quantify parameters such as the amount of water that's retained on small scale (or plot scale), the impact of these projects have never been quantified on a large scale in terms of amount of water retained, degrees of temperature change, increase of biomass and vegetation water content.

1.3. Monitoring land restoration using remote sensing

Surface temperature and soil moisture, which are influenced by the Justdiggit interventions, are generally measured well with in-situ sensors. However, these measurements are often not available, especially in remote regions like Africa. Furthermore, as temperature and soil moisture often have high spatial and temporal variability, expensive dense in-situ networks are required to measure this effect. Using satellite remote sensing observations instead of in-situ sensors, provides data for large areas and covers the spatial variability well.

To observe vegetation with remote sensing, often the Normalized Vegetation Difference Index (NDVI) is used. NDVI is a method based on the visible (red) and near-infrared part of the electromagnetic spectrum. The larger the vegetation cover, the more visible light is absorbed by the chlorophyll in the leaves, while more near-infrared light is reflected. As a result, NDVI ranges between 0 (no green leaves) to 1 (healthy vegetation) (Griend and Owe, 1993). However, because NDVI measures in the optical (visible) part of the electromagnetic spectrum, the method is often affected by cloud cover, especially during the wet season. Furthermore, as the red channel only measures the surface of vegetation, NDVI often becomes saturated (and therefore not directly related) at high vegetation biomass (Gao, 1996; Santin-Janin et al., 2009). It is therefore difficult to quantify biomass from NDVI observations, which is why NDVI is often used as indicator for vegetation healthiness. First results of Sentinel-2 NDVI observations at 10x10m resolution have shown clear contrast between between the project areas of Justdiggit and the surrounding area, even two months after the rain season (Appendix A, figure A.1). However, as these observations have shown to be affected by cloud cover and satellites with high resolution imagery pass over only once every two weeks, they limit data availability.

An alternative for the optical (and thermal) devices, is to use satellites which inspect the microwave bands of the electromagnetic spectrum. Microwaves between the 0.3GHz and 100GHz frequencies, can 'see' through clouds and can measure over night, and thus provide data in most atmospheric circumstances. Using the Land Parameter Retrieval Model (LPRM), soil moisture, surface temperature and vegetation optical depth (parameter for vegetation water content and vegetation thickness) can be derived from the microwave signal, which has proven to be very accurate (de Jeu et al., 2008, 2014; Liu et al., 2018, 2012; Owe et al., 2001, 2008; van der Schalie et al., 2015). However, despite the direct relations between the microwave signal and these surface parameters, the resolutions of the (passive) microwave signals are low (up to 50x30km), which makes it hard to use the data for field-scale applications (Parinussa et al., 2013; Santi, 2010).

VanderSat B.V., a Dutch remote sensing company, has found a solution for these low resolutions by combining the data of multiple satellite footprints into one high resolution dataset for temperature, soil moisture and vegetation optical depth (de Jeu et al., 2017). This results in daily data, with global coverage and spatial resolutions of 100x100m. Furthermore, as the satellite devices that are used by VanderSat have a long history, tracing back to 40 years ago, this results in a long dataset which helps putting droughts and wet periods that occur nowadays, in better perspective. Finally, a comparison done by VanderSat between their downscaled soil moisture product and a comic-ray in-situ network in the semi-arid climate of Kenya, has shown good consistency and correlations between both datasets, as presented in appendix B.

1.4. Aim of this research

The main goal of this research is to determine whether the impact of the Justdiggit project can be measured using the downscaled remote sensing products of VanderSat. This means that the 100x100m resolution soil moisture, surface temperature and vegetation optical depth data, based on passive microwave remote sensing and downscaled by VanderSat, will be tested on the project sites of Justdiggit in the Kuku group ranch in Kenya. The main research question is therefore defined as following:

Can the impact of land restoration projects using water-retaining semi-circular bunds in Kenya, be monitored in terms of soil moisture, surface temperature and vegetation optical depth, after implementation of the projects in 2016, based on downscaled (100x100m) passive microwave remote sensing products?

Sub research questions and -goals of this research are defined as following:

1. *What is the hydrological effect of the bunds on a small scale?*

By installing in-situ sensors inside and outside the bunds, the different hydrological and temperature effect between inside and outside along the rootzone is shown. These in-situ sensors were installed during a field-work in Kenya at the project locations of Justdiggit in March, 2018.

2. *For cross-validation; How do the downscaled passive microwave products relate to measurements of the in-situ stations and alternative optical and thermal remote sensing products?*

By comparing the in-situ temperature and soil moisture with the downscaled surface temperature and soil moisture products of VanderSat, comparing MODIS day- and night-time thermal derived surface temperature with the downscaled night-time temperature product of VanderSat and finally, comparing optical derived NDVI from MODIS and Sentinel-2 with the downscaled vegetation optical depth product of VanderSat. Taking into account that comparing point measurements (in-situ) with spatially averaged data (remote sensing) introduces errors, optical and thermal remote sensing data might be affected by atmospheric conditions and comparing VOD with NDVI introduces errors as both vegetation indices measure different parameters (vegetation thickness/water content and vegetation greenness respectively).

3. *What is the difference between the project areas with bunds and the reference area, in terms of soil moisture, surface temperature and vegetation optical depth, based on downscaled passive microwave remote sensing?* By doing a statistical analysis between the project areas of Justdiggit and the reference area, using the downscaled soil moisture, temperature and vegetation optical depth products of VanderSat.

4. *By modelling raw brightness temperatures; what signal is needed to measure a significant difference with the passive microwave remote sensing products?*

Using the Tau-Omega model, which calculates brightness temperatures from a soil surface with given moisture content, surface temperature and overlain by a given canopy thickness.

1.5. Thesis outline

In this thesis, first a description of the study area, with the project sites of Justdiggit in Kuku, Kenya, is given in chapter 2. Next, in chapter 3, a background is given on passive microwave remote sensing and a general introduction is given on obtaining soil moisture, surface temperature and vegetation optical depth data based on the land parameter retrieval model and the VanderSat downscaling method. In chapter 4, the materials and methods used during this research are discussed. After this, the results of this research are presented and discussed in chapter 5. Finally, the research questions will be answered and a conclusion on this thesis is given in chapter 6, together with recommendations for future research.

2

Project area Justdiggit

The project sites of the Justdiggit interventions, which are focussed on in this thesis, are located in Kajiado County in southern Kenya, close to the Tanzanian border and about 200 kilometers from capital city Nairobi. The local area is called Kuku Group Ranch and is bordered by Mount Kilimanjaro in the south and by the Chyulu Hills in the north-east. Furthermore, the Kuku Group Ranch is in between two major National Parks at the eastern and western borders, called Tsavo West National Park and Amboseli National park respectively. The area therefore serves as an important migration corridor for wildlife and is home to iconic African animals such as Lions, Elephants, Leopards, Giraffes and Zebra.

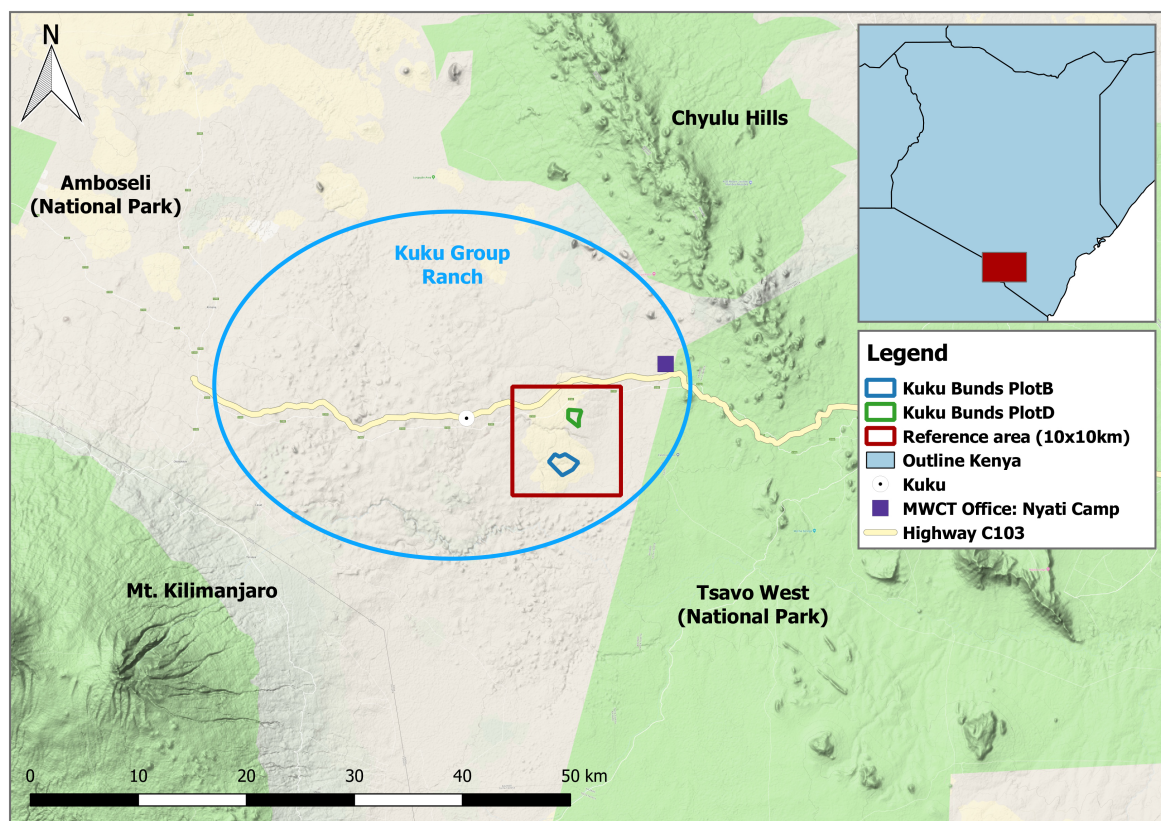


Figure 2.1: Location of the project sites (plot B and plot D) of Justdiggit in the Kuku Group Ranch in between Mount Kilimanjaro, the Chyulu hills and the national parks Amboseli and Tsavo West, in Kajiado County, southern Kenya.

The Kuku Group Ranch is home to about 17,000 people, which are primarily part of the Maasai community. For most of these people the area is of importance as grazing ground for their cattle (mostly cows, goats and sheep), while the forests provide resources such as logging. But, the area does not only provide resources for the local people, as its rivers and springs provide fresh water for over 7 million people, who are living in the coastal area around Mombasa, which is Kenya's second largest city.

Figure 2.1 shows an overview of the Kuku Group Ranch, where two project sites of Justdiggit are located in which over 72,000 water harvesting bunds were constructed in total, in 2016. The two project sites are called Plot B and Plot D, located just down the road of Kuku village. Each bund has a diameter of roughly 6m and was dug by hand, with help of the local community and in cooperation with Justdiggit's local partner, the Maasai Wilderness Conservation Trust (MWCT). Plot B and D were chosen as project locations based on the fact that these areas were most degraded compared to the surrounding area in the Kuku group ranch. The red 10x10 kilometer rectangular box in figure 2.1 is used as reference area in this thesis and is used for comparison with the plots later on in the analysis. As the water is retained behind the bunds after the start of the rain season (figure 1.1), vegetation starts growing inside the bunds (figure 1.3), but over time also should expand to outside, due to the moist soil and the seeds that are still present in the soil.

2.1. Topography and climate

The Kuku Group Range in southern Kenya, is located on the southern hemisphere between 2.5° and 3° S and 37° and 28° E. The area is around 800 to 1200 meters above mean sea level (AMSL) of the Indian Ocean. The Chyulu hills are going up to 2000m, while the Kilimanjaro is a distinct landmark in the surroundings with almost 5600m. The project sites of Justdiggit are in the lower elevated part of the region with altitudes between 880m and 950m AMSL, and are gentle sloped with slopes between 0 and 5%. Water therefore runs in south-eastern direction and discharges into the Tsavo river, which flows to the coastal region in which Mombasa is located. Most rivers in the area are rain dependent and therefore only flow during the rain season.

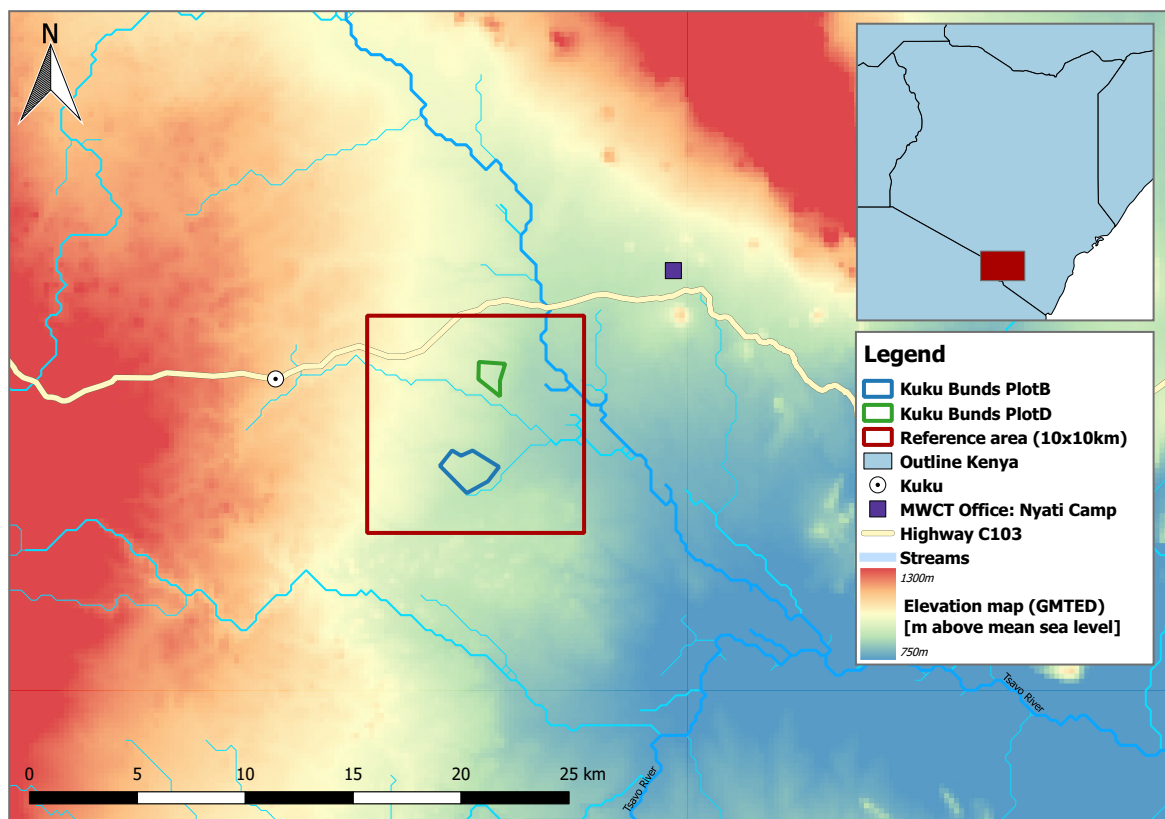


Figure 2.2: Elevation map of the Kuku Group Ranch area around the Justdiggit sites, with elevations roughly between 800 and 1200m.

The location of the Kuku Group Ranch in between the Chyulu hills and Mount Kilimanjaro and at the equator on the East African continent, results in two distinct dry and wet seasons during the year. A short but severe dry season in January and February, an intense but 'long' wet season from March to May, a dry season from May until October and finally a short and intense wet season from November until December. The alternating wet and dry seasons are the result of the inter tropical convergence zone (ITCZ) moving over the area because of the alternating summer and winter on the northern and southern hemisphere.

Precipitation data generated by the Tropical Rainfall Measuring Mission (TRMM) of NASA shows an average annual rainfall of 546mm since the year 2000 in the study area. The climatology shows an average amount of rain of 300mm during the 'long' rain season with peaks in March and April and about 250mm of rain during the short rain season with peaks in November and December, as shown in figure 2.3. In combination with the hot temperatures throughout the year, and the alternating wet and dry seasons, the climate can be defined as semi-arid. This climate results in droughts and floods through the year, which are magnified by the effects of el Niño from time to time.

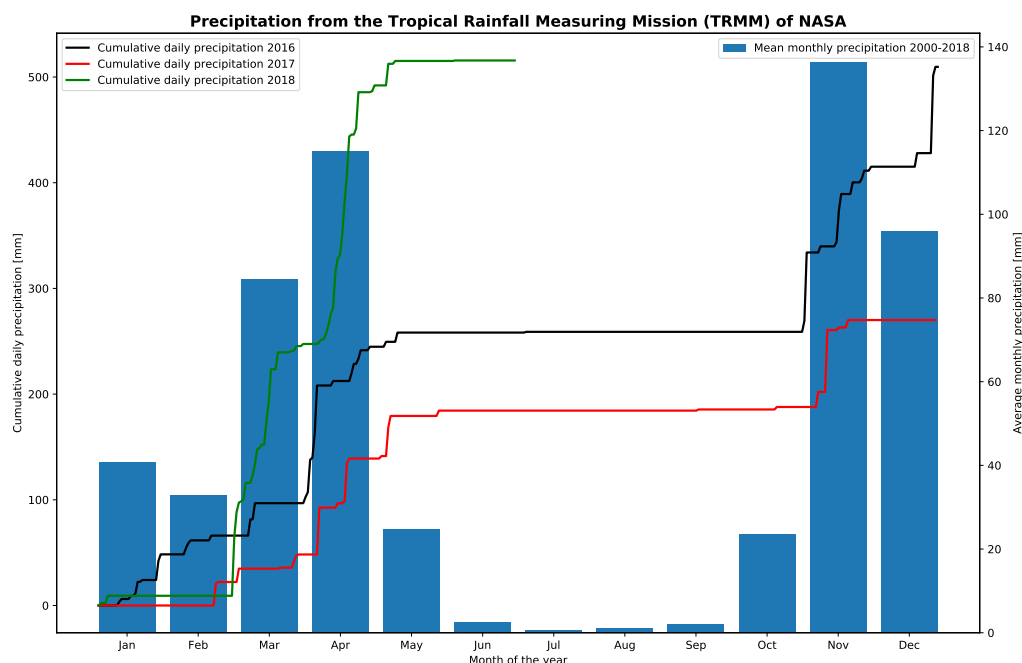


Figure 2.3: Daily accumulated precipitation for 2016, 2017 and 2018 (until July 1) and monthly averaged precipitation between 2000 and 2018, based on the Tropical Rainfall Measuring Mission (NASA Goddard Earth Sciences Data And Information Services Center, 2018)

2.2. Extreme wet and dry conditions in 2017 and 2018

Recently, Kenya was struggling with both floods and droughts. For reference, with roughly 510mm of precipitation, 2016 was just below an average year based on the period 2000-2018. However, 2017 has shown to be a very dry year with a significant lack of rainfall, in especially March and December, as shown in figure 2.3. With only 270mm of precipitation, the total amount of rainfall in 2017 was only half of the yearly average between 2000 and 2018. As a result, over 2.7 million people were in need of food aid and large numbers of cattle and wildlife died. The effects lasted until February 2018, but on the contrary, the first half of 2018 turned out to be an extremely wet year. With over 515mm during the first six months, the amount of precipitation in 2018 equalled the amount of rainfall in 2016 and nearly doubled the total amount of rainfall in 2017. As a result of the heavy rainfall, most of the project area (also outside the bunds) turned green as shown in figure 2.4. Finally, the rains also caused problems all around Kenya, with flooded neighbourhoods in Nairobi and broken bridges at the C103 road in the Kuku group ranch (figure 2.5).



Figure 2.4: Most of the area has turned green as a result of intense rainfall in March at April 12, 2018.



Figure 2.5: Broken bridge at C103 road, nearby Kuku

2.3. Land cover and soil texture

Based on the ESA CCI Land Cover map, the main land cover type in the area is classified as shrubland. Especially plot D is completely covered with shrubland as can be seen in figure 2.6, while plot B is largely covered in grassland. While both plots were chosen by Justdiggit based on the fact that these were most degraded according to the MWCT, especially land degradation in plot B was most severe, also in combination with the very dry circumstances in 2017.

Based on the FAO soil texture map, the area around the project sites is defined as clayey and well drained, as water is often no longer logged than two days. Furthermore, a fieldwork in the project area in March 2018, has shown that the areas are prone to a lot of erosion, with many sediment flows and big gullies as a result of heavy rainfall. Also, the main streams showed to be transporting sediment at sediment carrying capacity.

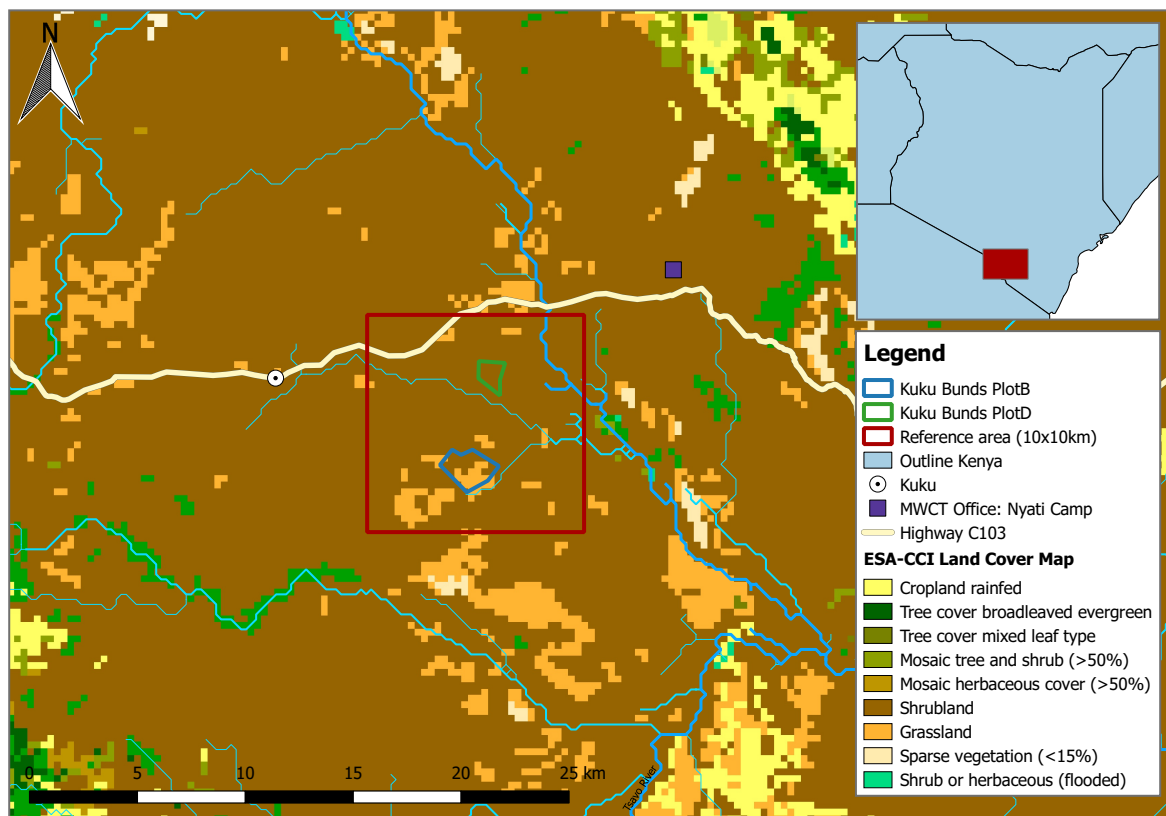


Figure 2.6: ESA-CCI Land Cover map, showing that most of the area around the Justdiggit project sites is covered by shrubs.

3

Microwave remote sensing

The term 'remote sensing' is often used to describe the technology to measure, observe or identify an object without being in direct contact with that object, often via satellite. Remote sensing can be applied along different frequencies and wavelengths of the electromagnetic spectrum. Optical remote sensing is for example applied along the visible spectrum, while thermal remote sensing focusses on the infrared part of the electromagnetic spectrum. Depending on the surface and atmospheric characteristics, each frequency and wavelength is absorbed or reflected differently. Remote sensing makes use of this when observing an object, which is why for example in the optical spectrum an object or surface is identified as red, blue, green, et cetera. As a result, the disadvantage of optical and thermal remote sensing is that it is often affected by cloud cover, which limits data availability.

3.1. Microwave remote sensing

The remote sensing products of VanderSat are based on satellite measurements in the microwave spectrum. The microwave spectrum lays between the infrared and radio spectrum, with frequencies roughly between 0.3 and 100 GHz and wavelengths between 100 and 0.3 cm respectively, as shown in figure 3.1 (ESA, 2018). The advantage of this spectrum, in contrast to the optical and thermal spectrum, is that it penetrates clouds and therefore can deliver valuable information about the Earth's surface under most atmospheric conditions. Each microwave band (P, L, S, C, X, K, Q, V and W) provides information about different object characteristics, which can be obtained by active or passive remote sensing (Ulaby et al., 1981). The band designations along the microwave spectrum are also shown in figure 3.1.

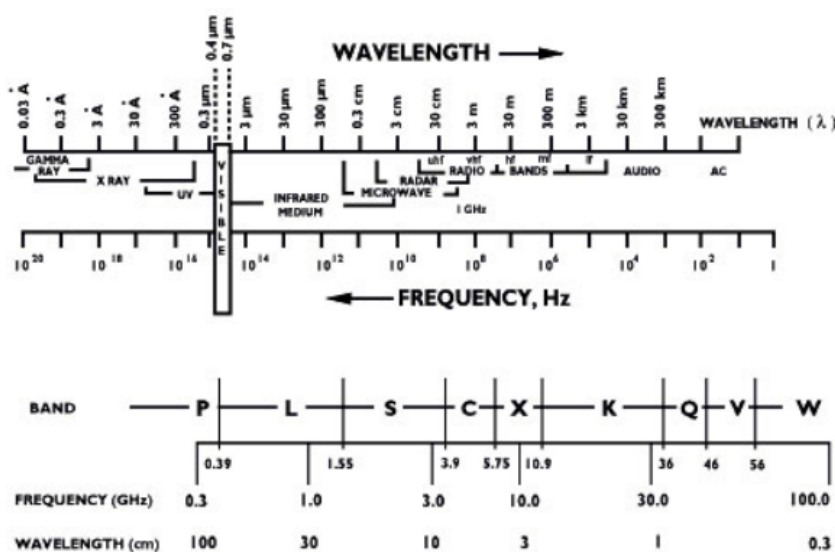


Figure 3.1: Electromagnetic spectrum with band designations within the microwave spectrum (ESA, 2018)

In active remote sensing, information is obtained by radar, which sends a pulse to the object under observation while the antenna measures the reflected radiation. In passive remote sensing, radiation is emitted by the object itself, or reflected from a natural source such as the sun, and measured by a device called radiometer. The disadvantage of passive microwave remote sensing is that it results in large resolutions ($\approx 50 \times 30 \text{ km}$), as the antenna needs to cover a large area ('field of view') to get a significant signal, due to the low amount of energy that's emitted. Furthermore, the energy that's measured by the radiometer is coming from the first few centimetres of the soil and depends on the frequency and wavelength. A general rule of thumb for the penetration depth in the soil is about 1/3 of the wavelength. However, the sensing depth depends on the surface characteristics as well. A dry soil for example has a larger penetration depth than a wet soil.

Passive microwave remote sensing has been retrieved as brightness temperature by satellites since the 1970s (SSMR, SSMI, AMSR-E, AMSR-2, SMOS) and can be translated to parameters such as soil moisture, surface temperature and vegetation optical depth, by using for example the land parameter retrieval model (LPRM) (Owe et al., 2008).

3.2. Passive microwave obtained brightness temperatures

In passive microwave remote sensing, microwave radiation is often represented by the surface brightness temperature (T_B), which is determined by the physical temperature (T) and the smooth-surface emissivity (e_s) of the radiating object under observation (Owe et al., 2001). The brightness temperature, at a given frequency (f), wavelength (λ) and polarization (p), is often defined as:

$$T_B = e_s * T \quad (3.1)$$

According to Njoku and Entekhabi (1996), the brightness temperature from a soil is strongly dependent on the soil moisture content, due to the direct relation between emissivity and dielectric constant, as the contrast between dielectric constant of water (80) and dry soil (about 3.5) is large. Besides soil moisture, the brightness temperature of a surface is also affected by soil surface roughness, attenuation and emission by vegetation cover, surface heterogeneity, soil texture and variability in temperature of the soil and overlaying vegetation (Njoku and Entekhabi, 1996; Owe et al., 2001). However, as for example vegetation and surface roughness have different spectral effects on the brightness temperature than soil moisture, it's possible to correct for these effects by using different frequencies and polarizations. In general, horizontal polarized brightness temperature is more sensitive to changes in soil moisture and vegetation than vertical polarized brightness temperature. The vertical polarization is better suited for temperature sensing than the horizontal polarization (de Jeu et al., 2008; Njoku and Li, 1999).

Furthermore, the lower frequencies at L- and C-band (1 – 6 GHz) are most frequently used for measuring soil moisture, due to the larger wavelengths and penetration depth through vegetation and soil (Owe et al., 2008), while Ka band (37 GHz) is most suitable for measuring surface/skin temperature (T_s), due to the smaller penetration depth and reduced sensitivity to the soil surface characteristics (Holmes et al., 2008). A third parameter, which is called Vegetation Optical Depth (VOD), is strongly related to the canopy density and shows a linear relation with the vegetation water content for frequencies lower than 10 GHz (< X-band) (Owe et al., 2001).

3.3. Land Parameter Retrieval Model

To convert brightness temperatures, obtained by passive microwave radiometers, to soil moisture, surface temperature and vegetation optical depth, the Land Parameter Retrieval Model (LPRM) was developed by researchers from the VU University Amsterdam and the NASA Goddard Space Flight Center from the mid-1990s onward (de Jeu et al., 2014). The LPRM uses a forward modelling approach to solve for the observed and modelled brightness temperatures. What makes the LPRM unique, is the fact that it can retrieve soil moisture, surface temperature and vegetation optical depth simultaneously, for multiple frequencies and it combines different datasets.

As vegetation affects the microwave emissions from the surface by absorbing or scattering radiation which is emitted from the soil, and by emitting its own radiation, these effects need to be distinguished. Because, when the canopy density increases, the soil radiation becomes completely masked by the vegetation, while the radiation from the canopy increases (Owe et al., 2008). The LPRM uses a radiative transfer equation by

Mo et al. (1982), also called the *tau – omega model*, which takes into account these vegetation effects and is defined as following:

$$T_{B_p} = T_S e_{r_p} \Gamma_p + (1 - \omega_p) T_C (1 - \Gamma_p) + (1 - e_{r_p}) (1 - \omega_p) T_C (1 - \Gamma_p) \Gamma_p \quad (3.2)$$

In which T_B is the brightness temperature, e_r the rough surface emissivity, ω the single scattering albedo and Γ the transmissivity, all at polarization p . T_S and T_C are defined as the soil and canopy temperature respectively. The first term of the radiative transfer equation defines the upwelling radiation from the soil, which is attenuated by the overlaying vegetation. The second term describes the direct upwelling radiation from the vegetation, while the third term defines the downward radiation from the canopy, which is reflected upward by the soil and attenuated again by the vegetation, before radiating into atmosphere. An important assumption to distinguish between radiation from soil and canopy, is that the surface soil temperature and surface canopy temperature are equal (Liu et al., 2018). As a result, the night time temperatures are therefore more favourable due to the small temperature gradients in space.

The transmissivity of vegetation is defined in terms of the optical depth (τ_v), which is strongly related to the canopy density, and incidence angle (u), and is based on the following equation:

$$\Gamma = e^{-\tau_v / \cos u} \quad (3.3)$$

The rough surface emissivity (e_r) is solved in three steps. First, the dielectric constant is calculated through the dielectric mixing model of Wang and Schmugge (1980), based on values of soil porosity and wilting point from the FAO soil texture map. Second, the smooth surface emissivity (e_s) is calculated using the Fresnel equations for both polarizations and with the values for the dielectric constant and incidence angle. Third, by using the model of Wang and Choudhury (1981), the rough surface emissivity is calculated (van der Schalie, 2017). By using the analytical formula by Meesters et al. (2005) and the Microwave Polarization Difference index (MPDI), the vegetation optical depth is calculated. The MPDI is calculated using the following equation:

$$MPDI = (T_{B(V)} - T_{B(H)}) / (T_{B(V)} + T_{B(H)}) \quad (3.4)$$

Polarization ratios such as MPDI are often used to normalize for the temperature dependence according to Owe et al. (2008). As a result the MPDI is highly related to the dielectric properties of the emitting surface, with the lower frequencies being more sensitive to the dielectric properties of the soil, while the higher frequencies contain more information on both the canopy and soil emission.

As a forward modelling approach is used in the LPRM method, the model first tries to partition the surface emission into soil and canopy emission, and then optimizes for the vegetation optical depth and soil moisture (Owe et al., 2008). This is done by using a wide range of soil moisture conditions, while the LPRM uses a forward approach to calculate the brightness temperature. When convergence is reached between the modelled brightness temperature values of the LPRM and the observed values of the satellite, the LPRM method uses the soil moisture value which results in the smallest residual between calculated and observed brightness temperature values (van der Schalie, 2017).

As the resolutions of passive microwave remote sensing are coarse, the retrieved soil moisture, surface temperature and vegetation optical depth data from the LPRM method aren't always useful in climate studies. By downscaling the microwave brightness temperatures obtained from satellite, using for example the smoothing filter-based intensity modulation (SFIM) downscaling method (Parinussa et al., 2013; Santi, 2010), the resolution of the LPRM was much improved. Using AMSR-E brightness temperature observations at Ka-band (8 x 14km footprint), the observations at C-band (75x43km footprint) were downscaled in a case study over the Iberian Peninsula. First, the high resolution Ka-band pixels were upscaled to match the dimensions of the C-band footprint. By using the SFIM processing equation, the C-band images were scaled according to the ratio between the original Ka-band resolution and the upscaled Ka-band low-resolution images. Besides making use of the C-band frequency, any band can be used in the LPRM. The SFIM processing equation is defined as following:

$$T_{B_{C\text{-bandHighRes}}} = \frac{T_{B_{Ka\text{-bandOrgRes}}}}{T_{B_{Ka\text{-bandLowRes}}}} T_{B_{C\text{-bandOrgRes}}} \quad (3.5)$$

This approach turned out to be very successful over the Iberian Peninsula, as after use of the SFIM downscaling method, the soil moisture product showed better agreement with two other soil moisture products (de Jeu et al., 2014).

3.4. VanderSat downscaling method

The data used in this thesis, is based on a downscaling method which is developed by VanderSat (de Jeu et al., 2017). VanderSat downscales the raw brightness temperatures to a resulting product of 100x100m resolution, which is a significant improvement from the original resolution of for example AMSR-2 at C-band (62x35km). The resolution of this ellipse-shaped satellite footprint at C-band frequency, is the resolution when the AMSR-2 signal is decreased to 3dB, which is 50% of the original signal intensity. By taking into account a Gaussian distribution inside the satellite footprint, it can be assumed that the center of a single footprint contributes more to the observed brightness temperature signal than the edges of that footprint. By using this Gaussian distribution, also footprints at for example 25% and 75% signal-intensity can be established, which results in footprints of different resolutions. Finally, by combining these different footprints, the geographical area of interest is overlain by multiple ellipses, in which pixels inside small footprints have larger weights than pixels inside large footprints.

A high detailed land cover map is used to distinguish between land cover and open water. For each footprint that is overlaying the geographical area of interest, the percentage of land and water inside that footprint is determined. By using the percentage of land and water cover, and by using fixed brightness temperature values for pixels covering water, the brightness temperature values for each high resolution land pixel can be calculated from the observed brightness temperature in the satellite footprint (taking into account the Gaussian distribution inside footprints).

The resulting high resolution brightness temperature map is used as input in the land parameter retrieval model to calculate soil moisture, surface temperature and vegetation optical depth at 100x100m resolution. By downscaling the raw brightness temperature data instead of downscaling soil moisture, temperature and VOD, the method becomes more efficient, but also performs better around large water bodies such as lakes and along the coast, as can be seen in figure 3.2. First results, based on AMSR-2 C-band and SMAP L-band have shown high correlations of soil moisture observations with phreatic ground water levels in the Netherlands (de Jeu and de Nijs, 2017). High correlations were found all around the Netherlands, including areas along the coast and Wadden islands. All in all, the L-band observations of SMAP perform better than the C-band observations of AMSR-2, which makes sense given that the L-band frequency generally has a larger penetration depth through vegetation, into the soil.

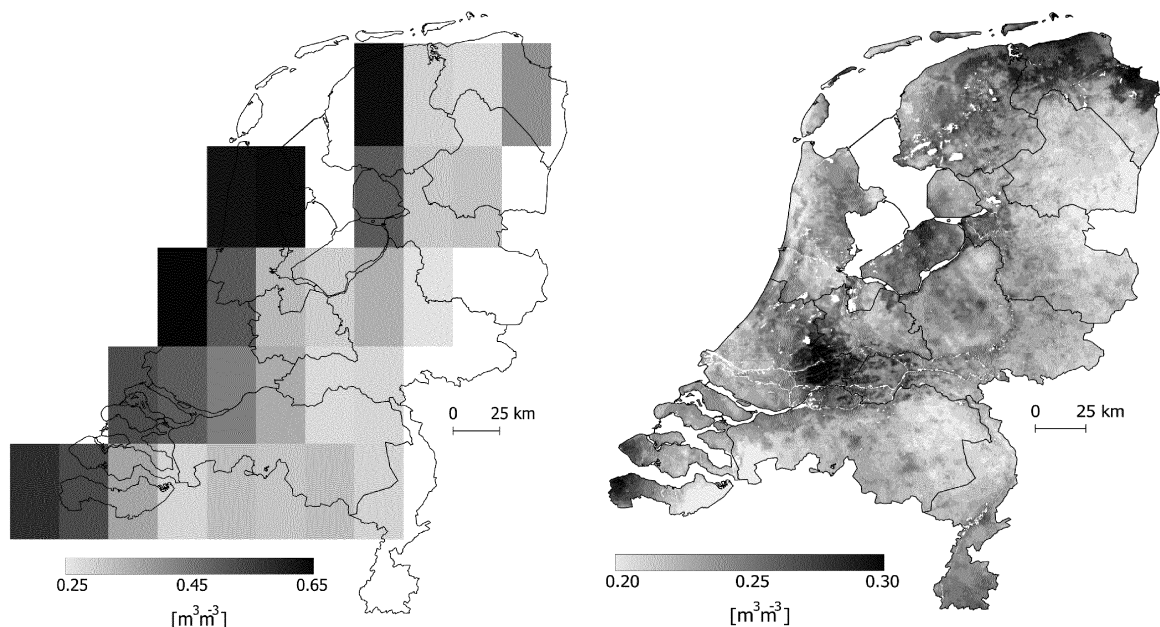


Figure 3.2: Soil moisture maps of the Netherlands, based on SMAP level 3 data with a resolution of 36x36km (left), and based on the downscaling algorithm of VanderSat, resulting in a resolution of 100x100m (right).

4

Materials and methods

In this chapter the materials and methods which are used in this thesis, are discussed. First of all, the installation and calibration of the in-situ sensors, which were installed in Kenya, is explained. Second, the used remote sensing products that were used in the analysis, are discussed. Finally, the applied methods for the analysis of the remote sensing data are explained.

4.1. Fieldwork Kenya: Installation of in-situ sensors

In order to install and calibrate four soil moisture stations, a fieldwork around Kuku, Kenya was carried out in March 2018. Each soil moisture station consists of five soil moisture sensors, of which one measures temperature as well. The five sensors were installed in such a way that they measure both the soil moisture in the top layer of the soil and over the depth along the root zone. The advantage of the sensors in the deeper layer is that those provide data which can not be measured by satellite. Furthermore, the in-situ stations help to better understand the different hydrological behaviour between the areas inside and outside the bunds.

4.1.1. Volumetric water content

The sensors installed in the field are using the Capacitance / Frequency domain technology, which is a widely applied technique and determines the volumetric water content (VWC). The capacitance-technique is used to measure the dielectric constant of the soil, which is influenced by the moisture content of that soil. So, when the moisture content of a soil changes, so do the dielectric constant and consequently the capacitance of that soil. By measuring the capacitance of the sensors, this can be directly related to the water content of a soil. And, by using the 70MHz frequency, salinity and soil texture effects are minimized, which makes the sensors suitable for any type of soil (METER Group, 2017).

Where the gravimetric water content measures the ratio of the weight of water to weight of the soil column, the VWC measures the ratio of water volume to total soil volume. VWC can therefore be defined as:

$$\theta = \frac{V_w}{V_t} * 100\% \quad (4.1)$$

In which V_w is the volume of water and V_t is the total volume.

4.1.2. Set-up of soil moisture stations

The four soil moisture stations each consist of a *Decagon ECH₂O EM50* Data Logger. Each EM50 data logger contains five ports, to which different types of sensors can be connected. The logger can store more than 36,000 scans from the connected sensors and each scan saves the date, time and measurements from each of the five sensors. By connecting a laptop via cable into the communication port of the logger, data can be downloaded manually from the logger. The devices run on 5 AA alkaline batteries and can run in environments up to 100% relative humidity (RH), and between temperatures of -40°C to 60°C.

The EM50 data loggers installed in Kenya, are set at a measurement interval of one hour, storing data for 1500 days. However, as the soil moisture stations are installed in collaboration with the Maasai Wilderness Conservation Trust (MWCT), data is downloaded once every month on average.

To every EM50 logger, five sensors have been connected via 3.5mm stereo plug connectors. Four *Decagon ECH₂O EC5* soil moisture sensors and one *Decagon ECH₂O 5TM* soil moisture and temperature sensor. Both sensors have a resolution of $0.001\text{m}^3/\text{m}^3$ and an accuracy of $0.03\text{m}^3/\text{m}^3$, which is equal to 3% VWC. In addition the 5TM sensor can measure temperatures between -40°C and 60°C , which is compatible with the EM50 logger, with a resolution of 0.1°C and an accuracy of 1°C . The five probes are installed along the rootzone, each at an angle of 45. The 5TM is installed at 5cm depth together with one EC5 sensor. The three remaining EC5 sensors are installed in the soil at depths of 10cm, 20cm and 40cm below the surface. The set-up of the in-situ stations at plot D is shown in figure 4.1 and 4.2.



Figure 4.1: In-situ station, installed at Plot D in Kenya.



Figure 4.2: 5TM and EC5 sensors installed at the soil surface.

Two of the four soil moisture stations are installed at plot D, while two stations are installed at Nyati Camp, the head office of the MWCT. At plot D, one station is installed inside a bund, while one is installed outside. Both stations are only 5m apart. Before the fieldwork, it was planned to install two sensors at the grass seed bank, another project of Justdiggitt. However, due to extreme wet circumstances in Kenya in March 2018, most of the roads were inaccessible and the only bridge to cross a local river broke down (figure 2.5). As a result, it was impossible to reach the project sites most of the time and therefore two stations have been installed near the office. Both stations near the office are installed 200m apart and can be used to validate the VanderSat soil moisture and surface temperature products. Unfortunately, one of the sensors at the MWCT office broke down after a couple of weeks.

4.1.3. Calibration of in-situ sensors

Although standard calibrations for different soil types are available for both the EC5 and 5TM sensors, a calibration was done during the fieldwork in Kuku, Kenya. Using 100cm^3 volumetric soil sample rings, samples were taken in the field at each location (Bunds and Nyati Camp) and depth (5cm, 10cm, 20cm, 40cm). With each sample, a raw measurement was done by the EC5 and 5TM sensor at that specific location. The samples were taken back to the office and, after weighing, oven dried at 90°C for approximately 30 hours. By comparing the wet weight and dry weight, and dividing by the volume of the sample ring, the VWC was obtained. Using the raw measurements of the EC5 and 5TM sensors, a calibration curve was constructed that will be applied on the data of the soil moisture stations. The calibration curves for all locations are presented in appendix C, in equations C.1-C.4 and figure C.1.

Furthermore, bulk density and porosity measurements are presented in table C.1 and C.2 respectively. Despite that the soil is classified as clayey, low bulk densities and high porosities were observed during the fieldwork. An explanation for this might be that samples were often taken inside the bunds, but as observed most of the bunds were filled with sediments which were transported via overland flow. This probably has affected the measurements as these sediments were not fully compacted yet. Finally, there is also the possibility that the soils inside the bunds were affected during the construction phase, as these were dug by hand.

4.2. Remote sensing data

To monitor the impact of the land restoration projects of Justdiggitt, microwave, thermal and optical remote sensing data are used within this Thesis. Passive microwave remote sensing data is retrieved as brightness temperature by the AMSR-E and AMSR-2 devices, installed at NASA's Aqua and JAXA's GCOM-W1 satellites

respectively. The microwave data at C-band is downscaled by VanderSat's downscaling algorithm and processed by the Land parameter retrieval model to soil moisture, surface temperature and vegetation optical depth data at 100x100m resolution (see chapter 3). In the data analysis, these data products are compared to optical and thermal remote sensing data from Sentinel-2 and MODIS, which deliver NDVI and land surface temperature products.

4.2.1. Raw brightness temperatures from AMSR

Raw brightness temperatures are retrieved from the Advanced Microwave Scanning Radiometer (AMSR) which has operated on three satellites, of which two (AMSR-E and AMSR-2) are used in this thesis. AMSR is a multi-frequency radiometer which is developed by JAXA to observe atmospheric, land, oceanic and cryospheric parameters. AMSR-E was launched in 2002 on board of NASA's Aqua satellite and stopped rotating in October 2011. From October until May 2012 a data gap in brightness temperatures occurred, after which AMSR-2 was launched on board of JAXA's GCOM-W1 satellite. The key feature of the AMSR instruments, by using microwave observations, is their ability to 'see' through clouds, which provides almost continuous data over all regions on Earth (Remote Sensing Systems, 2018). Specifications of the AMSR-E and AMSR-2 devices are presented in table 4.1. As shown, AMSR-2 has one additional frequency compared to AMSR-E. Furthermore, due to the larger antenna size, the resolutions of AMSR-2 are higher compared to AMSR-E.

Alternatives to the datasets generated by the AMSR devices are passive microwave datasets derived from the SMAP (Soil Moisture Active Passive) and SMOS (Soil Moisture Ocean Salinity) missions at L-band frequency. However, both devices map the Earth's surface within 3 days, with overpass times around 6:00 am.

Table 4.1: Specifications of Advanced Microwave Scanning Radiometers AMSR-E and AMSR-2

Specifications of AMSR-E and AMSR-2			
	AMSR-E		AMSR-2
<i>Satellite Platform</i>	Aqua (NASA)		GCOM-W1 (JAXA)
<i>Dates of operation</i>	May 2002 - Oct 2011		May 2012 - Present
<i>Altitude</i>	705km		700km
<i>Swath width</i>	1450km		1450km
<i>Antenna size</i>	1.6m		2m
<i>Equator Crossing time</i>	1:30pm (Ascending) & 1:30am (Descending)		1:30pm (Ascending) & 1:30am (Descending)
<i>Frequencies (and resolutions)</i>	6.93GHz	(75x43km)	6.93GHz (62x35km)
	10.7GHz	(51x29km)	7.30GHz (62x35km)
	18.7GHz	(27x16km)	10.7GHz (42x24km)
	23.8GHz	(32x15km)	18.7GHz (22x14km)
	36.5GHz	(14x 8km)	23.8GHz (19x11km)
	89.0GHz	(6x 4km)	36.5GHz (12x 7km) 89.0GHz (5x 3km)

4.2.2. VanderSat soil moisture, temperature and vegetation optical depth data

The soil moisture, surface temperature and vegetation optical depth products of VanderSat are derived from the raw brightness temperature data, which are obtained by AMSR-E and AMSR-2. After downscaling these to high resolution maps of 100x100m using their algorithm, the high resolution brightness temperatures are used as input in the land parameter retrieval model (LPRM) to calculate soil moisture, surface temperature and vegetation optical depth. The LPRM uses the descending (night-time 1:30am equator crossing) brightness temperatures. As, the project areas in Kenya are close to the equator, the overpass time of the satellite at the study sites of Justdiggit is roughly at the same time. Due to the location of the project areas close to the equator, data is available roughly twice every three days. Furthermore, in this thesis, the data is calculated at C-band frequency. By combining datasets of different satellites, the dataset of VanderSat is available from 1978. However, this is a 0.25 degree product, while the 100x100m resolution product is available from 2002, after launching of AMSR-E. Therefore, the period of interest in this thesis is between 2002 and 2018.

Soil moisture content is measured as the volume of water per volume of soil (m^3/m^3), while surface temperature is measured in Kelvin (K). Vegetation Optical Depth (VOD) is a dimensionless parameter which describes the thickness of the canopy layer at the surface. High VOD values correlate to high biomass and vegetation water content (kg/m^3), while low VOD values relate to low biomass and low water content at the Earth's surface that's under observation.

4.2.3. MODIS thermal derived land surface temperature

Besides using temperature data from the microwave spectrum, also surface temperatures from the thermal spectrum are analysed in this thesis, for comparison. MODIS, which is installed on the same satellite (Aqua) as the AMSR-E device, provides day- and night-time thermal infrared temperature observations at $1000 \times 1000 \text{m}$ resolution. This adds the opportunity to compare the night-time passive microwave derived temperature product of VanderSat with daytime observations. During daytime, the spatial temperature gradients in the study area are larger, while the surface temperature during night-time is more homogeneously distributed (Liu et al., 2018). The disadvantage of using the MODIS thermal infrared observations, is that these are sometimes affected by cloud cover which is therefore already filtered out. Similar to the passive microwave obtained surface temperature data, MODIS has data available since May 2002.

4.2.4. Sentinel-2 & MODIS Normalized Difference Vegetation Index

Finally, also optical remote sensing data from Sentinel-2 and MODIS is used in this thesis. The Normalized Difference Vegetation Index (NDVI) images of Sentinel-2 at $10 \times 10 \text{m}$ resolution, which are presented in appendix A, are calculated from both the near-infrared and red bands, using equation 4.2 (Griend and Owe, 1993).

$$NDVI = \frac{NIR - RED}{NIR + RED} \quad (4.2)$$

NDVI is based on the principle that chlorophyll in the leaves of plants absorbs the red light, while the cell structure of the leaves reflects the near-infrared light. As the optical light can not penetrate through the leaves, NDVI is a parameter that describes the greenness and healthiness of canopy on the Earth's surface, which often saturates at high vegetation density. NDVI is therefore not linearly related to vegetation biomass and, as a result, is a different parameter than vegetation optical depth. VOD measures vegetation thickness which has a linear relation with biomass and vegetation water content for frequencies below 10GHz, which is the case for C-band that's used in this research.

Besides providing day- and night-time surface temperatures, MODIS also provides an NDVI-product, at $250 \times 250 \text{m}$ resolution. The NDVI-product of MODIS has a temporal resolution of 16 days and pixels containing clouds are filtered out, which makes it very consistent. The MODIS NDVI-product will be used in the analysis as it is delivering data since 2002, while Sentinel-2 is only providing data since the end of 2015.

4.3. Temporal smoothing of downscaled soil moisture, temperature and vegetation optical depth products

A first look on the time series of the downscaled soil moisture, temperature and VOD products has shown unusual temporal variability, as shown in figure 4.3. Especially looking at VOD, the temporal variability is not reasonable, given that it represents a parameter for vegetation thickness. When taking a look at the spatial maps, gridded artefacts are present in the data, as shown in figure 4.4. These grid artefacts are a familiar problem at VanderSat and are the result from downscaling and deriving surface temperatures at Ka-band (36.5GHz). As the satellite-footprints at this frequency are too small to overlap with each other, these grids appear, with clear contrast around the edges. Because the downscaled temperature product is used to derive soil moisture and vegetation optical depth, the temperature artefacts are also present in those datasets. Despite the clear contrasts inside the grid, the differences between the edges of the artefacts are small (soil moisture $\pm 2\%$, temperature $\pm 1\text{K}$ and VOD ± 0.02). And because of temporal variability in the location of the artefacts, this causes small fluctuations in the time series of soil moisture, temperature and VOD. Currently, VanderSat has already solved this issue in their datasets, but for this research a workaround is needed.

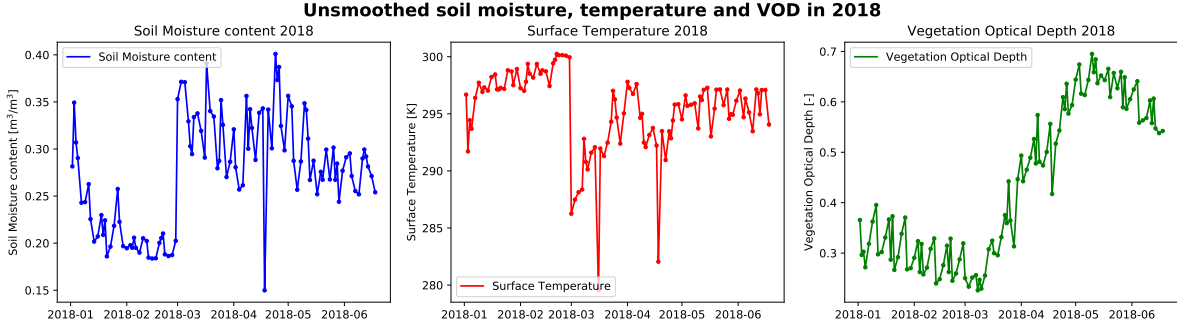


Figure 4.3: Time series of soil moisture, surface temperature and VOD for the reference area

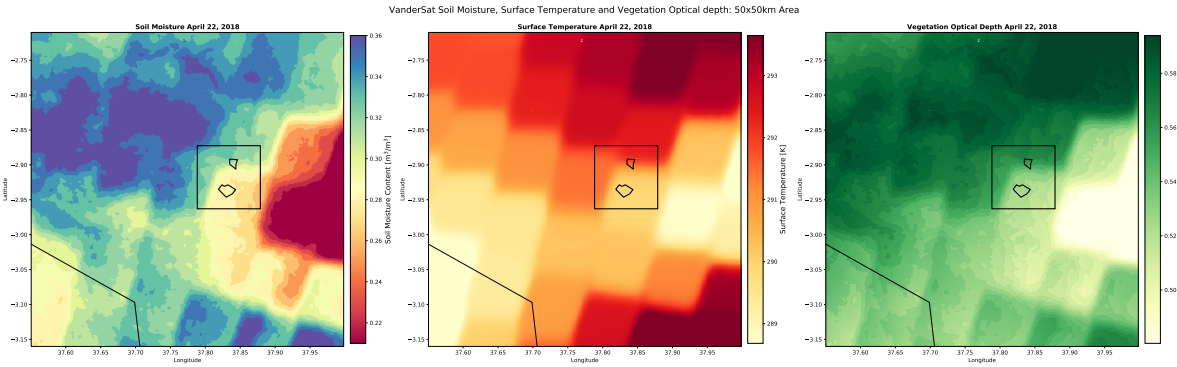


Figure 4.4: Spatial plots (50x50km) of soil moisture, surface temperature and VOD, showing the 36.5GHz temperature grid artefacts.

As temporal averages over the course of several months have shown to remove the artefacts (see also figure 5.14 & 5.15), a workaround needs to be found to solve for the temporal and spatial variability on smaller time frames. For this reason, smoothing filters are tested on the time series data. Instead of using a simple moving average, the Gaussian and Epanechnikov kernels are considered, as both give higher weights to the (nearest) neighbouring observed data. Both kernels are applied within the Nadaraya Watson kernel estimator, which is given by equation 4.3, in which K is the Kernel or weight which is applied on the data. In general, kernels are defined based on equation 4.4 and 4.5.

$$\hat{y}(x_0) = \frac{\sum_{i=1}^n K_\lambda(x_0, x_i) y_i}{\sum_{i=1}^n K_\lambda(x_0, x_i)} \quad (4.3)$$

$$K_\lambda(x_0, x_i) = D\left(\frac{|x_i - x_0|}{\lambda}\right) = D(t) \quad (4.4)$$

$$t = \left(\frac{|x_i - x_0|}{\lambda}\right) \quad (4.5)$$

The Gaussian kernel is based on an exponential function, while the Epanechnikov kernel is a parabolic function. The Gaussian kernel therefore is a wide kernel without cut-offs near the edges, while the Epanechnikov kernel has no weight function to data far away for absolute values of t larger than 1. Formulas for the Gaussian and Epanechnikov kernels are shown in equation 4.6 and 4.7 respectively.

$$\text{Gaussian Kernel: } D = e^{-t^2} \quad (4.6)$$

$$\text{Epanechnikov Kernel: } D = \begin{cases} \frac{3}{4}(1 - t^2) & |t| \leq 1 \\ 1 & \text{otherwise} \end{cases} \quad (4.7)$$

The bandwidth, or smoothing window of the kernel is defined by λ . In appendix D, figures D.1-D.6, smoothing windows of 6, 8 and 10 days are presented for soil moisture and temperature, while for vegetation optical depth smoothing windows of 13, 15 and 17 days are shown.

To choose an appropriate smoothing window for soil moisture, temperature and vegetation optical depth, the kernels should smooth out the temporal variability caused by the grid artefact in the time series, but should also not remove too much detail. Figure D.1 in appendix D for example, shows how the Gaussian kernel at all smoothing windows (6-10 days) is generally too smooth. As a result, it causes the significant increase in soil moisture after the first rains to happen up to two weeks in advance of the actual increase and rainfall, at March 1. The same happens in terms of surface temperature, where temperature decreases two weeks in advance of the big rain events in March (figure D.2). The Gaussian kernel is also a clear example of how almost all of the temporal variability is smoothed out of the soil moisture and temperature time series, except for major precipitation events. However, the smoothing windows of 13-17 days for VOD are more accurate.

All in all, the Epanechnikov kernel seems to better take into account the variabilities of soil moisture, temperature and VOD, compared to the Gaussian kernel. For the data-analysis in this thesis, therefore the Epanechnikov smoothing kernel is used to improve the VanderSat data, although the effects of the grid artefacts are not entirely removed, as shown in appendix D, figures D.4-D.6. Finally, for soil moisture and surface temperature, smoothing windows of 8 days are used, while for VOD a smoothing window of 15 days is used.

4.4. Data analysis

This section discusses which analyses have been carried out on the AMSR-2 raw brightness temperatures, the VanderSat soil moisture, surface temperature and vegetation optical depth data and the MODIS land surface temperature and NDVI data. Before the analysis, the soil moisture, temperature and vegetation optical depth data have been smoothed according to section 4.3, to solve for the temperature artefacts that are present in this data, which cause unusual temporal and spatial variability.

4.4.1. Analysis of raw brightness temperature data

Besides an analysis on the 100x100m soil moisture, temperature and vegetation optical depth products of VanderSat, also an analysis is carried out on the raw brightness temperature data of AMSR-E and AMSR-2. This analysis focusses on the Ka-band (36.5GHz), as this frequency has the finest spatial resolution. Besides a regular time series of plot B, plot D and the reference area, also anomalies, error plots and the microwave polarization difference index is calculated. As for each frequency, the raw brightness temperature is delivered with coordinates for latitude and longitude, the gridpoints with a 1km radius around its coordinates that are overlapping the project sites are selected. This criteria is based on the Gaussian distribution that VanderSat assumes within the satellite footprints in which the center of the footprints contributes more to the observed brightness temperature value than the footprint's edges. As a result, the smaller Justdiggitt plots have less overlapping gridpoints than the 10x10km reference area.

Results of the analysis of the raw brightness temperature data are shown in appendix E. The time series haven't shown any differences between the project sites and the reference area. Furthermore, it can be noticed that the horizontal polarized brightness temperatures are on average lower than the vertical polarized data. Also in terms of anomalies no significant differences are present between the project sites and the reference area. The error plots at 36.5GHz for comparison of 2016 and 2017 with the period 2003-2015, show that there are again no significant differences between the Justdiggitt plots and the reference area, while 2016 and 2017 have both higher brightness temperature values at vertical and horizontal polarizations during January until April. Finally, as the results of the microwave polarization difference index (MPDI) have shown higher variability in MPDI during the AMSR-E period than the AMSR-2 period in appendix E, for the analysis of the remote sensing data of VanderSat, only soil moisture, temperature and VOD data during the AMSR-2 period (2012-2018) will be analysed.

4.4.2. Time series and differences between plots

After smoothing of the remote sensing data of VanderSat, time series for soil moisture, temperature and vegetation optical depth are plotted for the AMSR-2 period, for all project areas. Furthermore, the differences between the project areas (plot B and plot D) and the 10x10km reference area are calculated and plotted over time. This shows if and when there are significant differences between the project areas and the reference area over time. For each day spatial averages are calculated for each project area and the reference area is subtracted from the daily spatial averages from plot B and plot D. Positive differences result in larger soil moisture, temperatures and vegetation optical depth values inside the plots compared to the reference area while negative differences show lower values inside the plots.

4.4.3. Climatology and anomalies

To get insight in the seasonal behaviour of the project areas in terms of soil moisture, surface temperature and vegetation optical depth, the climatology and anomalies are calculated for the AMSR-2 period. Both are commonly used in climate studies.

The climatology is defined as a long-term average of the parameter under observation, at a given time-range. The given time-range can be daily, weekly or monthly for example. The long-term average is calculated over multiple years. A daily climatology of temperature, for a term of ten years, will therefore calculate the average temperature at each day of the year over the ten year period. In this thesis, the daily climatology will be used for soil moisture, temperature and vegetation optical depth over the AMSR-2 time period between July 3, 2012 and June 19, 2018. The climatology \bar{Y}_d , at a given day d , for N years, can be calculated with equation 4.8. In which y_{dj} is the measurement at a given day d in year j .

$$\bar{Y}_d = \frac{\sum_{j=1}^N y_{dj}}{N} \quad (4.8)$$

Anomalies can be defined as the deviation from the mean, or climatology. The anomalies help determining whether seasonal variations are present in the data. By subtracting the climatology of a given day from the observed measurements, the anomaly at this day is calculated, as shown in equation 4.9. In which the anomaly is calculated at a given day d in year j .

$$Anomaly_{dj} = y_{dj} - \bar{Y}_d \quad (4.9)$$

4.4.4. Histograms and cumulative distribution functions

Histograms and cumulative distribution functions (CDF's) are calculated to represent the distribution of the remote sensing data of VanderSat. For this method, a distinction is made between the data before and after implementation of the Justdiggit projects in 2016. The data is therefore divided in 'pre-Justdiggit' and 'post-Justdiggit'. Furthermore, first the normalized histograms of both periods are calculated, after which the histograms for the differences between the plots and the reference area are computed.

The CDF's are calculated to give the distribution of soil moisture, temperature and vegetation optical depth for each area in a given year. The functions thereby give the probability that for example soil moisture has a specific value or less, in a given year. The results will be used to identify if plots B and D for example have a cooler distribution in temperature during the post-intervention years than the outer reference area.

To compute the histograms, the standardized histogram function in python is used from the matplotlib package, which is shown in equation 4.10

$$Axes.hist(Y, bins = 100, normed = True, cumulative = False, histtype = 'bar') \quad (4.10)$$

In which Y is the dataset, the number of bins is set at 100 and the histograms are normalized. For the cumulative distribution functions, the same equation is used. However, cumulative is set at '*True*' and histtype at '*step*'.

4.4.5. Temporal averaging during wet season

While the climatologies, anomalies and histograms were primarily focussed on analysing the time series of the remote sensing data, temporal averaging focusses on the spatial variability during the wet season. As shown, the long wet season often occurs between the end of February until the end of May, and especially 2018 has proven to be a significant wet year so far. Therefore, for each year, the period between day 50 (February 19) and day 150 (May 30) is averaged and presented in spatial plots. For 2016, 2017 and 2018 it's expected that the project areas of Justdiggit stand out in terms of soil moisture and VOD, while surface temperatures should be lower in this area.

4.4.6. Spearman correlation coefficient

To determine the correlation between two variables, the Pearson correlation, Spearman rank test and coefficient of determination can be used. In this thesis the Spearman correlation is used to determine the relationships between the in-situ soil moisture sensors in Kenya and the VanderSat soil moisture data. Furthermore,

they're used for comparison between the VanderSat surface temperature, the temperature from the in-situ sensor and MODIS temperature of day and night time. Finally, also the vegetation optical depth data of VanderSat is compared to MODIS NDVI (250x250m) and Sentinel-2 NDVI (10x10m), although for the latter we need to take into account that two different vegetation parameters are used (section 4.2.4).

The Spearman rank test is based on equation 4.11 and is calculated in python using the scipy package, with `scipy.stats.spearmanr(a, b)`, in which a and b are the datasets which are tested.

$$\rho = 1 - \frac{6 \sum d_i^2}{n(n^2 - 1)} \quad (4.11)$$

4.5. Modelling of brightness temperature signal using tau-omega model

4.5.1. Brightness temperature modelling

To better understand the effect of the bunds and to get insight in what signal is needed from the bunds to measure a significant difference between the project areas, the brightness temperature signal is modelled using the tau-omega model. The tau-omega model (Mo et al., 1982) is used in the land parameter retrieval model (LPRM) to solve for the soil moisture content and vegetation optical depth, using brightness temperatures obtained from AMSR-2, as discussed in chapter 3, and expressed in equation 4.12.

$$T_{Bp} = T_S e_{r_p} \Gamma_p + (1 - \omega_p) T_C (1 - \Gamma_p) + (1 - e_{r_p}) (1 - \omega_p) T_C (1 - \Gamma_p) \Gamma_p \quad (4.12)$$

First of all, the dielectric constant is calculated using the dielectric mixing formula of Wang and Schmugge (1980), which requires soil texture information and soil moisture content as input. The dielectric mixing model is given in equation 4.13.

$$\text{Dielectric Mixing Model: } k = \begin{cases} \theta k_x + (P - \theta) k_a + (1 - P) k_r & \theta \leq \theta_t \\ \theta_t k_x + (\theta - \theta_t) k_w + (P - \theta) k_a + (1 - P) k_r & \theta > \theta_t \end{cases} \quad (4.13)$$

In which k is the dielectric constant, θ the soil moisture content, θ_t the transition soil moisture content (which describes the transition between the bound- and free water phase), P the porosity, k_a and k_r the dielectric constants of air (1) and rock (5.5) respectively and k_x is the dielectric constant of initially absorbed water, which is calculated from equation 4.14.

$$\text{Initially Absorbed Water: } k_x = \begin{cases} k_i + (k_w - k_i) \frac{\theta}{\theta_t} y & \theta \leq \theta_t \\ k_i + (k_w - k_i) y & \theta > \theta_t \end{cases} \quad (4.14)$$

In which k_w and k_i are the dielectric constants of water (78) and ice (3.2) respectively, while y is a parameter to fit the data, which is given by equation 4.15.

$$y = -0.57 \theta_{WP} + 0.481 \quad (4.15)$$

In which θ_{WP} is the soil moisture content at wilting point, which is calculated using equation 4.16.

$$\theta_{WP} = 0.06774 - 0.00064 * \text{Sand}P + 0.00478 * \text{Clay}P \quad (4.16)$$

Where θ_{WP} is calculated based on the sand and clay mass fractions ($\text{Sand}P$ and $\text{Clay}P$) in the soil. As the soil of the project areas in Kenya is described as a Chromic Luvisol by the FAO soil texture map, the sand and clay fractions are approximately 10 and 60% respectively, while the porosity is around 40% (Sari et al., 2018). Finally, the transition soil moisture content can be calculated from equation 4.17.

$$\theta_t = 0.165 + 0.49 \theta_{WP} \quad (4.17)$$

Second, using the dielectric constant k from the Dielectric Mixing Model and an incidence angle u of 55° , the Fresnell equations are used to solve for the smooth surface emissivity, using equation 4.18 for the horizontal polarized smooth surface reflectivity and equation 4.19 for the vertical polarized smooth surface reflectivity.

$$R_H = \left| \frac{\cos(u) - \sqrt{k - \sin^2(u)}}{\cos(u) + \sqrt{k - \sin^2(u)}} \right|^2 \quad (4.18)$$

$$R_V = \left| \frac{k \cos(u) - \sqrt{k - \sin^2(u)}}{k \cos(u) + \sqrt{k - \sin^2(u)}} \right|^2 \quad (4.19)$$

Third, using the rough surface emissivity model of Wang and Choudhury (1981), the rough surface emissivity is calculated for both polarizations, as shown by equations 4.20 and 4.21 (van der Schalie, 2017).

$$e_{r(H)} = 1 - \left((1 - Q)R_H + QR_V \right) e^{-h \cos(u)} \quad (4.20)$$

$$e_{r(V)} = 1 - \left((1 - Q)R_V + QR_H \right) e^{-h \cos(u)} \quad (4.21)$$

In which Q is the polarization mixing factor, which is often 0 (Njoku and Li, 1999), and h the dimensionless roughness parameter, which is often between 0 and 2 (Njoku and Li, 1999). In this research therefore, a value of 1 is used for h . The transmissivity Γ in the tau-omega model is calculated using equation 4.22. In which τ_v is the vegetation optical depth for a given type of canopy and vegetation thickness.

$$\Gamma = e^{-\tau_v / \cos u} \quad (4.22)$$

Finally, using the tau-omega model as described in equation 4.12, the brightness temperature can be modelled for a given soil moisture content and vegetation optical depth. In which the soil temperature T_S and canopy temperature T_C are assumed equal (298K). While, ω is the single scattering albedo for vegetation, which is assumed 0.1 for African savanna and the Sahel at C-band frequency (Van de Griend and Wigneron, 2003).

4.5.2. Modelling scenarios

To better understand the effect of the bunds on the passive microwave signal and to get insight in what signal is needed from the project areas to measure a significant difference in brightness temperature (to overcome the accuracy of 1K of the AMSR-2 radiometer), the effect of the bunds is modelled. First of all, a sensitivity analysis is done on the brightness temperature signal by varying soil moisture content (between 0 and 1 m^3/m^3 , and a fixed vegetation optical depth of 0.50) and vegetation optical depth (between 0.2 and 0.7, using a fixed soil moisture content of 0.25 m^3/m^3). Taking into account a surface temperature of 298K. Furthermore, a colormap shows the sensitivity of brightness temperature to soil moisture and vegetation optical depth between 0 and 1 m^3/m^3 and 0.2 and 0.7 respectively.

Secondly, two scenarios are used to model the effect of the bunds. Scenario 1 describes the reference situation without bunds and what signal is needed to measure 1K brightness temperature difference. This is compared to the current signal with 10% of bunds in the project area. Scenario 1 takes into account a VOD of 0.2 for the area containing bare land (Open shrubland), while the area with bunds are assigned a value of 0.5 for VOD, which corresponds to a woody savanna according to Konings et al. (2017). This scenario therefore assumes that all bunds are fully vegetated at this stage. By varying the percentage of bunds P_{Bunds} in the project area between 0 and 100%, using equation 4.23, the effect of the bunds is modelled.

$$T_B = P_{Bunds} T_{B_{Bunds}} + (1 - P_{Bunds}) T_{B_{Bare}} \quad (4.23)$$

Scenario 2 describes the current situation with 10% of bunds and takes into account the increase of vegetation cover inside the area for the first 15 years after implementation of the projects, in order to simulate the number of years needed to measure a 1K difference in brightness temperature. Scenario 2 assumes a vegetation optical depth of 0.2 for bare land and 0.3 for bunds at year 0. However, these values are increased over time, by multiplying their effect by 5% every year ($\tau_{yearly} = \tau_{initial} * 1.05^{N_{years}}$). This simulates the development of vegetation inside the project areas over time, for example from an open shrubland ($\tau = 0.2$) to a closed shrubland ($\tau = 0.4$) for the area outside the bunds (Konings et al., 2017). Furthermore, by increasing the area of the bunds every year by 10%, it is assumed that the effect of the bunds increases in space as well.

Discussion of results

In this chapter the results of the analyses are discussed. First of all, the measurements from the in-situ sensors in Kenya are presented. Second, a cross-validation is done between the in-situ data, the downscaled passive microwave derived soil moisture, temperature and vegetation optical depth products of VanderSat and the thermal derived temperature and optical derived NDVI from MODIS. Third, the impact of the project areas of Justdiggitt is analysed using the soil moisture, temperature and VOD data, by comparing time series, calculating climatologies, anomalies, histograms, cumulative distribution functions. In addition, also the time series of surface temperatures from MODIS are presented. Four, the results of the modelling approach using the tau-omega model are presented. And finally, a synthesis reflects on the results of the analyses.

5.1. Measurements from in-situ sensors

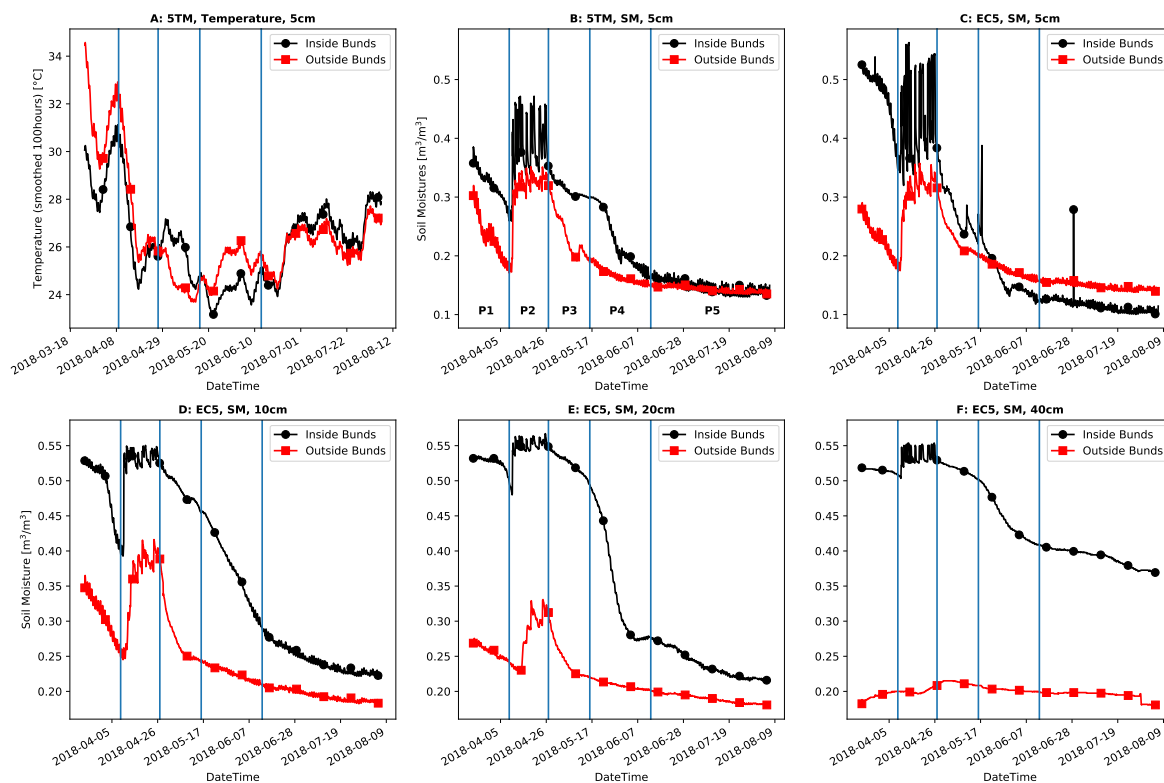


Figure 5.1: Time series of in-situ sensors installed inside and outside the bunds at plot D, with 5TM temperature at 5cm depth (A), 5TM soil moisture content at 5cm depth (B) and EC5 soil moisture content at depths of 5cm (C), 10cm (D), 20cm (E) and 40cm (F). Blue lines represent four periods, P1: March 23 - April 9, P2: April 9 - April 27, P3: April 27 - May 16, P4: May 16 - June 13 and P5: June 13 - August 6.

Figure 5.1 presents the data which is obtained by the in-situ sensors that were installed in March 2018 at plot D. Panels A till F show the results of the 5TM temperature sensors at 5cm, 5TM soil moisture at 5 cm and EC5 soil moisture at 5cm, 10cm, 20cm and 40cm depth respectively. Each graph shows the results of the two stations installed inside (black line) and outside (red line) the bund. These in-situ stations were installed only 5m apart and are used to get insight in the hydrological behaviour along the rootzone, around the bunds.

Both stations were installed on the 23rd of March 2018, roughly three weeks after the first rains and therefore show a dry down until the 9th of April in all layers (Period P1). However, this dry down is less pronounced in the deeper layers. Between the 9th of April and the 27th of April (Period P2), a second rain period occurred, causing a rapid decrease of temperature both inside and outside the bund ($\pm 7^\circ\text{C}$), and an instantaneous rise of soil moisture in the upper layers, with increases of approximately 15%. Furthermore, panels D and E show significant increases of soil moisture at 10cm and 20cm depth ($\pm 15\%$ and 7.5% respectively), both inside and outside the bunds. The response of soil moisture to rainfall however, slightly lags at the sensors outside the bund, while the response inside is instantaneous. Finally, at 40cm depth, an immediate increase of soil moisture ($\pm 5\%$) is present in figure 5.1 panel F, while the response at the sensor outside the bund is minimal.

After the rain period, an immediate dry down occurred outside the bunds in the layers at 5cm, 10cm and 20cm (Period P3). In addition, this resulted in a further decrease of the surface temperature outside the bund, which is possibly due to vegetation growth outside the bunds. As shown in figure 2.4, due to the intense rainfall in 2018, most of the area had turned green in contrast to December 2017 as shown in figure 1.3. This resulted in more vegetation outside the bunds compared to inside, which was probably because of ponding of water inside the bunds (as observed during the fieldwork and shown in figure 1.1). As a result, the soils were therefore too wet for vegetation growth inside the bunds. As shown in figure 5.1, this seems reasonable as the dry down of soil moisture at all depths inside the bund was less pronounced during period P3, except for the EC5 sensor at 5cm depth, which followed the pattern of the EC5 sensor outside the bund at the same depth. Because vegetation growth outside the bunds was more significant than inside, this explains the significant dry down outside the bund and the fact that surface temperatures are lower outside than inside the bund, probably as a result of increased transpiration.

Between the 16th of May and the 13th of June (Period P4) the temperature outside the bund increased, while the temperature inside continued its decrease at first. As a result, the temperature inside the bund was lower than outside, while at the same time a rapid dry down of soil moisture occurred at all depths, probably due to the fact that vegetation has started growing inside the bunds. Meanwhile, the soil layers outside the bund ran out of water, due to transpiration. All in all, the time lag in dry down between inside and outside the bunds is roughly a month. And, the soil still contains higher soil moisture contents inside the bund compared to outside, at depths of 10cm, 20cm and 40cm during Period P5, with even a double amount of soil moisture content (40% instead of 20%) inside the bund at the beginning of August, three months into the dry season.

Table 5.1: Results of a simple T-test between in-situ data inside and outside the bunds

Independent two-sample t-test between in-situ data inside and outside the bund						
Sensor	5TM 5cm (Temp)	5TM 5cm (SM)	EC5 5cm	EC5 10cm	EC5 20cm	EC5 40cm
<i>p</i>	0.271	$6.04 \cdot 10^{-6}$	0.005	$1.03 \cdot 10^{-22}$	$1.54 \cdot 10^{-29}$	$8.87 \cdot 10^{-135}$

The results of a simple independent two-sample t-test between the in-situ measurements inside and outside the bund, which are presented in table 5.1, show that the differences between the sensors are most significant on the deeper layers. Using a significance level of 0.05 (5% probability), only the temperature measurements inside and outside the bund can be assumed to have the same distribution. From the soil moisture observations, the EC5 sensor at 5cm comes closest to having the same relation between the measurements inside and outside the bunds, while the probability decreases for the observations at deeper locations. The results in table 5.1 therefore show that the effect of the bunds in terms of moisture content is most significant at the deeper layers. While, for surface temperature there is no significant difference between inside and outside the bunds during the measurement period of March-August.

5.2. Cross-validation between remote sensing products and in-situ data

In figures 5.2, 5.3 and 5.4, time series are shown for the soil moisture, temperature and vegetation optical depth remote sensing products of VanderSat, versus the soil moisture and temperature in-situ data, and versus the MODIS daytime & night-time temperature data and the NDVI products of Sentinel-2 and MODIS.

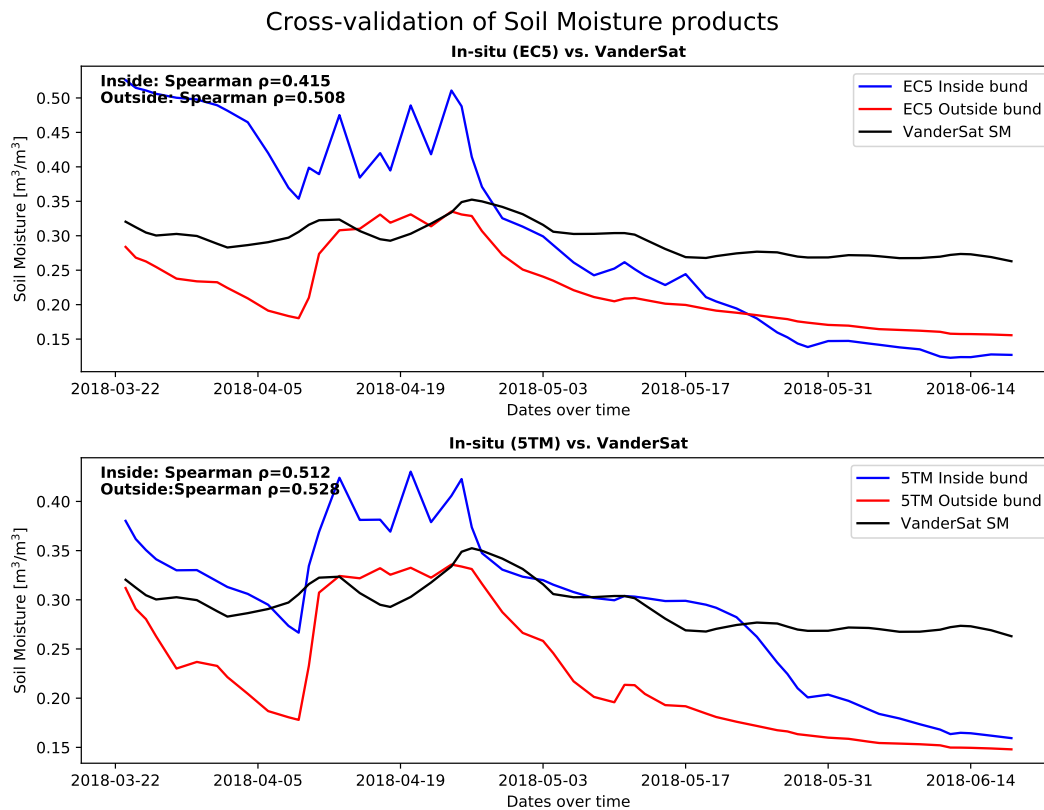


Figure 5.2: Time series of VanderSat soil moisture vs. In-situ sensors soil moisture inside and outside the bunds

Figure 5.2 shows the time series of the soil moisture data of VanderSat versus the soil moisture from the EC5 and 5TM in-situ stations, which are installed inside and outside a bund in plot D. In general, the Spearman correlations of the in-situ sensors with the VanderSat soil moisture product are quite similar, with values of $\rho \approx 0.5$. The EC-5 sensor inside the bund is the only sensor with a lower correlation, of $\rho = 0.415$, which is probably caused by the high soil moisture values between the 22nd of March and the 10th of April. Furthermore, the in-situ sensors have a stronger amplitude between dry and wet conditions, where the soil moisture product of VanderSat shows a more smooth time series, probably as a result of the area averaged data. We have to take in to account that the in-situ sensors have run since March 2018 only and are being compared to the VanderSat remote sensing products until the 19th of June. Due to missing data, these are only 56 days.

Figure 5.3 shows the time series of the temperature data of VanderSat versus the temperature data of the 5TM in-situ sensors inside and outside the bund and versus the daytime and night-time temperature products of MODIS. As shown, both the 5TM sensors inside and outside the bund have low Spearman correlations with the downscaled temperature product ($\rho \leq 0.23$), probably as a result of the short measurement period. Furthermore, the temperature product of VanderSat has lower temperatures than the in-situ sensors during the wet period until May. The MODIS products have higher correlations than the in-situ sensors, where the night-time temperatures of MODIS ($\rho = 0.622$) perform better than the daytime values ($\rho = 0.373$). This also makes sense, as the night-time temperature products of VanderSat and MODIS have similar overpass times and daytime naturally has larger temporal variability. Any differences can be explained from the fact that MODIS measures in a different spectrum (Thermal), which is therefore sometimes covered by clouds and MODIS uses a larger resolution (1000m). The advantage of comparing the temperature products of VanderSat and MODIS is that both products are available during longer time series than the in-situ stations and that we're comparing remote sensing products instead of point measurements versus remote sensing.

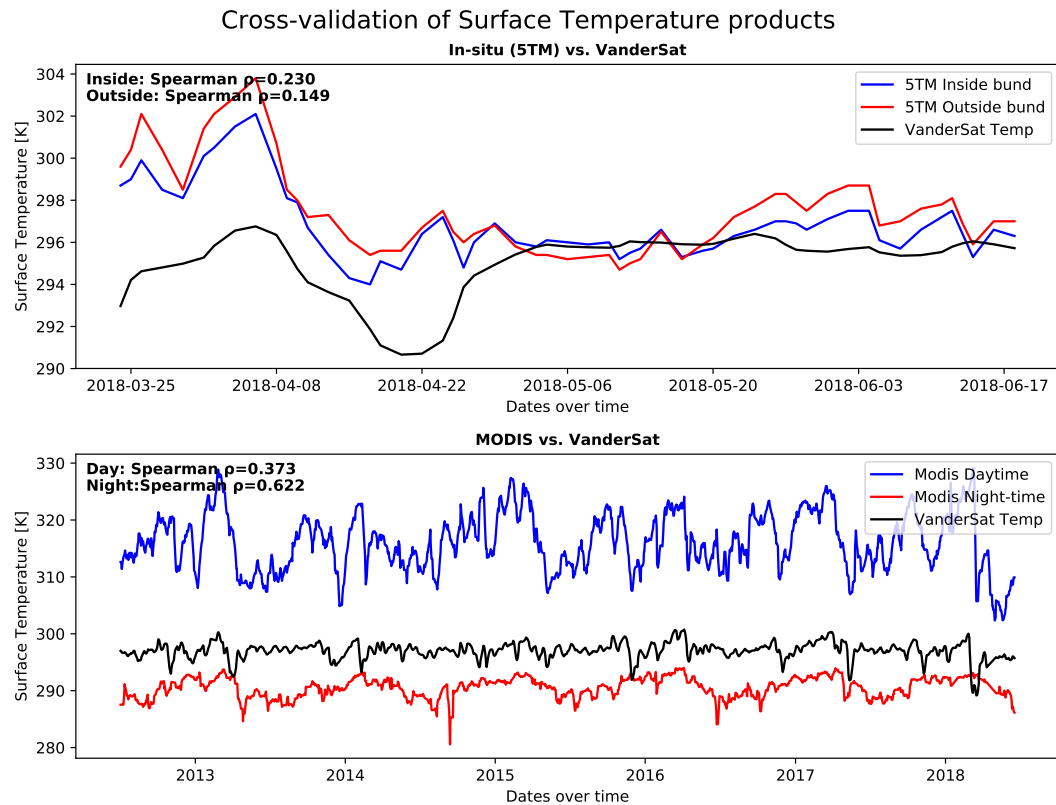


Figure 5.3: Time series of VanderSat night-time temperature vs. In-situ sensors temperature inside and outside the bunds & MODIS LST

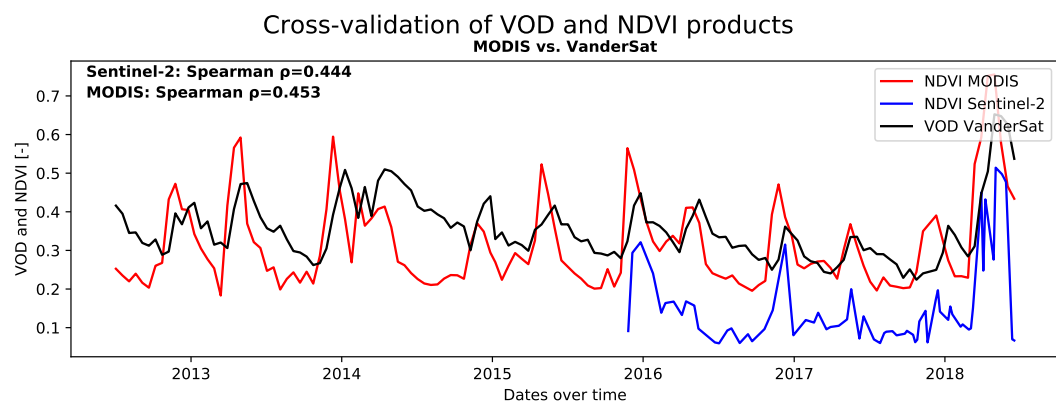


Figure 5.4: Time series of VanderSat vegetation optical depth vs. MODIS & Sentinel-2 NDVI

In terms of vegetation optical depth, time series versus MODIS and Sentinel-2 NDVI are presented in figure 5.4, while taking into account we're comparing different parameters (section 4.2.4). Overall, the MODIS NDVI values are higher compared to the Sentinel-2 values. Furthermore, the NDVI values generally have a higher amplitude in variability compared to VOD. But all in all, they're consistent and show low VOD/NDVI values during the dry periods and high VOD/NDVI values during wet periods. As a result, therefore the Spearman correlations are similar ($\rho \approx 0.45$)

5.3. Analysis of project areas, using soil moisture, surface temperature and vegetation optical depth data

5.3.1. Time series of downscaled soil moisture, temperature and vegetation optical depth

In figure 5.5 the time series of soil moisture, surface temperature and vegetation optical depth are shown for the AMSR2 period (2012-2018), until the 19th of June. Each graph shows the spatial means on a given day for plot B (red line), plot D (blue line) and the 10x10km reference area (black line). All graphs are smoothed using the Epanechnikov smoothing kernel, with smoothing windows of eight days (soil moisture and surface temperature) and 15 days (vegetation optical depth).

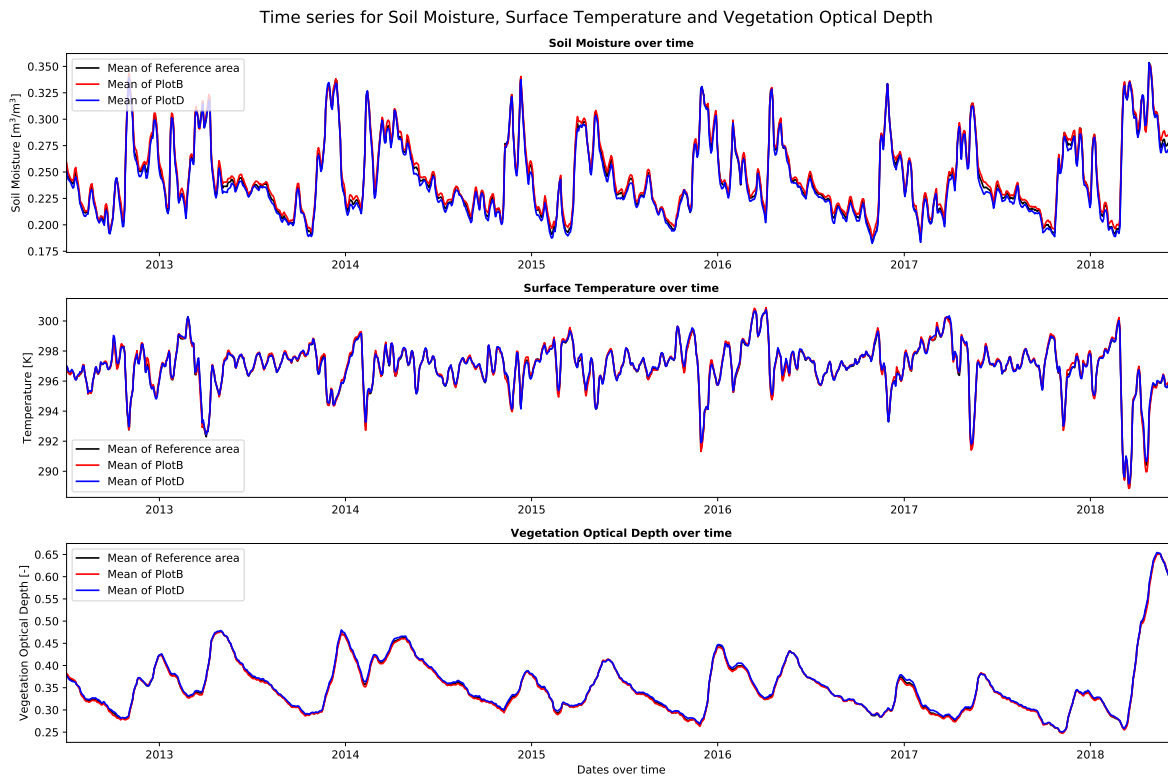


Figure 5.5: Time series of VanderSat Soil Moisture, Surface Temperature and Vegetation Optical Depth data, for the daily spatial means of plot B (red), plot D (blue) and the 10x10km reference area called Justdiggit Area (black).

Although a longer smoothing window is applied on VOD, it is shown that soil moisture and surface temperature are fluctuating more than VOD. This is because soil moisture and temperature are more sensitive to atmospheric effects such as heating by sun and small precipitation events. Both parameters therefore often also show a diurnal pattern due to evaporation and condensation because of warming up by sun and cooling down over night. In addition, vegetation has a delay in its response to precipitation events and high soil moisture contents as can be seen in figure 5.5. Peaks in VOD always occurred after the soil moisture peaks. But, despite this delay, the time series of soil moisture, VOD and temperature have shown to be very consistent.

The soil moisture, temperature and VOD peaks clearly coincide with the two wet and dry seasons through the year. A first decline often sets in during January and February until the start of the rain season in March, after which rapid increases in soil moisture and VOD occur until May. A strong decline in VOD and soil moisture content kicks in until the last months of the year, when due to the second rain season new soil moisture peaks occur in November and December, with often high peaks in VOD around new year. As can be seen from figure 5.5, often the second dry season is more severe than the first one for VOD, as a result of the longer drought. This is also shown in the climatology for soil moisture and VOD in figure 5.7. The extreme wet start of 2018, with already an annual amount of rainfall during March and April ($\approx 500\text{mm}$) has also resulted in an exceptional peak in VOD. The peak reaches up to a VOD of 0.65, which is 30% higher than previous peaks in 2013 and 2014. This is in contrast to the extreme dry season in 2017, which resulted in very low peaks (< 0.3).

5.3.2. Differences between plots of Justdiggit and reference area

By comparing the difference between each plot and the 10x10km reference area over time, it's possible to detect any trend changes. The results are shown in figure 5.6 for soil moisture, surface temperature and vegetation optical depth. The graph represents spatial averages for each single day, which are smoothed using the Epanechnikov kernel, with again smoothing windows of eight days for soil moisture and surface temperature, and 15 days for vegetation optical depth. The red lines represent the differences between plot B and the reference area, while the blue lines represent the differences between plot D and the reference area.

Although the differences are very small in terms of soil moisture, temperature and VOD (roughly 0.5%, 0.4°C and 0.005 respectively), some things are notable during the AMSR2 period. On average plot B is wetter than the reference area, while plot D is drier. The temperature in both plots is comparable with the reference area and not constantly cooler or hotter. In terms of VOD, the thickness of vegetation is slightly higher in plot D than in plot B, in comparison with the reference area.

Although it was expected that the areas with bunds have higher soil moisture contents and VOD, with lower surface temperatures, we don't see this in the results of the differences in figure 5.6. We would expect a trend change after implementation of the projects in 2016, compared to the outer reference area, but this is not visible in the results yet.

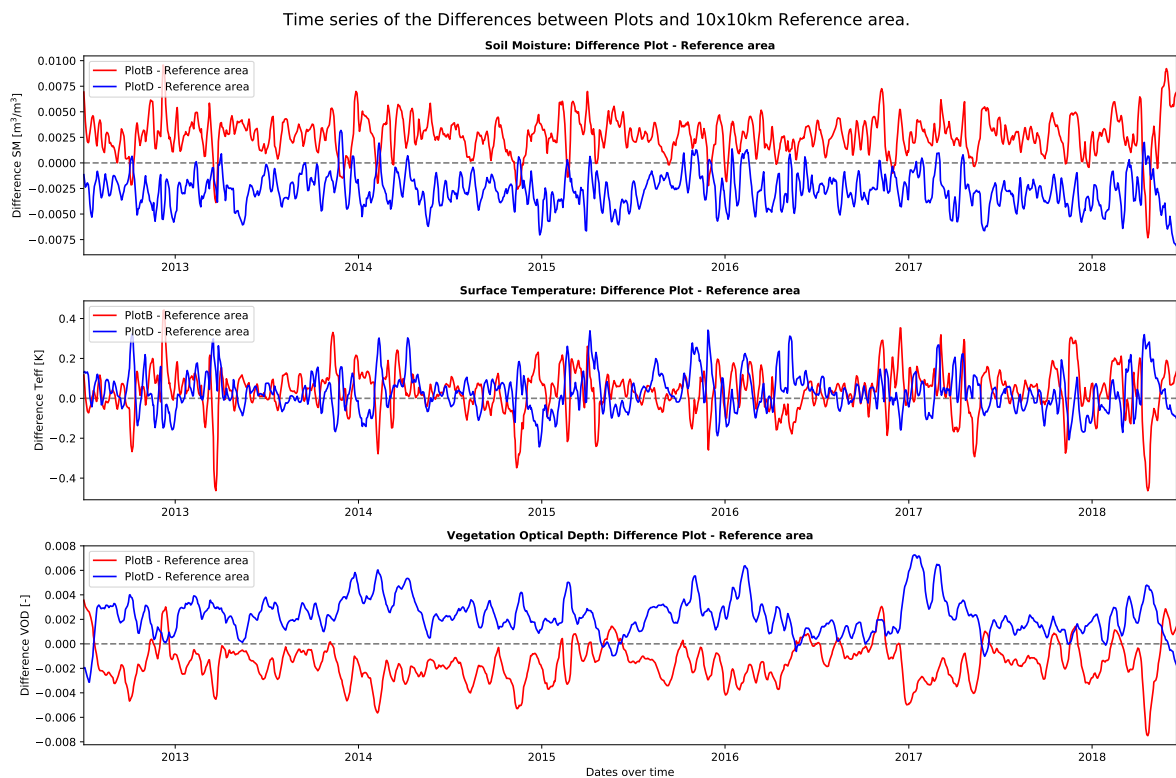


Figure 5.6: Time series of the differences between Plot B (red) and Plot D (blue) with the reference area, for VanderSat Soil Moisture, Surface Temperature and Vegetation Optical Depth data for the AMSR2 time period.

5.3.3. Climatologies and anomalies

Figure 5.7 shows the climatology of soil moisture, surface temperature and vegetation optical depth for the AMSR2 period, for plot B, plot D and the 10x10km reference area. The black line represents the climatology of the reference area, the red line shows the climatology of plot B and the blue line represents plot D.

The climatologies show the same pattern which we've already seen in the time series of figure 5.5. Furthermore, there is no significant difference between the climatologies of plot B, plot D and the reference area. Plot B is often a bit more wet than the reference area and plot D, while there are almost no differences in surface

temperature. In terms of VOD, plot D is slightly higher than plot B. Furthermore, there is a clear distinction between the wet and dry seasons. In periods with no, or limited amount of rainfall, low soil moisture contents are found with lows in VOD, while temperatures are generally highest at the end of the dry seasons. A steady decline in soil moisture and VOD is visible between May and October, as a result of the long dry season. Finally, the highest peaks in soil moisture are generally in December, while for VOD, the highest peaks occur at the end of the first wet season around April and May. This is probably because vegetation has more benefits from a longer wet season, instead of a short rain season, as water has more time to infiltrate into the soil.

Figures 5.8, 5.9 and 5.10 show the anomalies of soil moisture, surface temperature and VOD respectively for the AMSR2 period for all study areas. The blue colors represent positive anomalies, meaning that the soil moisture content or vegetation optical depth is higher at a given day compared to its climatology, while red values represent a negative anomaly, meaning that the soil moisture content or VOD at a given day is lower than its climatology. For temperature it is the other way around, where lower temperature anomalies are blue and higher anomalies are shown as red.

The anomalies look very similar for soil moisture temperature and VOD and there are, again, no significant differences between the plots and the reference area. After implementation of the Justdiggit projects in 2016, we would expect more positive anomalies for soil moisture and VOD in plot B and D during the wet seasons, while more negative anomalies are expected in temperature. Furthermore, if an effect is visible in the plots, this effect would also be visible during the first weeks into the dry season, but this is not the case.

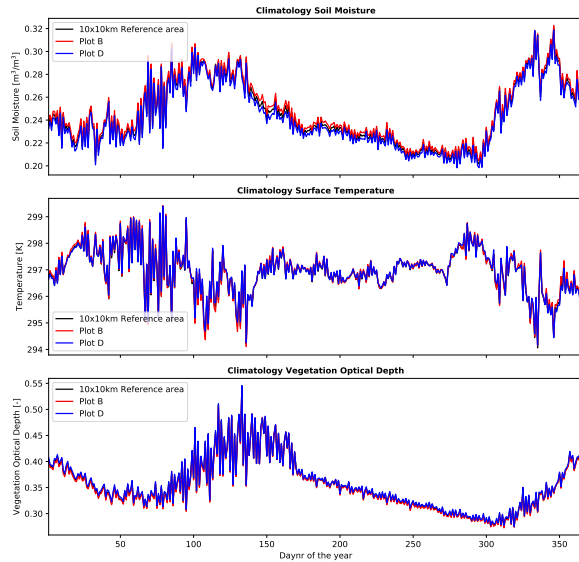


Figure 5.7: Climatology of VanderSat Soil Moisture, Surface Temperature and Vegetation Optical Depth 2012-2018

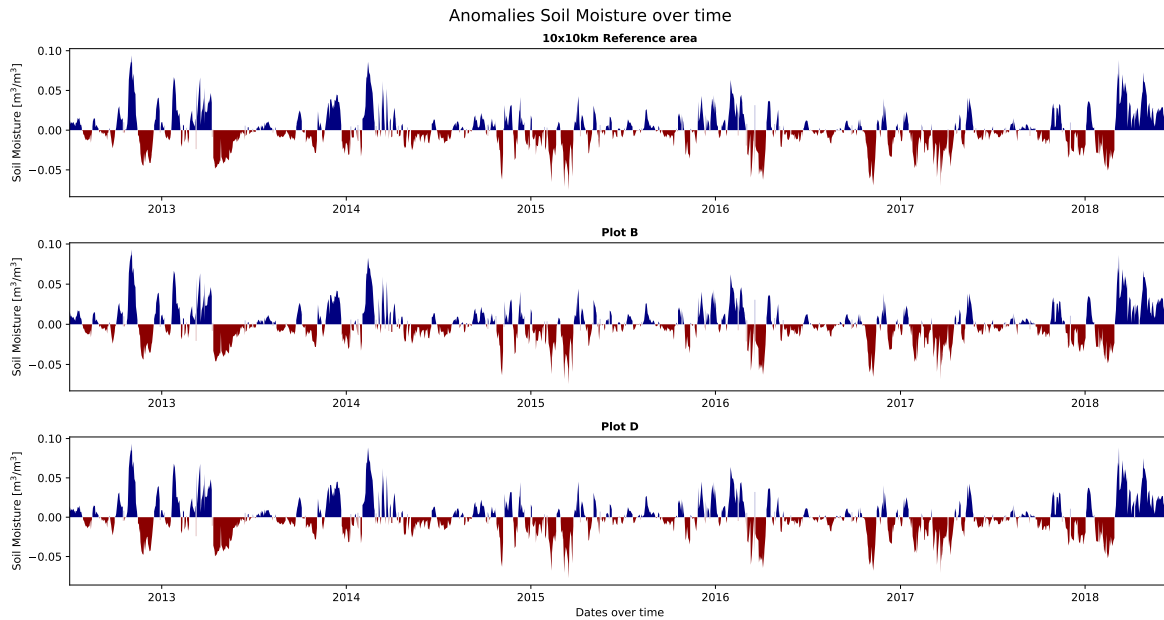


Figure 5.8: Anomalies of VanderSat soil moisture data for AMSR2 period, for all study areas.

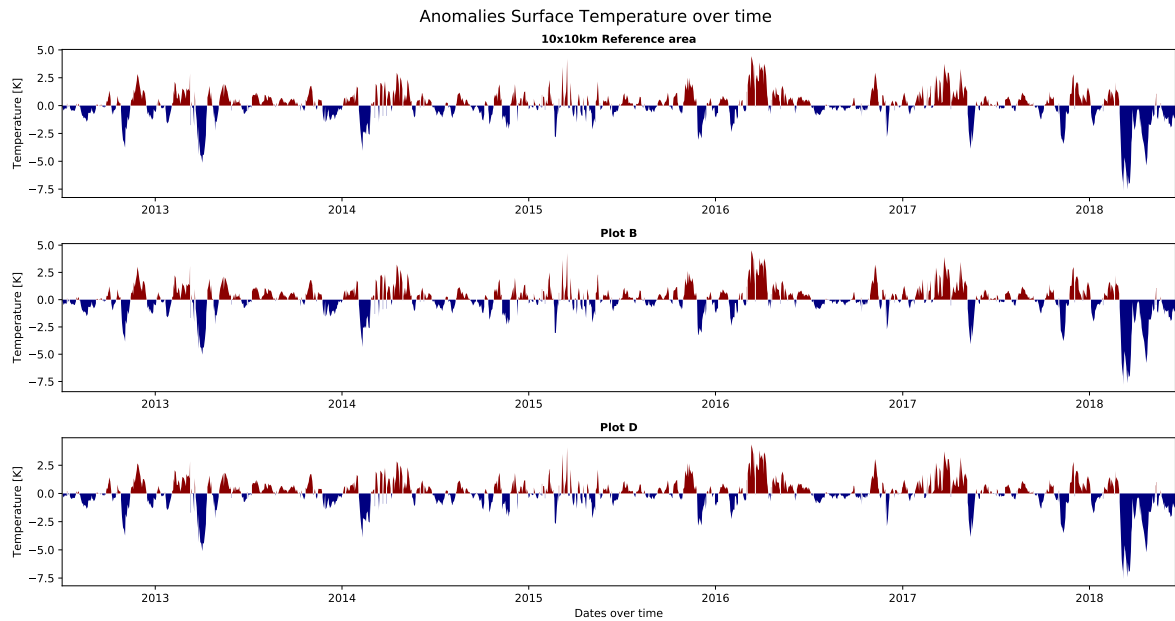


Figure 5.9: Anomalies of VanderSat surface temperature data for AMSR2 period, for all study areas.

Independently of the longer smoothing window that is applied, VOD is more smooth than temperature and soil moisture. This is probably because of the fact that vegetation growth has a time lag in response to precipitation due to the fact that it uses moisture from the deeper layers. The data of the in-situ sensors in figure 5.1 have also shown that the deeper soil layers of undisturbed soil have a time lag, due to infiltration of the water, while the dry down is slower compared to the upper layers. The VOD therefore acts as a 'memory' of the system. Furthermore, this has to do with the fact that vegetation uses moisture from the deeper soil layers, while the radiometers measure the surface layer of the soil only, which is more variable and sensitive to evaporation and small precipitation events. As a result, the wet and dry seasons are visible in the anomalies of vegetation optical depth in figure 5.10. Furthermore, the exceptional dry period in 2017 is very clear and lasts until February 2018, while the big VOD peak in the time series in figure 5.5 follows with a significant anomaly as well.

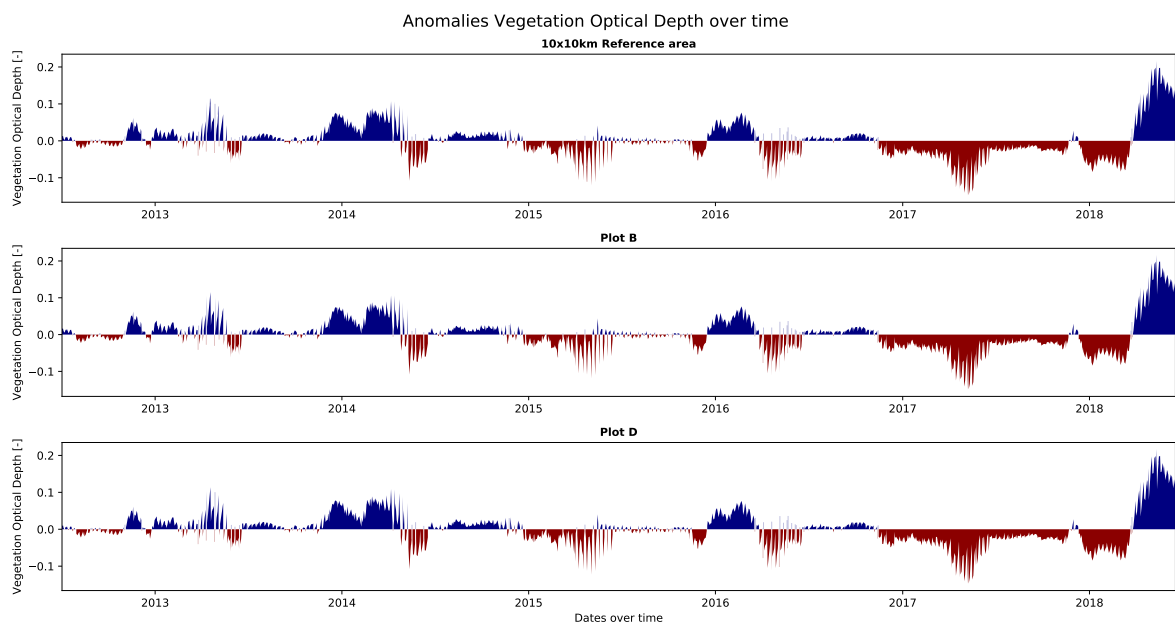


Figure 5.10: Anomalies of VanderSat vegetation optical depth data for AMSR2 period, for all study areas.

5.3.4. Histograms and cumulative distribution functions

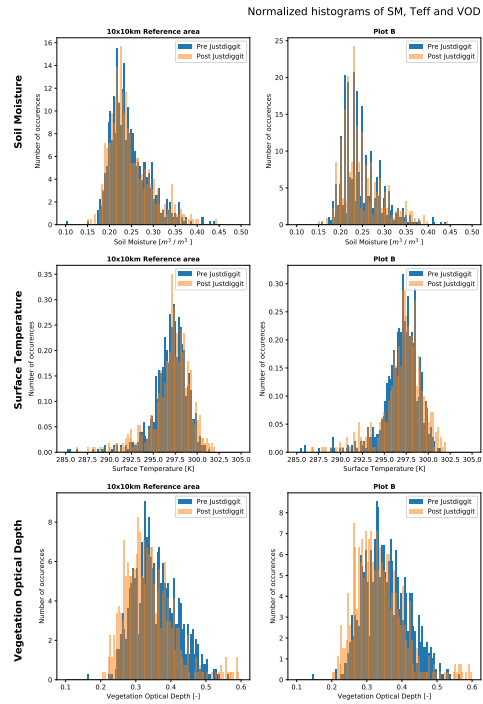


Figure 5.11: Histograms of Normalized data

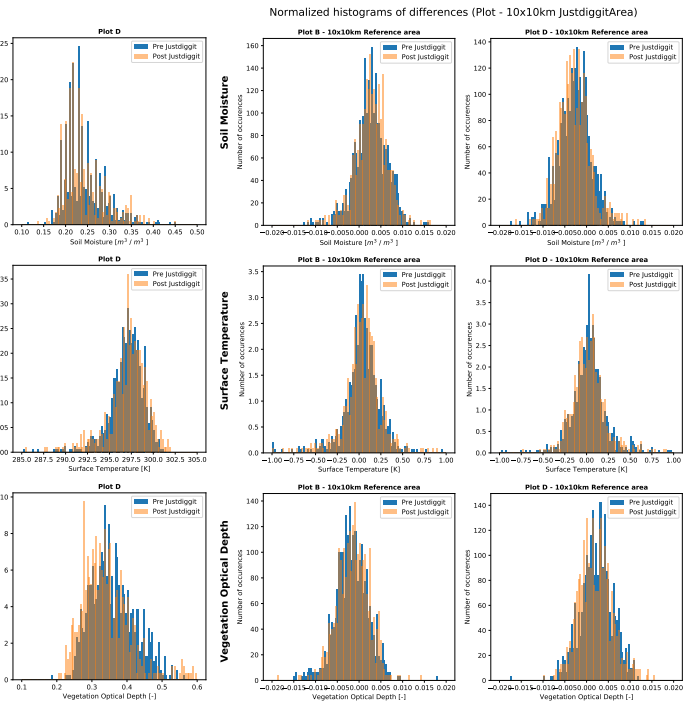


Figure 5.12: Histograms of differences between plots and reference area

In figure 5.11 the normalized histograms of the reference area, plot B and plot D for soil moisture, surface temperature and vegetation optical depth are presented. The blue histograms show the period before the implementation of the water-retaining bunds in 2016, while the orange bars show the results of the period after implementation. Despite the distinction between pre- and post- intervention, both histograms are on top of each other for soil moisture and surface temperature and show no significant differences. For VOD however, the histograms which display the data after intervention show a lower distribution than the histograms that show the data before implementation. This probably has to do with the exceptional dry year in 2017, which covers 30% of the data in the period after implementation in 2016. Furthermore, almost all histograms show similar (normal) distributions for all areas, which are slightly skewed. Besides normalized histograms for each area of interest, normalized histograms of the differences between the plots and the 10x10km reference area are presented in figure 5.12. Again, no differences are present between the period before and after implementation of the Justdiggit projects in 2016. All histograms show similar normal distributions.

Finally, in figure 5.13 the cumulative distribution functions are shown for the period between 2013 and 2017. The years 2012 and 2018 are neglected for the AMSR2 period, as these contain missing data and would show incomplete distributions. For each area, the cumulative distribution functions are shown for soil moisture, surface temperature and vegetation optical depth. In general, the distribution for each of these parameters is quite similar for every area.

In the case of soil moisture, for all years, there roughly is an 80% probability that soil moisture is between 0.2 and $0.3\text{m}^3/\text{m}^3$, with a 50% probability that it is between 0.22 and $0.27\text{m}^3/\text{m}^3$. Most outliers are below 0.17 and above $0.35\text{m}^3/\text{m}^3$ for soil moisture in all years. There is no clear distinction between the plots in terms of the Justdiggit intervention. In accordance to the TRMM data, 2017 turns out to be the driest year in the period of observation, while 2016 is an average year. In terms of surface temperature, the distribution through the years for all areas are similar as well. There is an 80% probability that night surface temperatures are between 295 and 299K , with a 50% probability that the temperatures are between 297 and 298K for all areas. While the distribution of temperature is steeper than that of soil moisture, most outliers are in the lower part of the distribution, with a 5% probability that temperatures are below 292.5K . Although the differences in the

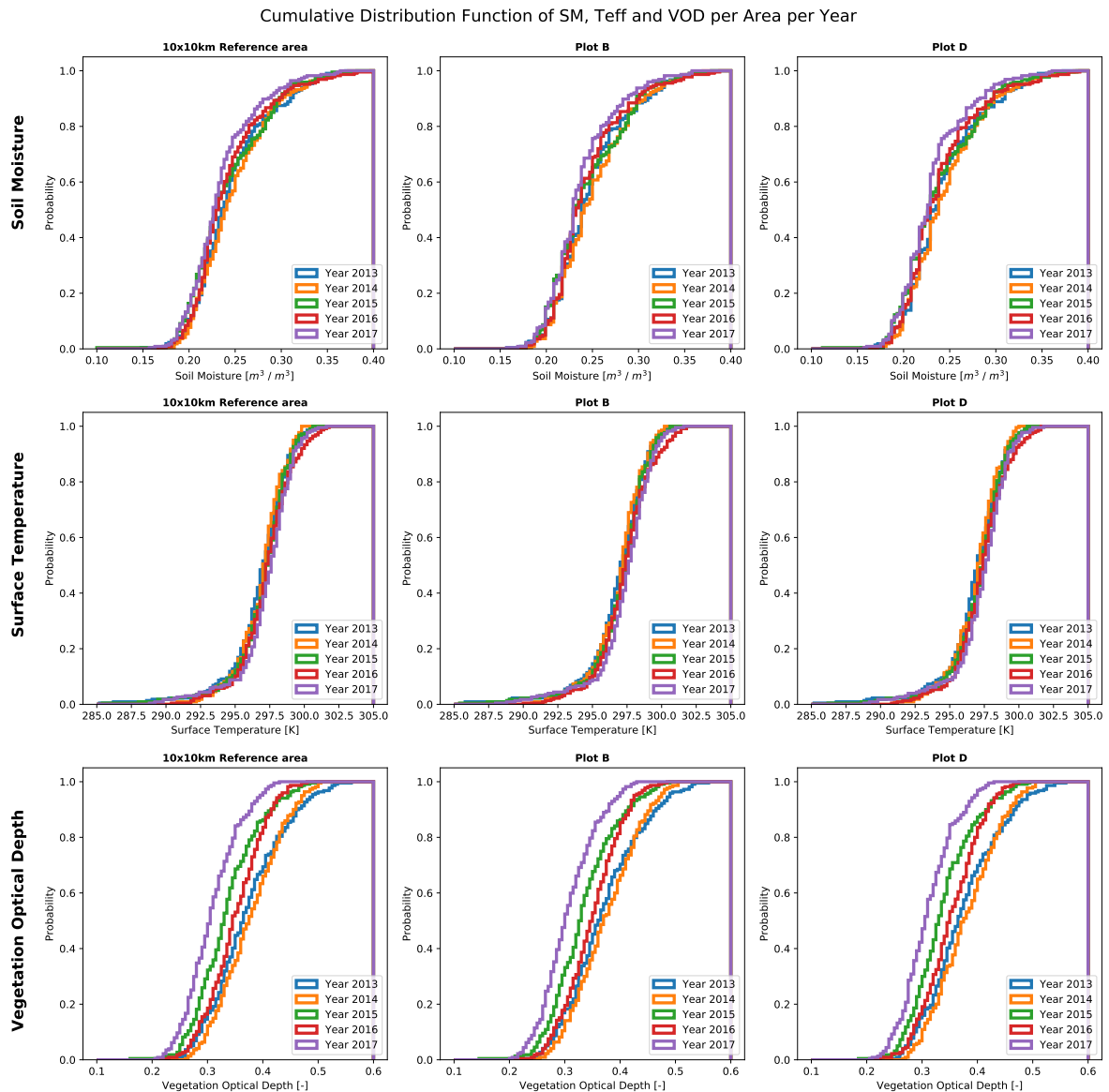


Figure 5.13: Cumulative Distribution Functions of individual years between 2013 and 2017, for soil moisture, temperature and vegetation optical depth.

years are very small, 2016 turns out to have the hottest distribution. The distinction between wet and dry years is, comparable to figure 5.10, clearest for VOD. As turns out, 2017 is the year which was most affected by the drought and shows lowest VOD. The distributions in all three areas are similar, however those of the drier years 2014, 2016 and 2017 show steeper distributions with less outliers to the upper end (VOD > 0.5) of the distribution. On average, there is a 50% probability that the VOD is between 0.3 and 0.4. Despite the fact that NDVI has shown positive results for Sentinel-2, there is no clear difference between the project areas of Justdiggit and the reference area in terms of VOD.

5.3.5. Temporal averages during wet season

In figures 5.14 and 5.15, the temporal averages for soil moisture, surface temperature and vegetation optical depth are presented for the wet season for 2013 until 2018. The wet season is defined as the time period between day 50 (February 20) and 150 (May 31) of each year and therefore covers the long rain season. The color bars are individually set for each spatial map, to provide as much as detail as possible. As a result, the spatial variabilities in the project area are visible, especially in soil moisture and vegetation optical depth. Although these spatial differences are small, the same spatial patterns occur every year. In terms of soil moisture, the differences are in a range of 2% for all years, while the variability in temperature is in the range of 1K and

vegetation optical depth less than 0.02. Furthermore, it seems that the spatial artefacts which were present in the unsmoothed soil moisture, temperature and vegetation optical depth data, are not present any more in the temporally averaged maps, probably due to the small differences which were present in on the artefact edges.

Despite the small spatial variabilities, the soil moisture maps show dry areas in the north-eastern part of the project area every year. Especially the eastern part shows a clear wet area, while also southern and western areas are wet. Taking a look at the Justdiggitt plots, shows that the southern area, plot B, has the same spatial soil moisture pattern every year, while plot D is drier and shows average soil moisture contents compared to the 10x10km reference area. The spatial patterns in soil moisture are probably caused by different soil texture patterns in the soil. Unfortunately, although plot B is for example more wet than the outer area, the project areas of Justdiggitt don't show any significant impact after the start of the interventions in 2016.

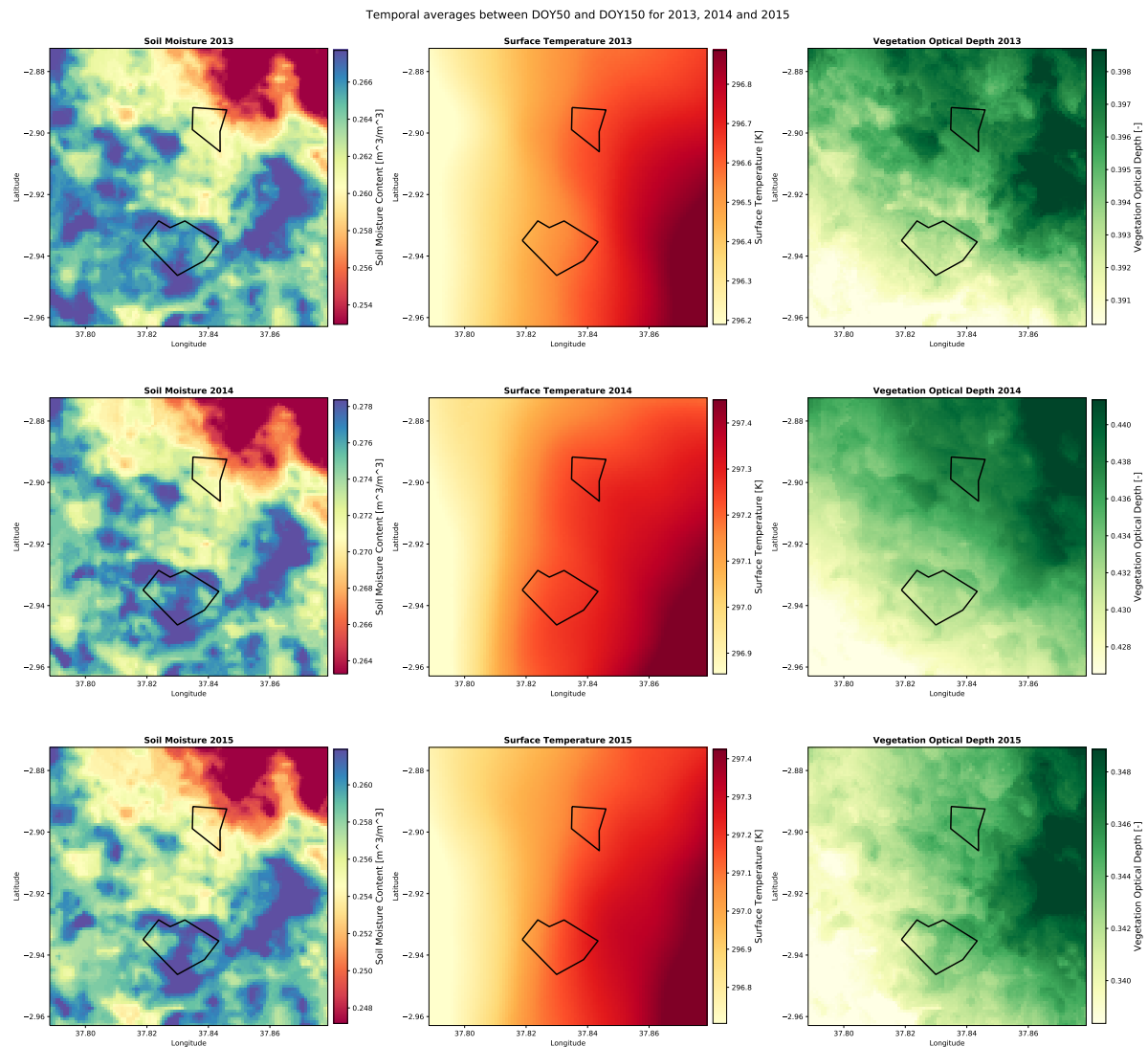


Figure 5.14: Temporal average between DOY50 and DOY150 for years 2013, 2014, 2015

In terms of surface temperature a clear west-east gradient is present in the project area, with highest surface temperatures in the east, while coolest areas are in the west, which seems reasonable with the wetter areas over here. However, this is not in accordance with the wet areas in the east and in plot B. The surface temperature maps clearly show less spatial variability compared to the soil moisture maps, which might have to do with the assumption that surface temperatures are homogeneously distributed over night.

For vegetation optical depth, similar spatial patterns are visible as present in soil moisture. The patterns which are present in plot B are the same spatial (soil texture) patterns which we saw in soil moisture. However, despite the small differences, highest VOD values are in the north-eastern part of the study area, which is consistent with the Sentinel-2 NDVI images from figure A.1 in appendix A and observations during the fieldwork in March due to the fact that a river is flowing through the north-eastern part of the Study area.

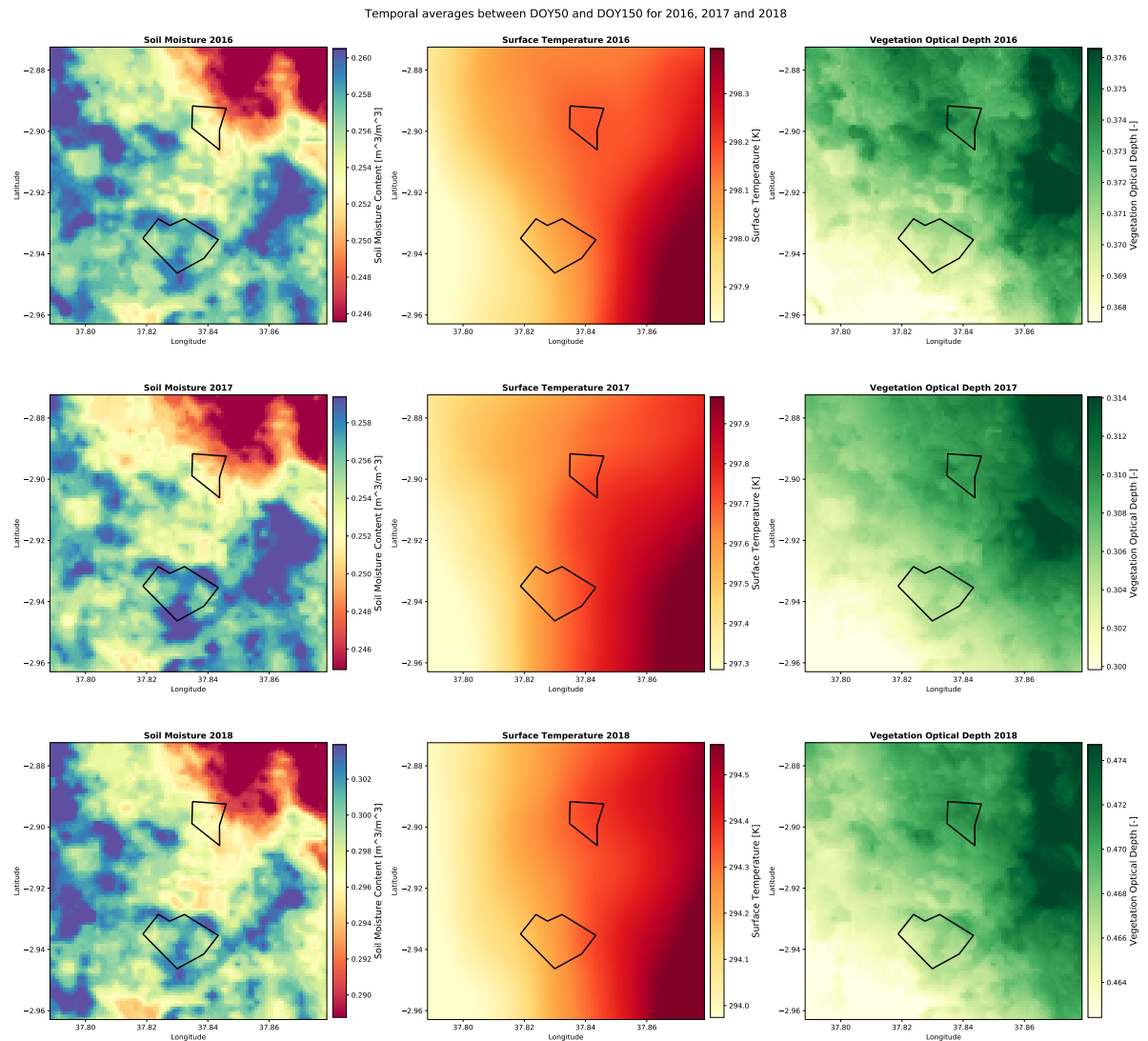


Figure 5.15: Temporal average between DOY50 and DOY150 for years 2016, 2017, 2018

5.3.6. MODIS land surface temperature and NDVI

In figure 5.16 the time series for MODIS land surface temperature for daily and night-time data are presented, together with MODIS NDVI, for plot B, plot D and the 10x10km reference area. Figure 5.17 shows the differences for these parameters between the plots and the reference area, with red the differences between plot B and the reference area, while in blue the differences between plot D and the reference area are plotted.

As can be seen from figure 5.16, the daytime surface temperatures of MODIS show more and larger fluctuations than the night time temperatures. This makes sense, given the fact that the night time temperatures are more stable under night time atmospheric conditions, without influence from the sun. Furthermore, despite the fact that the daytime surface temperatures result in higher temperature gradients over the area (Liu et al., 2018), no significant differences (figure 5.17) are spotted between the Justdigg plots and the reference area. Although, we see that the daytime temperature data shows more and larger variability than the night time temperatures between the project areas.

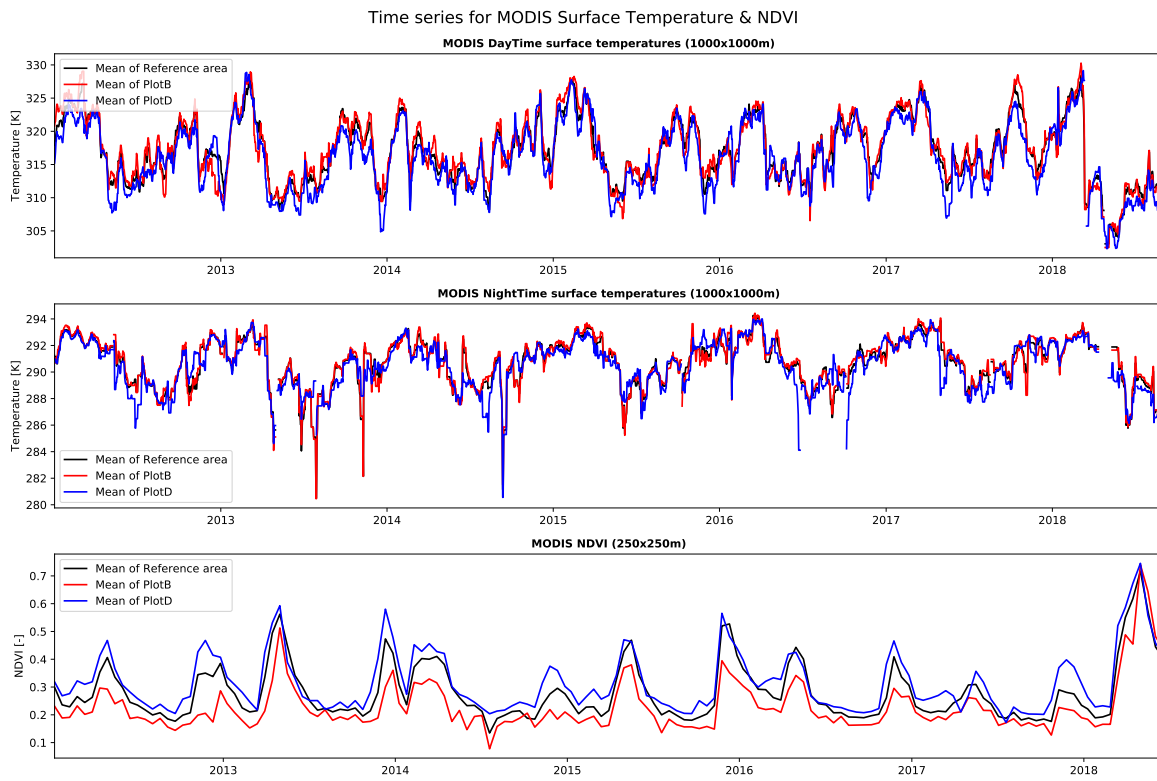


Figure 5.16: Time series of MODIS LST daytime and night-time (1000x1000m) and MODIS NDVI (250x250m)

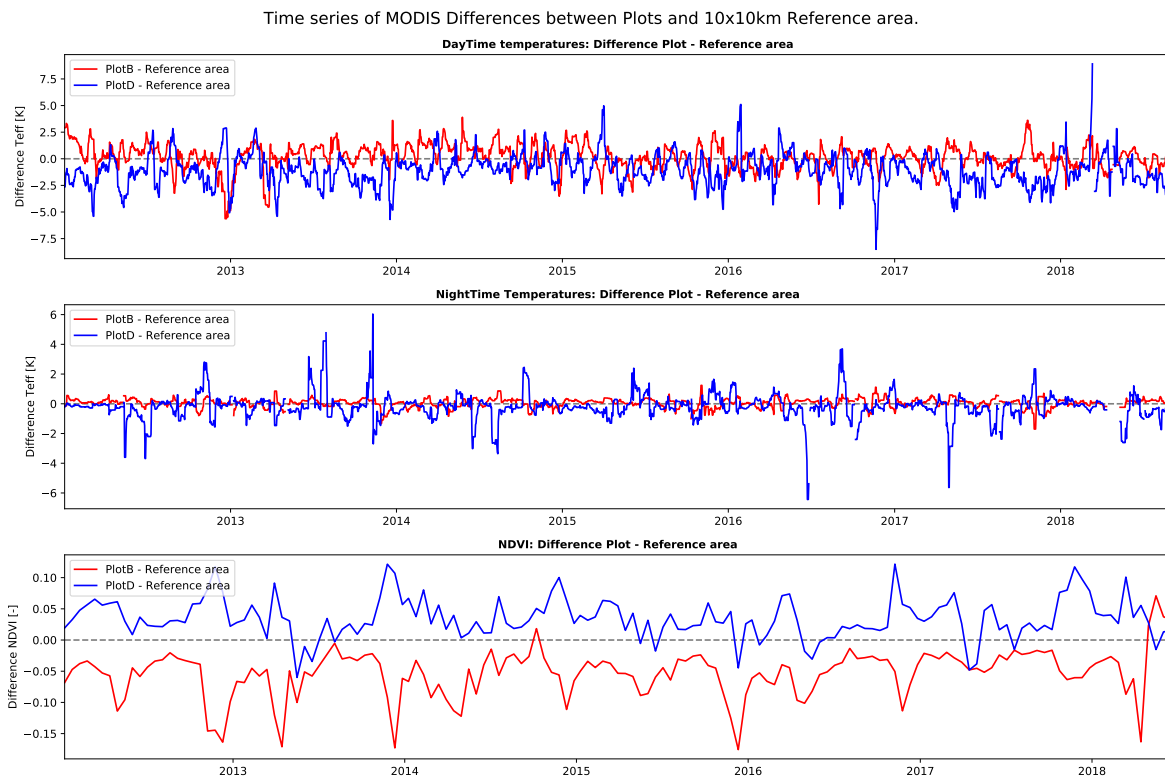


Figure 5.17: Time series the differences between plot B, plot D and the reference Justdigg area of MODIS LST daytime and night-time (1000x1000m) and MODIS NDVI (250x250m)

For NDVI, we see a similar seasonal pattern as the vegetation optical depth time series in figure 5.5. However, due to less frequent data (once every 16 days) the time series for MODIS NDVI are less smooth than those of vegetation optical depth. Often plot D has higher NDVI values than the reference area, while plot B has lower NDVI values than the reference area. This is in accordance with what was found with vegetation optical depth and observations from the Maasai Wilderness Conservation Trust, who described plot B as most degraded compared to its surroundings. Overall, there is no clear change of trend after implementation of the projects in 2016. However, the last observations of MODIS NDVI in June 2018, show increased NDVI values in plot B in comparison to plot D and the reference area. This might be a signal that MODIS NDVI is actually starting to measure the Justdiggitt interventions, as no clear peak in the differences between plot B and the reference area was observed before in the period 2012-2018 (figure 5.17). Figure 5.18 and 5.19 show the spatial maps of MODIS NDVI at the 2nd of June and the 18th of June, which clearly show that plot B contains higher NDVI values than the outer reference area, which is comparable to what we saw in the Sentinel-2 NDVI maps which are presented in Appendix A.

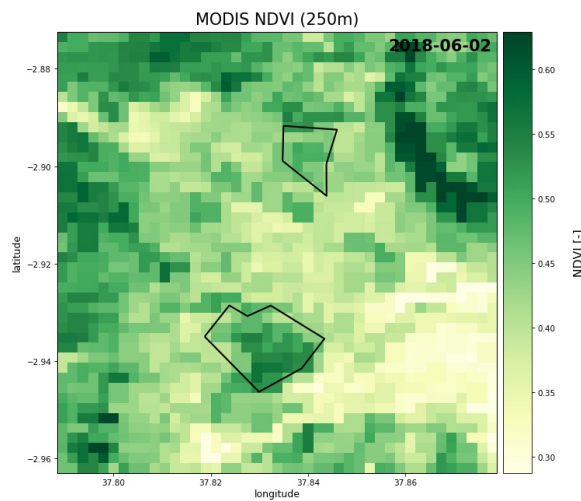


Figure 5.18: MODIS NDVI (250x250m) at June 2, 2018

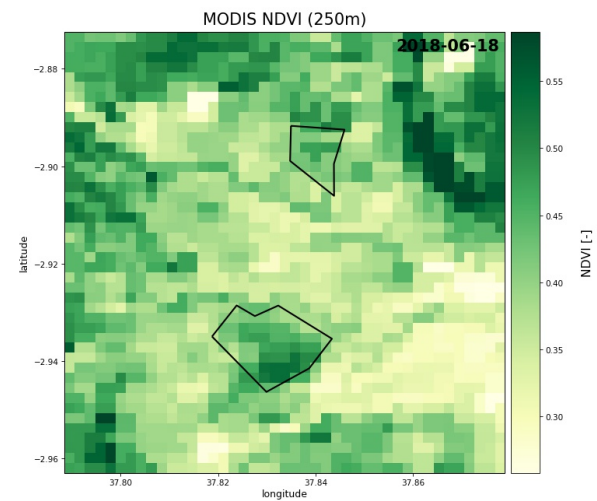


Figure 5.19: MODIS NDVI (250x250m) at June 18, 2018

5.4. Modelling brightness temperatures using tau-omega model

This section discusses the results of the sensitivity analysis of brightness temperature and the modelled signal which is expected from the project areas, using the tau-omega model as described in chapter 3 and section 4.5.1. The results give better understanding of the brightness temperature signal and give more insight in what signal is needed from the project areas.

5.4.1. Sensitivity analysis of brightness temperature

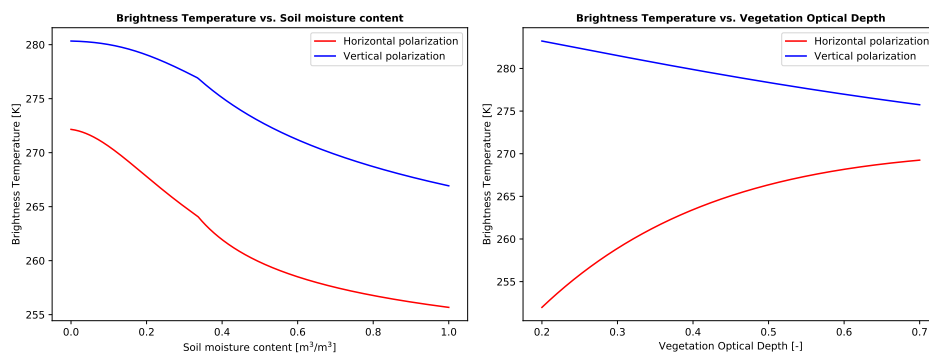


Figure 5.20: Brightness temperature sensitivity to increasing soil moisture content and vegetation optical depth.

Figure 5.20 shows a sensitivity analysis of brightness temperature to soil moisture content and vegetation optical depth. When varying soil moisture between 0 and $1 \text{ m}^3/\text{m}^3$, a fixed VOD of $\tau=0.5$ is used. While, when varying VOD between 0.2 and 0.7, a fixed soil moisture content of $\theta=0.25 \text{ m}^3/\text{m}^3$ is used. The results in figure 5.20 show that the horizontal polarized brightness temperature is more sensitive to changes in soil moisture and vegetation than the vertical polarization, which is comparable to the results of Owe et al. (2001) for emissivity. The reason that the horizontal polarized brightness temperature is increasing with increased vegetation optical depth, can be explained from the fact that, as vegetation density is increasing, the radiation from the canopy increases as well, which is assumed by the tau-omega model (chapter 3). However, as the vegetation density increases, the vertical polarized brightness temperature decreases, which is more sensitive to surface temperatures than the horizontal polarization (Holmes et al., 2008).

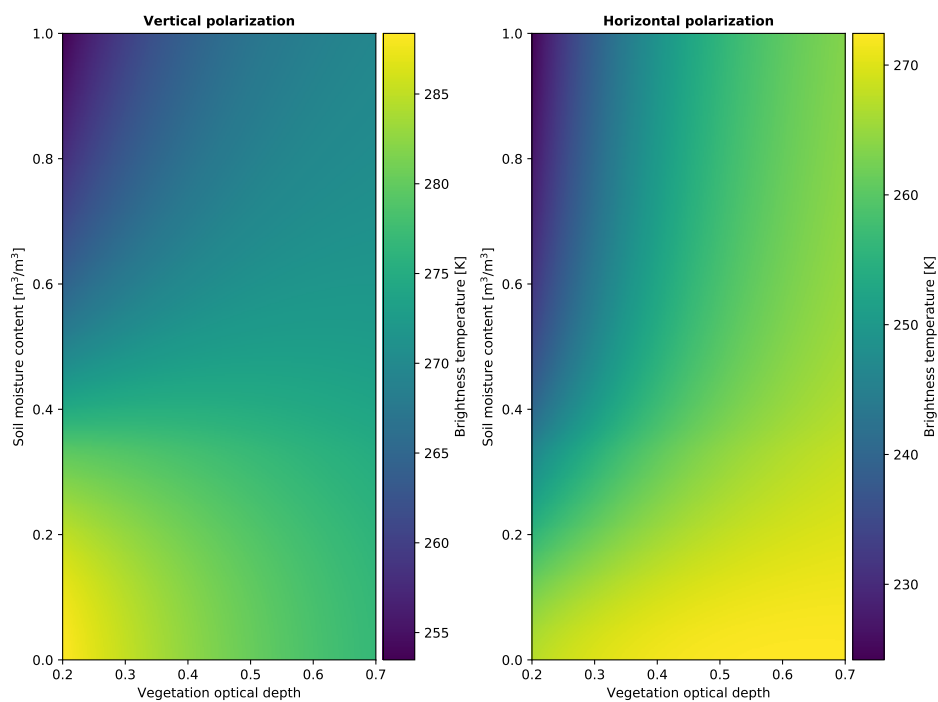


Figure 5.21: Brightness temperature (horizontal and vertical polarization) sensitivity to soil moisture content and vegetation optical depth.

In figure 5.21, the horizontal and vertical polarized brightness temperatures are presented for varying soil moisture content ($0-1 \text{ m}^3/\text{m}^3$) and vegetation optical depth ($0.2-0.7$). As can be seen from both vertical and horizontal polarization, the brightness temperature decreases for increasing soil moisture content. For a soil moisture content of $0-0.3 \text{ m}^3/\text{m}^3$, the vertical polarized brightness temperature decreases with increasing VOD, while for higher soil moisture contents, the brightness temperature increases with increasing VOD, at vertical polarization, which is because the wet soil is masked by the overlying canopy. At horizontal polarization, the brightness temperature increases with increasing VOD, which is due to the increasing radiation from canopy. Furthermore, the horizontal polarization is more sensitive to increasing VOD but saturates for soil moisture contents below $0.2 \text{ m}^3/\text{m}^3$. Meanwhile, the brightness temperature at vertical polarization saturates for an optical depth of roughly 0.5.

5.4.2. Brightness temperature signal from bunds

The results of scenario 1, in figure 5.22, show that from the reference situation without bunds, roughly 20% of the bare land ($\tau=0.2$) needs to be covered by bunds ($\tau=0.5$), to have a brightness temperature difference of at least 1K, to overcome the AMSR-2 accuracy. In the current situation, roughly 10% of the area is covered by bunds, which therefore explains why no significant differences were found in terms of passive microwave remote sensing products. From the current situation, the amount of bunds therefore needs to be doubled, or vegetation of larger density/water content ($\tau=1.0$) should develop inside the bunds over time, for example similar to evergreen broad-leaf forest (Konings et al., 2017).

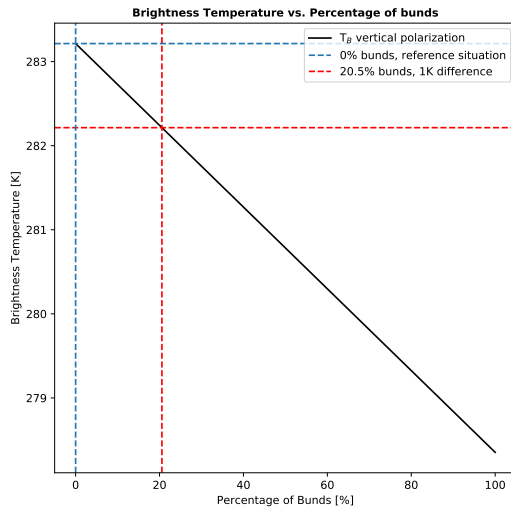


Figure 5.22: Results of Scenario 1: Vertical polarized brightness temperature decreases with increasing percentage of bunds.

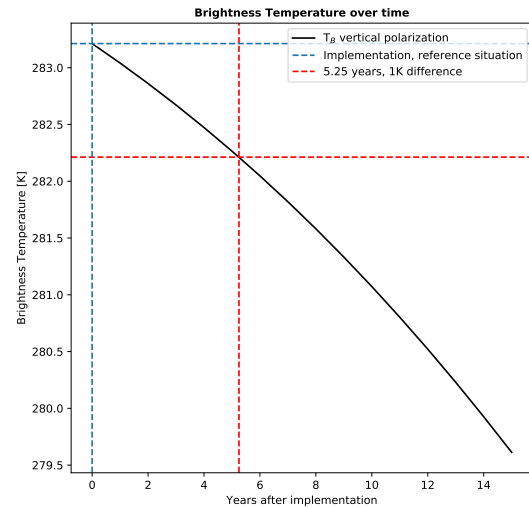


Figure 5.23: Results of Scenario 2: Vertical polarized brightness temperature decreases over time.

Furthermore, the results of scenario 2, presented in figure 5.23, have shown that the project areas are developing over time and need at least five years and three months after implementation before a difference of 1K in brightness temperature is measured. This scenario takes into account that both the area with and without bunds are becoming more vegetated over time. Figure 5.24 shows how the vegetation optical depth of the project area for scenario 2 increases over time, as a result of increasing VOD values inside and outside the bunds, which after 15 years correspond to woody savanna and closed shrubland respectively (Konings et al., 2017). Finally, besides the development of vegetation, this scenario also assumes that the effect of the bunds increases due to the development of vegetation from inside the bunds to the area outside the bunds. Therefore, an expand (10% per year) of the area of bunds is taken into account, as shown in figure 5.24.

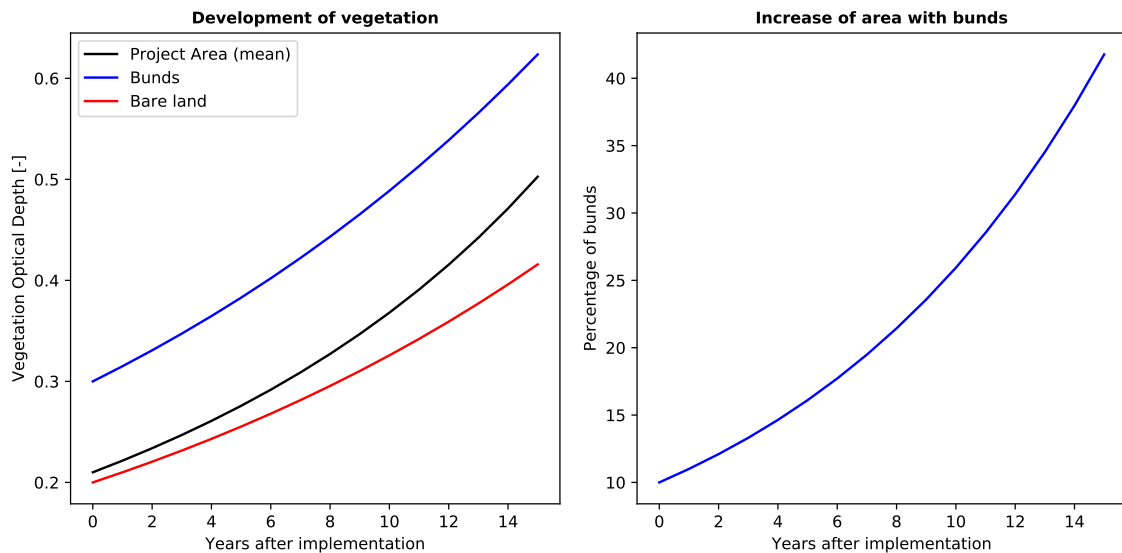


Figure 5.24: Development of vegetation (increasing VOD) and increased area with bunds over time.

5.5. Synthesis

The measurements of the in-situ sensors inside and outside the bunds have shown that soil in the water-retaining bunds is significantly more wet than the soil outside the bunds. The effect of the bunds turned out to be most significant for the deepest soil layers, with differences of up to 35% for the sensors at 40cm depth. Besides higher soil moisture content inside the bund, also a time lag occurred between the dry down inside and outside the bund, where the sensors inside the bund started drying down roughly a month after the sensors outside. Again, the effect is most significant on the deepest layers, where the sensor at 40cm depth even measured a double amount of soil moisture in August 2018, three months after the end of the rain season. However, the sensors in the surface layer have shown a rapid dry down both inside and outside, except for the 5TM sensor inside the bund (figure 5.1, panel C).

The difference between the 5TM and EC5 sensor inside the bund can possibly be explained by the large spatial variability in the soil. But, this alone seems unlikely given the fact that the 5TM and EC5 sensor inside the bund were installed only 10cm apart, while the bunds during the fieldwork in March have shown to be filled with water after precipitation events (figure 2.1). Therefore this could also be due to a measurement error in one of the sensors. Additional calibration of the sensors and a longer measurement period are advised for future research. This is also to make sure that soil moisture information before the first rains is captured and infiltration of moisture is measured along the rootzone.

Although the downscaled passive microwave soil moisture, surface temperature and vegetation optical depth (VOD) products, based on the Land Parameter Retrieval Model (LPRM), have shown to be consistent (figure 5.5), accurate (de Jeu et al., 2008, 2014; Liu et al., 2018, 2012; Owe et al., 2001, 2008; van der Schalie et al., 2015), and have shown good correlation with a cosmic-ray in-situ network in Kenya (Appendix B), the cross-validation with the MODIS temperature and NDVI products and especially the in-situ stations have shown low correlations. The latter can be explained based on the fact that point measurements (in-situ) were compared with area averaged data (remote sensing). As a result of the large variability in soil moisture and surface temperature in space, it is difficult to relate point measurements to remote sensing observations (Western and Blöschl, 1999). The results in figure 5.1 have for example already shown large differences between the sensors inside and outside the bund, which are only 3 meters apart.

Furthermore, the low correlations between the downscaled soil moisture and surface temperature products and the in-situ stations can be explained based on the short overlapping period between both datasets. As the in-situ sensors were installed on March 23, 2018, while the dataset of VanderSat was calculated until the 19th of June, there were only 88 days to validate the VanderSat data. And, as the VanderSat data was available roughly every 2 out of 3 days due to the location of the projects close to the equator, this left in this case only 56 days to validate. In addition, right now only the dry down after the first wet season was validated, while a measurement period of a full year is needed to do a proper validation based on in-situ data. This is also the reason why for example the MODIS temperature products have higher correlations due to the longer measurement period, where the night-time observations consequently have the highest correlation. Finally, the cross-validation between NDVI and VOD has shown that both vegetation parameters are related, despite different aspects of vegetation were measured. As a result, MODIS and Sentinel-2 performed similar in comparison to vegetation optical depth.

The analysis of the downscaled soil moisture, temperature and vegetation optical depth data has shown that the Justdigg project cannot be measured yet based on passive microwave remote sensing and the downscaling method of VanderSat. No significant differences between plots B, plot D and the reference Justdigg area were present, while also the climatologies, anomalies, histograms, cumulative distribution functions and the temporally averaged spatial maps have shown no results. This is contrary to what is observed from the in-situ observations, Sentinel-2 NDVI images and fieldwork photos which have shown clear impact from the bunds. As Sentinel-2 NDVI at 10x10m resolution has shown a clear contrast between the project sites and the reference areas and also MODIS NDVI at 250x250m resolution has shown promising results at the start of the dry season, this shows that the fact that we don't see the impact in the 100x100m resolution passive microwave products is a resolution problem alone. Although, the effect of MODIS NDVI was mainly visible at the beginning of the dry season in 2018, as shown in figures 5.18 and 5.19.

Looking at the downscaling method, the processed soil moisture and VOD are based on C-band microwaves, which at 3dB intensity, result in large footprints with resolutions of 62x35km for AMSR2. As, due to the low intensity of passive microwaves, a large field of view is required to obtain enough energy by the radiometer. These large resolutions result in multiple overlapping footprints at the geographical area of interest, which improves the downscaled product (de Jeu et al., 2017). However, this might also result in the fact that the project area is sometimes only covered by the footprint's edges, which contribute less to the brightness temperature signal than the center, based on the assumption of a Gaussian distribution inside the footprints. This, in addition to the already low intensity of the passive microwave signal, might result in the fact that the interventions of the Justdigg project are not present in the soil moisture, temperature and vegetation optical depth products of VanderSat.

Besides the low intensity radiation of passive microwaves (Parinussa et al., 2013; Santi, 2010) and the multiple overlapping satellite footprints, also the temperature artefacts which were presented in figure 4.4, might be an explanation for the fact that the impact of the interventions of Justdigg is not present in the data. The artefacts are the result from the Ka-band frequency (36.5GHz), with a footprint resolution of 12x7km for AMSR2 approximately. As these footprints are too small to overlap with each other, they result in a grid pattern in north-west to south-east direction. Furthermore, these temperature artefacts are also present in the soil moisture and VOD data and resulted in homogeneous distributions for soil moisture, temperature and VOD inside the artefacts. And, as these artefacts only have small differences near the edges, the spatial variability of the resulting soil moisture, temperature and VOD products is low. Although smoothing has resulted in higher spatial variability around the project areas (figure D.4, D.5 and D.6), the spatial differences are small.

Independently of the passive microwave signal, in terms of soil moisture it makes sense that the impact of the Justdigg project is not directly measured, as soil moisture is very variable, especially in the surface layer of the soil. This is due to the diurnal pattern (evaporation and condensation during day and night respectively) and the fact that soil moisture in the surface layer of the soil evaporates quickly after rainfall, especially in a semi-arid and hot climate such as in Kenya (Njoku and Entekhabi, 1996). This results in only small differences in soil moisture between the surface soil layers inside and outside the bunds. This was also confirmed by the in-situ stations which showed that the effect of the bunds is largest at the deeper soil layers.

In addition, as C-band frequency is used for the soil moisture observations, the penetration depth from the soil is small, which also limits the possibility of measuring an effect of the bunds in the surface soil layer. Furthermore, it could also be at this frequency that the signal is saturated by overlaying vegetation. By using L-band instead of C-band, the signal sensing depth is increased, which probably results in a better soil moisture signal (de Jeu et al., 2014). As microwave remote sensing has a lot of potential, because it can directly obtain and quantify soil moisture, temperature and VOD (Owe et al., 2001), it is recommended to also investigate L-band measurements. However, we have to take into account that using L-band results in larger satellite footprints, which could further reduce the signal strength of the low intensity microwave radiation.

In terms of surface temperature, the fact that no differences were measured between the project areas and the reference area, could have been because the temperatures were derived from the descending night time overpasses from the AMSR2 device. As a result, the temperature gradients are smaller over night (Holmes et al., 2008; Liu et al., 2018) and therefore caused smaller differences between the project areas. As daytime surface temperatures were not processed for this research, a comparison was done with MODIS temperatures from both day- and night-time. Despite the clear contrast in NDVI between the project areas, also the day-time product of MODIS has not shown any effect from the project areas of Justdigg.

Although NDVI has shown a clear contrast between the areas with and without bunds (which indicates larger vegetation cover and more greenness inside the project areas), no difference is present in terms of vegetation optical depth. It could be that the vegetation cover inside the areas with bunds was larger than outside the project areas, but that the difference in vegetation density was not significant enough to affect the emissivity of the microwave signal. As NDVI is mainly affected by the plant structure and photosynthetic cells inside leaves and it mainly measures the surface instead of seeing through the leaves (as NDVI uses optical remote sensing instead of microwaves), it is more sensitive to vegetation cover than vegetation density. VOD however, is linearly related to the vegetation density and water content at frequencies below 10GHz (Owe et al., 2001).

As the projects of JustdiggIt are only running for three years, mainly grasses and small types of vegetation are found inside the bunds. As a result, inside the areas with bunds we therefore find a larger grass vegetation cover compared to outside the bunds (and these areas are therefore more green). However, the vegetation density (and therefore also vegetation water content) between the project area and reference area is not significantly different. So, despite the larger leaf cover inside the bunds, the emissivity was probably not significantly different between inside and outside. This explains why vegetation optical depth shows no clear contrast between the project areas and reference area, like NDVI.

Finally, the microwave signal from the bunds was modelled using the tau-omega model, to model the signal from the project areas and to confirm if the emissivity of the bunds is indeed (still) too low. The results in section 5.4 have shown that it is reasonable that we don't see any significant differences yet between the project areas and the reference area, as at least 20% of the area should be covered by bunds as shown in figure 5.22, while in the current situation roughly only 10% of the area is covered by bunds. Furthermore, the second scenario (figure 5.23), has also shown that the effect of the bunds is increasing over time, as vegetation in the project area develops. It is therefore still too early after implementation, to measure a significant difference in terms of brightness temperature from the project areas. However, the results of the model need to be further improved by for example calibrating and comparing the model with downscaled brightness temperatures.

6

Conclusions and recommendations

This chapter answers the research questions that were defined in the Introduction and will give recommendations for future research. The main research question is answered using four sub-questions:

1. *What is the hydrological effect of the bunds on a small scale?*

Observations of the in-situ sensors installed at plot D have shown significant increases of soil moisture content inside the bunds compared to outside, at all measurement depths (5, 10, 20 and 40cm) along the root-zone. The effect turned out to be most significant at the deeper layers. Besides higher moisture contents inside the bund right after rain events, the dry down of the soil inside the bund showed a time lag compared to the soil outside the bund. As a result, the soil moisture content measured inside the bund at 40cm depth, was twice as high compared to outside, even three months after the end of the rain season.

2. *For cross-validation; How do the downscaled passive microwave products relate to measurements of the in-situ stations and alternative optical and thermal remote sensing products?*

The cross-validation between the downscaled passive microwave soil moisture, surface temperature and vegetation optical depth (VOD) and measurements of the in-situ stations and optical and thermal remote sensing, have shown low correlations in general. The in-situ sensors measuring soil moisture had higher correlations with the passive microwave soil moisture product (*Spearman* $\rho \approx 0.5$) than the sensors measuring surface temperature with the passive microwave surface temperature product (*Spearman* $\rho \approx 0.2$). However, by comparing point measurements with spatially averaged data, errors were introduced. Furthermore, low correlations were caused as a result of the short measurement period of the in-situ stations. Comparing the downscaled surface temperatures to thermal derived temperatures from MODIS (between 2012-2018) have shown higher correlations for night-time (*Spearman* $\rho = 0.62$) than daytime (*Spearman* $\rho = 0.37$), which is reasonable given that the downscaled passive microwave surface temperature product is derived during night-time (1:30). A cross-comparison between the downscaled VOD product and NDVI, has shown similar correlations (*Spearman* $\rho \approx 0.45$) for MODIS and Sentinel-2. However, as VOD and NDVI represent different parameters of vegetation (thickness/water content and greenness/healthiness respectively), this should be taken into account.

3. *What is the difference between the project areas with bunds and the reference area, in terms of soil moisture, surface temperature and vegetation optical depth, based on downscaled passive microwave remote sensing?*

The downscaled passive microwave soil moisture, surface temperature and vegetation optical depth products were analysed by comparing the project areas (plot B and D) of Justdiggitt with the 10x10km reference area. The analyses of differences between the time series, climatologies, anomalies, histograms, cumulative distribution functions and temporal averaging have not shown any significant differences between the project areas and the reference area. However, the datasets have shown to be very consistent over time and have shown high correlations with an in-situ cosmic-ray network in Kenya. The fact that no differences are measured by the downscaled passive microwave products, is caused by a combination of a too low intensity of the microwave signal (resulting in large 'field-of-view' satellite footprints, which represent a regional signal instead of the 100x100m resolution) and temperature artefacts which are present in the data and caused by the

downscaling method (at Ka-band frequency). Furthermore, the soil moisture product was derived from C-band, which has limited penetration sensing depth into the soil and saturates over dense vegetation cover. In addition, the land surface temperature product was derived during night-time, where using a daytime product would have resulted in larger spatial temperature gradients, which possibly would have shown the effect of the bunds in the project areas. However, an analysis done with MODIS thermal land surface temperatures, has not shown any effect during daytime as well. As NDVI from MODIS and Sentinel-2 has shown a clear contrast between the project areas, it can be concluded that the project areas did have a larger vegetation cover and were more green compared to the reference area. However, VOD was not significantly different as a result of the fact that the difference in vegetation water content was not significantly different and therefore didn't affect the microwave emissivity sufficiently.

4. *By modelling raw brightness temperatures; what signal is needed to measure a significant difference with the passive microwave remote sensing products?*

The modelling approach using the Tau-Omega model has also shown that the effect of the project areas after implementation in 2016, was not significant enough yet in terms of emissivity. The analysis has shown that the percentage of bunds in the current situation ($\approx 10\%$) is too low, as roughly a double amount of bunds ($\approx 20\%$) is needed to measure a significant difference in brightness temperature to overcome the 1K accuracy of the AMSR-2 device. When taking into account the development of vegetation in the project areas over time, the modelling approach has shown that it should be possible to measure the effect of the bunds roughly five years after implementation of the projects.

Finally, the main research question in this thesis was defined as following:

Can the impact of land restoration projects using water-retaining semi-circular bunds in Kenya, be monitored in terms of soil moisture, surface temperature and vegetation optical depth, after implementation of the projects in 2016, based on downscaled (100x100m) passive microwave remote sensing products?

It can be concluded that the land restoration projects of Justdiggit, using semi-circular bunds, definitely work, as shown by fieldwork observations, the in-situ stations and Sentinel-2 and MODIS NDVI, but it is not possible (yet) to monitor the projects using downscaled passive microwave obtained soil moisture, surface temperature and vegetation optical products from remote sensing. Although the passive microwave signal has proven to be consistent and accurate and has shown great potential for drought monitoring due to the direct relations with soil moisture, temperature and vegetation thickness/water content, the impact of the projects of Justdiggit is still too small in terms of passive microwave emissivity to be measured.

For future research it's recommended to further investigate whether passive microwave observations can be combined with active microwave remote sensing measurements to improve the high resolution brightness temperatures from the downscaling method. As radar has its own source of energy, active microwave remote sensing requires smaller satellite footprints to receive the same amount of energy, which thus results in higher resolutions than passive microwave remote sensing. Furthermore, a combination of radar and radiometers may have more potential than developing fine-resolution radiometers (Ulaby et al., 1981).

Furthermore, it is recommended to use ascending brightness temperature observations to derive daytime surface temperatures. During daytime, spatial surface temperature gradients are larger than during night-time (Holmes et al., 2008; Liu et al., 2018). When the land restoration projects of Justdiggit are implemented for a longer time, a difference in surface temperature will therefore be measured by the daytime product first. In terms of validation, it is recommended to do another comparison between the in-situ stations and remote sensing data when data of a longer measurement period is available. Furthermore, it is advised to reinstall the soil moisture stations that are currently installed at the office of Maasai Wilderness Conservation Trust, at the project sites as well. Due to bad weather conditions during the fieldwork in March this was not possible. Finally, for Justdiggit, besides monitoring vegetation growth using NDVI, monitoring soil moisture using a Cosmic-ray soil moisture observing system is a good alternative for satellite remote sensing. Cosmic-ray works on the principle that neutron intensity is inversely correlated with the hydrogen content of the surrounding hectometres of air and the top decimetres of the soil (Andreasen et al., 2017; Zreda, 2016). The technique is therefore a very good alternative to monitor soil moisture content in their project areas.

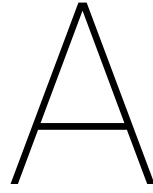
Bibliography

- W. R. L. Anderegg, J. W. Prall, J. Harold, and S. H. Schneider. Expert credibility in climate change. *Proceedings of the National Academy of Sciences*, page 201003187, June 2010. ISSN 0027-8424, 1091-6490. doi: 10.1073/pnas.1003187107. URL <http://www.pnas.org/content/early/2010/06/04/1003187107>.
- Mie Andreassen, Karsten H. Jensen, Darin Desilets, Marek Zreda, Heye R. Bogena, and Majken C. Looms. Cosmic-ray neutron transport at a forest field site: the sensitivity to various environmental conditions with focus on biomass and canopy interception. *Hydrology and Earth System Sciences*, 21(4):1875–1894, April 2017. ISSN 1607-7938. doi: 10.5194/hess-21-1875-2017. URL <https://www.hydrol-earth-syst-sci.net/21/1875/2017/>.
- W. Critchley and K. Siegert. Water Harvesting - A manual for the design and construction of water harvesting schemes for plant production. FAO Paper AGL/MISC/17/91, FAO, Rome, 1991. URL https://www.samsamwater.com/library/Water_harvesting_-_Critchley.pdf.
- R. A. M. de Jeu and A. H. A. de Nijs. Evaluatie van hoge resolutie satelliet bodemvochtproducten met behulp van grondwaterstandmetingen. *Stromingen*, 2017(2):12, 2017. URL https://www.nhv.nu/uploads/fileservice/stromingen/attachment/3590_3605.pdf.
- R. A. M. de Jeu, W. Wagner, T. R. H. Holmes, A. J. Dolman, N. C. van de Giesen, and J. Friesen. Global Soil Moisture Patterns Observed by Space Borne Microwave Radiometers and Scatterometers. *Surveys in Geophysics*, 29(4):399–420, October 2008. ISSN 1573-0956. doi: 10.1007/s10712-008-9044-0. URL <https://doi.org/10.1007/s10712-008-9044-0>.
- R. A. M. de Jeu, Holmes Holmes, T. R. H., Parinussa Parinussa, R. M., and M. Owe. A spatially coherent global soil moisture product with improved temporal resolution. *Journal of Hydrology*, 516:284–296, August 2014. ISSN 0022-1694. doi: 10.1016/j.jhydrol.2014.02.015. URL <http://www.sciencedirect.com/science/article/pii/S0022169414001139>.
- R. A. M. de Jeu, A. H. A. de Nijs, and M. H. W. van Klink. Method and system for improving the resolution of sensor data (Patent). *World Intellectual Property Organization*, page 51, December 2017. URL <https://patentscope.wipo.int/search/en/detail.jsf?docId=W02017216186&tab=PCTBIBLIO&maxRec=1000>.
- ESA. Radar Course 3 - Electromagnetic spectrum - ERS Radar Course 3 - ESA Operational EO Missions - Earth Online - ESA, 2018. URL https://earth.esa.int/web/guest/missions/esa-operational-eo-missions/ers/instruments/sar/applications/radar-courses/content-3/-/asset_publisher/mQ9R7ZVkkKg5P/content/radar-course-3-electromagnetic-spectrum.
- FAO. The state of the world's land and water resources for food and agriculture - Managing systems at risk. Technical report, Food and Agriculture Organization of the United Nations, New York, 2011. URL <http://www.fao.org/docrep/017/i1688e/i1688e.pdf>.
- L. Fleskens, L. Stroosnijder, M. Ouessar, and J. De Graaff. Evaluation of the on-site impact of water harvesting in southern Tunisia. *Journal of Arid Environments*, 62(4):613–630, September 2005. ISSN 0140-1963. doi: 10.1016/j.jaridenv.2005.01.013. URL <http://www.sciencedirect.com/science/article/pii/S0140196305000285>.
- J. A. Foley, R. DeFries, G. P. Asner, C. Barford, G. Bonan, S. R. Carpenter, F. S. Chapin, M. T. Coe, G. C. Daily, H. K. Gibbs, J. H. Helkowski, T. Holloway, E. A. Howard, C. J. Kucharik, C. Monfreda, J. A. Patz, I. C. Prentice, N. Ramankutty, and P. K. Snyder. Global Consequences of Land Use. *Science*, 309(5734):570–574, July 2005. ISSN 0036-8075, 1095-9203. doi: 10.1126/science.1111772. URL <http://science.sciencemag.org/content/309/5734/570>.

- Bo-cai Gao. NDWI—A normalized difference water index for remote sensing of vegetation liquid water from space. *Remote Sensing of Environment*, 58(3):257–266, December 1996. ISSN 0034-4257. doi: 10.1016/S0034-4257(96)00067-3. URL <http://www.sciencedirect.com/science/article/pii/S0034425796000673>.
- A. A. van de Griend and M. Owe. On the relationship between thermal emissivity and the normalized difference vegetation index for natural surfaces. *International Journal of Remote Sensing*, 14(6):1119–1131, April 1993. ISSN 0143-1161. doi: 10.1080/01431169308904400. URL <https://doi.org/10.1080/01431169308904400>.
- T. R. H. Holmes, R. A. M. de Jeu, M. Owe, and A. J. Dolman. Land surface temperature from Ka band (37 GHz) passive microwave observations. *Journal of Geophysical Research: Atmospheres*, 114(D4), 2008. ISSN 2156-2202. doi: 10.1029/2008JD010257. URL <https://agupubs.onlinelibrary.wiley.com/doi/abs/10.1029/2008JD010257>.
- Justdiggit. Kenya, Kuku, Digging for re-greening, 2018. URL <https://justdiggit.org/>.
- Alexandra G. Konings, Maria Piles, Narendra Das, and Dara Entekhabi. L-band vegetation optical depth and effective scattering albedo estimation from SMAP. *Remote Sensing of Environment*, 198:460–470, September 2017. ISSN 0034-4257. doi: 10.1016/j.rse.2017.06.037. URL <http://www.sciencedirect.com/science/article/pii/S0034425717302961>.
- Ralph Lasage and Peter H. Verburg. Evaluation of small scale water harvesting techniques for semi-arid environments. *Journal of Arid Environments*, 118:48–57, July 2015. ISSN 0140-1963. doi: 10.1016/j.jaridenv.2015.02.019. URL <http://www.sciencedirect.com/science/article/pii/S0140196315000555>.
- Y. Y. Liu, A. I. J. M. van Dijk, D. G. Miralles, M. F. McCabe, J. P. Evans, R. A. M. de Jeu, P. Gentine, A. Huete, R. M. Parinussa, L. Wang, K. Guan, J. Berry, and N. Restrepo-Coupe. Enhanced canopy growth precedes senescence in 2005 and 2010 Amazonian droughts. *Remote Sensing of Environment*, 211:26–37, June 2018. ISSN 0034-4257. doi: 10.1016/j.rse.2018.03.035. URL <http://www.sciencedirect.com/science/article/pii/S0034425718301366>.
- Yi Y. Liu, Albert I. J. M. Dijk, Matthew F. McCabe, Jason P. Evans, and Richard A. M. Jeu. Global vegetation biomass change (1988–2008) and attribution to environmental and human drivers. *Global Ecology and Biogeography*, 22(6):692–705, December 2012. ISSN 1466-822X. doi: 10.1111/geb.12024. URL <https://onlinelibrary.wiley.com/doi/full/10.1111/geb.12024>.
- S. A. Margulis. *Introduction to Hydrology*. Steven Margulis, 2017a edition, 2017. URL <https://itunes.apple.com/us/book/introduction-to-hydrology/id1272471780>.
- METER Group. EC-5 | Soil Moisture Sensor | METER Environment, 2017. URL <https://www.metergroup.com/environment/products/ec-5-soil-moisture-sensor/>.
- T. Mo, B. J. Choudhury, T. J. Schmugge, J. R. Wang, and T. J. Jackson. A model for microwave emission from vegetation-covered fields. *Journal of Geophysical Research: Oceans*, 87(C13):11229–11237, December 1982. ISSN 2156-2202. doi: 10.1029/JC087iC13p11229. URL <https://agupubs.onlinelibrary.wiley.com/doi/abs/10.1029/JC087iC13p11229>.
- NASA. Climate change evidence: How do we know?, 2018. URL <https://climate.nasa.gov/evidence>.
- NASA Goddard Earth Sciences Data And Information Services Center. TRMM (TMPA) Precipitation L3 1 day 0.25 degree x 0.25 degree V7, 2018. URL https://disc.gsfc.nasa.gov/datacollection/TRMM_3B42_Daily_7.html. type: dataset.
- E. G. Njoku and D. Entekhabi. Passive microwave remote sensing of soil moisture. *Journal of Hydrology*, 184(1):101–129, October 1996. ISSN 0022-1694. doi: 10.1016/0022-1694(95)02970-2. URL <http://www.sciencedirect.com/science/article/pii/0022169495029702>.
- E. G. Njoku and L. Li. Retrieval of Land Surface Parameters Using Passive Microwave Measurements at 6 to 18 GHz. *IEEE Transactions on Geoscience and Remote Sensing*, 37(1):79–93, 1999. doi: 10.1109/36.739125. URL <http://ieeexplore.ieee.org/stamp/stamp.jsp?tp=&arnumber=739125&isnumber=15962>.

- M. Owe, R. A. M. de Jeu, and J. Walker. A methodology for surface soil moisture and vegetation optical depth retrieval using the microwave polarization difference index. *IEEE Transactions on Geoscience and Remote Sensing*, 39(8):1643–1654, August 2001. ISSN 0196-2892. doi: 10.1109/36.942542.
- M. Owe, R. A. M. de Jeu, and T. R. H. Holmes. Multisensor historical climatology of satellite-derived global land surface moisture. *Journal of Geophysical Research: Earth Surface*, 113(F1):F01002, March 2008. ISSN 2156-2202. doi: 10.1029/2007JF000769. URL <http://onlinelibrary.wiley.com/doi/10.1029/2007JF000769/abstract>.
- R. M. Parinussa, M. T. Yilmaz, M. C. Anderson, C. R. Hain, and R. A. M. de Jeu. An intercomparison of remotely sensed soil moisture products at various spatial scales over the Iberian Peninsula. *Hydrological Processes*, 28(18):4865–4876, 2013. ISSN 08856087. doi: 10.1002/hyp.9975. URL <http://doi.wiley.com/10.1002/hyp.9975>.
- W. E. Rees. Ecological footprints and appropriated carrying capacity: what urban economics leaves out. *Environment and Urbanization*, 4(2):121–130, October 1992. ISSN 0956-2478, 1746-0301. doi: 10.1177/095624789200400212. URL <http://journals.sagepub.com/doi/10.1177/095624789200400212>.
- Remote Sensing Systems. Advanced Microwave Scanning Radiometer, 2018. URL <http://www.remss.com/missions/amr/>.
- E. Santi. An application of the SFIM technique to enhance the spatial resolution of spaceborne microwave radiometers. *International Journal of Remote Sensing*, 31(9):2419–2428, May 2010. ISSN 0143-1161. doi: 10.1080/01431160903005725. URL <https://doi.org/10.1080/01431160903005725>.
- H. Santin-Janin, M. Garel, J.-L. Chapuis, and D. Pontier. Assessing the performance of NDVI as a proxy for plant biomass using non-linear models: a case study on the Kerguelen archipelago. *Polar Biology*, 32(6): 861–871, June 2009. ISSN 1432-2056. doi: 10.1007/s00300-009-0586-5. URL <https://doi.org/10.1007/s00300-009-0586-5>.
- Mustafa Sari, Yusuf Kurucu, Erhan Akça, Muhsin Eren, Selahattin Kadir, Hikmet Günal, Claudio Zucca, İbrahim Atalay, Zülküf Kaya, Franco Previtali, Pandi Zdruli, Selim Kapur, and Ewart Adsil FitzPatrick. Luvisols. In Selim Kapur, Erhan Akça, and Hikmet Günal, editors, *The Soils of Turkey*, World Soils Book Series, pages 231–249. Springer International Publishing, Cham, 2018. ISBN 978-3-319-64392-2. doi: 10.1007/978-3-319-64392-2_15. URL https://doi.org/10.1007/978-3-319-64392-2_15.
- S. J. Scherr. A downward spiral? Research evidence on the relationship between poverty and natural resource degradation. *Food Policy*, 25(4):479–498, August 2000. ISSN 0306-9192. doi: 10.1016/S0306-9192(00)00022-1. URL <http://www.sciencedirect.com/science/article/pii/S0306919200000221>.
- W. Schiettecatte, M. Ouessar, D. Gabriels, S. Tanghe, S. Heirman, and F. Abdelli. Impact of water harvesting techniques on soil and water conservation: a case study on a micro catchment in southeastern Tunisia. *Journal of Arid Environments*, 61(2):297–313, April 2005. ISSN 0140-1963. doi: 10.1016/j.jaridenv.2004.09.022. URL <http://www.sciencedirect.com/science/article/pii/S0140196304002046>.
- K.C. Seto, B. Güneralp, and L. R. Hutyrá. Global forecasts of urban expansion to 2030 and direct impacts on biodiversity and carbon pools. *Proceedings of the National Academy of Sciences*, 109(40):16083–16088, October 2012. ISSN 0027-8424, 1091-6490. doi: 10.1073/pnas.1211658109. URL <http://www.pnas.org/content/109/40/16083>.
- D. Tilman, K. G. Cassman, P. A. Matson, R. Naylor, and S. Polasky. Agricultural sustainability and intensive production practices, August 2002. URL <https://www.nature.com/articles/nature01014>.
- F. T. Ulaby, R. K. Moore, and A. K. Fung. *Microwave Remote Sensing: Active and passive. Volume 1 - Microwave remote sensing fundamentals and radiometry*. Artech House Publishers, 1981. URL <https://ntrs.nasa.gov/search.jsp?R=19820039342>.
- UN. World population projected to reach 9.8 billion in 2050, and 11.2 billion in 2100, 2017. URL <https://www.un.org/development/desa/en/news/population/world-population-prospects-2017.html>.

- UNCCD. Water scarcity and desertification. Technical report, United Nations Convention to Combat Desertification, 2017. URL <http://www2.unccd.int/sites/default/files/relevant-links/2017-01/Desertificationandwater.pdf>.
- UNCCD. The Great Green Wall Initiative | UNCCD, 2018. URL <https://www.unccd.int/actions/great-green-wall-initiative>.
- University of Arizona. COSMOS Probe: KLEE Probe 50, 2018. URL <http://cosmos.hwr.arizona.edu/Probes/StationDat/055/index.php>.
- Adriaan A Van de Griend and Jean-Pierre Wigneron. Canopy extinction and single scattering albedo in the microwave region as a function of frequency, polarization, incidence angle and canopy type. *IEEE Transactions on Geoscience and Remote Sensing*, 2003.
- R. J. van der Ent, H. H. G. Savenije, B. Schaefli, and S. C. Steele-Dunne. Origin and fate of atmospheric moisture over continents. *Water Resources Research*, 46(9), September 2010. ISSN 1944-7973. doi: 10.1029/2010WR009127. URL <https://agupubs.onlinelibrary.wiley.com/doi/abs/10.1029/2010WR009127>.
- R. van der Schalie. *Advancing soil moisture climate records through the integration of SMOS observations*. PhD Thesis, Vrije Universiteit, Amsterdam, 2017. URL <https://www.vandersat.com/blog/successful-phd-defense-of-our-colleague-robin-van-der-schalie>.
- R. van der Schalie, R. M. Parinussa, L. J. Renzullo, A. I. J. M. van Dijk, C. H. Su, and R. A. M. de Jeu. SMOS soil moisture retrievals using the land parameter retrieval model: Evaluation over the Murrumbidgee Catchment, southeast Australia. *Remote Sensing of Environment*, 163:70–79, June 2015. ISSN 0034-4257. doi: 10.1016/j.rse.2015.03.006. URL <http://www.sciencedirect.com/science/article/pii/S0034425715001029>.
- P. M. Vitousek, H. A. Mooney, J. Lubchenco, and J. M. Melillo. Human Domination of Earth's Ecosystems. *Science*, 277(5325):494–499, July 1997. ISSN 0036-8075, 1095-9203. doi: 10.1126/science.277.5325.494. URL <http://science.sciencemag.org/content/277/5325/494>.
- J. R. Wang and B. J. Choudhury. Remote sensing of soil moisture content, over bare field at 1.4 GHz frequency. *Journal of Geophysical Research: Oceans*, 86(C6):5277–5282, June 1981. ISSN 2156-2202. doi: 10.1029/JC086iC06p05277. URL <https://agupubs.onlinelibrary.wiley.com/doi/abs/10.1029/JC086iC06p05277>.
- J. R. Wang and T. J. Schmugge. An Empirical Model for the Complex Dielectric Permittivity of Soils as a Function of Water Content. *IEEE Transactions on Geoscience and Remote Sensing*, GE-18(4):288–295, October 1980. ISSN 0196-2892. doi: 10.1109/TGRS.1980.350304.
- Andrew W. Western and Günter Blöschl. On the spatial scaling of soil moisture. *Journal of Hydrology*, 217(3):203–224, April 1999. ISSN 0022-1694. doi: 10.1016/S0022-1694(98)00232-7. URL <http://www.sciencedirect.com/science/article/pii/S0022169498002327>.
- World Bank. Restoring China's Loess Plateau, 2017. URL <http://www.worldbank.org/en/news/feature/2007/03/15/restoring-chinas-loess-plateau>.
- Marek Zreda. Land-surface hydrology with cosmic-ray neutrons: principles and applications. *J. Jpn. Soc. Soil Phys.*, 132:6, 2016. URL <http://cosmos.hwr.arizona.edu/Docs/zreda16-land-surface-hydrology-with-cosmic-ray-neutrons.pdf>.



Sentinel-2 NDVI results 2018

Sentinel-2 NDVI images between January and July 2018, which show the impact of the JustdiggIt projects, with a clear contrast between inside and outside the project areas after the wet season, in May, June and July. However, NDVI also shows its disadvantage, as it is affected by cloud cover during the rain season in March and April.

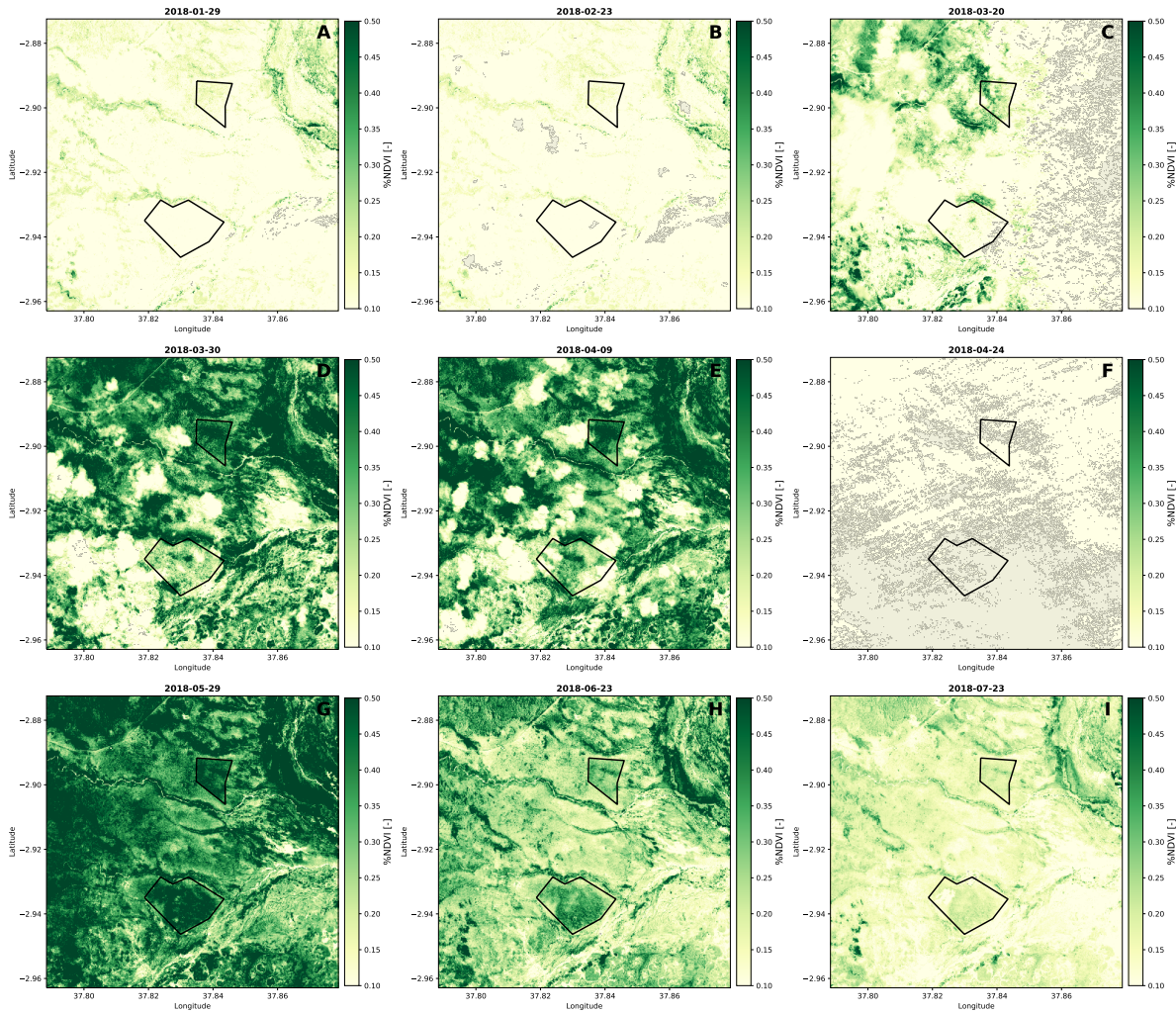


Figure A.1: NDVI images in 2018, showing impact of JustdiggIt projects and cloud cover

B

Validation of soil moisture product using cosmic-ray in-situ data

A validation of the downscaled passive soil moisture product with a cosmic-ray in-situ station in Kenya, which was carried out by VanderSat, has shown very good consistency and correlation between March 2015 and September 2018, as shown in figure B.1. As a result, this proves that the product is very accurate in semi-arid climates such as in Kenya and therefore can be used to monitor the land restoration projects of Justdigg in Kenya.

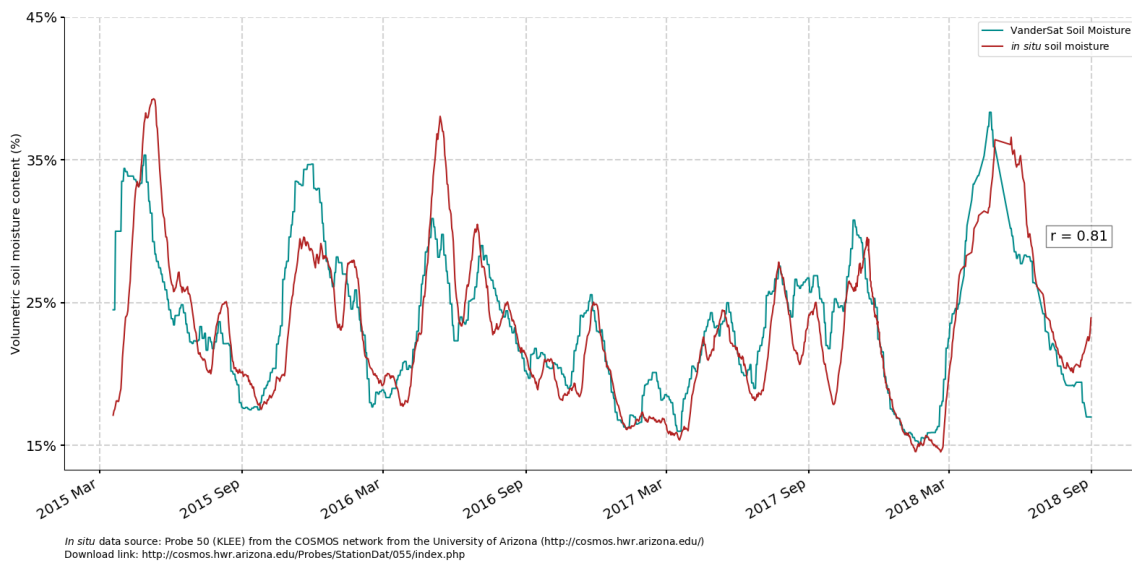
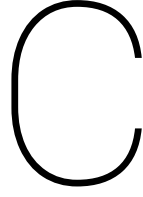


Figure B.1: Validation of downscaled soil moisture product using a Cosmic-ray in-situ station in Kenya (University of Arizona, 2018).



Calibration of in-situ sensors

In this chapter the results of the calibration of the in-situ sensors are presented. First of all, the raw sensor values obtained from the 5TM and EC5 sensors are plotted (figure C.1) against the soil moisture content, which are measured during the fieldwork by using the 5TM and EC5 sensors, around the bunds at Plot D and at Nyati camp. The linear fitted functions are used on the raw data of the in-situ sensors to calculate soil moisture content. Equations C.1-C.4 show the calibration coefficients for the EC5 and 5TM sensors.

C.1. Calibration curves & linearly fitted functions

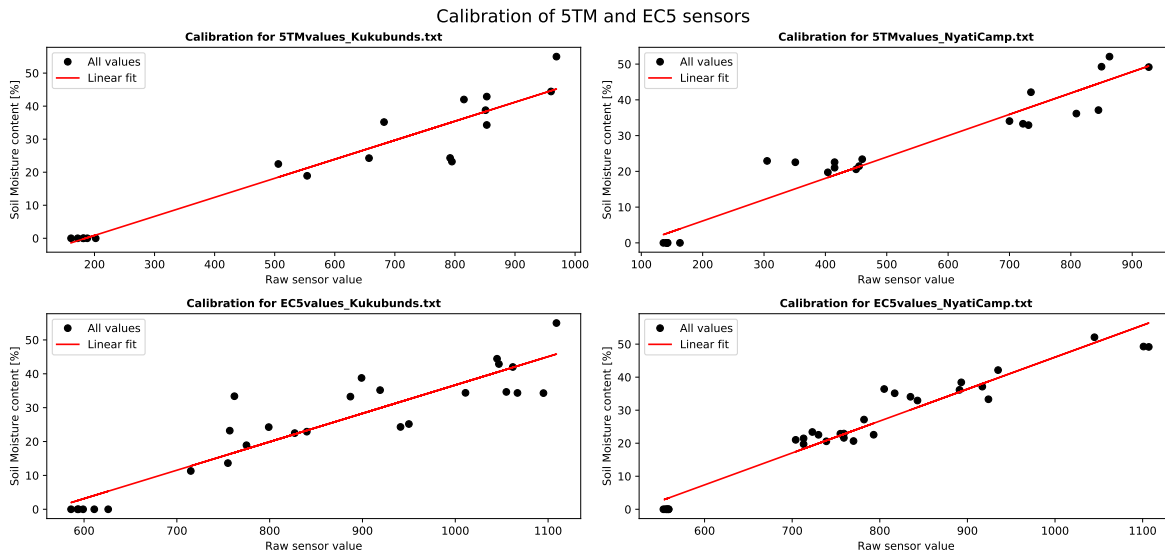


Figure C.1: Calibration of 5TM and EC5 in-situ sensors, installed around the bunds at plot B near Kuku and at the head office of the MWCT, Nyati Camp.

$$5TM \text{ sensor } \theta_{Bunds} = (Raw \text{ sensor value} * 0.0576) - 10.6681 \quad (C.1)$$

$$EC5 \text{ sensor } \theta_{Bunds} = (Raw \text{ sensor value} * 0.0838) + -47.1516 \quad (C.2)$$

$$5TM \text{ sensor } \theta_{Nyati} = (Raw \text{ sensor value} * 0.0596) - 5.7949 \quad (C.3)$$

$$EC5 \text{ sensor } \theta_{Nyati} = (Raw \text{ sensor value} * 0.0967) + -50.6190 \quad (C.4)$$

C.2. Bulk density & porosity

C.2.1. Bulk densities

Table C.1 presents the bulk density values, based on the 5TM and EC5 sensors, at the bunds in plot D and at Nyati Camp, MWCT's head office.

Table C.1: Bulk density values based on 5TM and EC5 sensors

	Kuku Bunds, Plot D		Nyati Camp, MWCT Office	
	5TM sensor	EC5 sensor	5TM sensor	EC5 sensor
Min	1.182	1.119	0.923	0.923
Max	1.475	1.475	1.301	1.301
Mean	1.322	1.284	1.110	1.130
Std Dev.	0.093	0.096	0.115	0.104

C.2.2. Porosities

Table C.2 presents the porosity values, based on the 5TM and EC5 sensors, at the bunds in plot D and at Nyati Camp, MWCT's head office.

Table C.2: Porosity values based on 5TM and EC5 sensors

	Kuku Bunds, Plot D		Nyati Camp, MWCT Office	
	5TM sensor	EC5 sensor	5TM sensor	EC5 sensor
Min	0.446	0.446	0.511	0.511
Max	0.556	0.579	0.653	0.653
Mean	0.503	0.518	0.583	0.575
Std Dev.	0.035	0.036	0.043	0.039

D

Epanechnikov and Gaussian smoothing filters

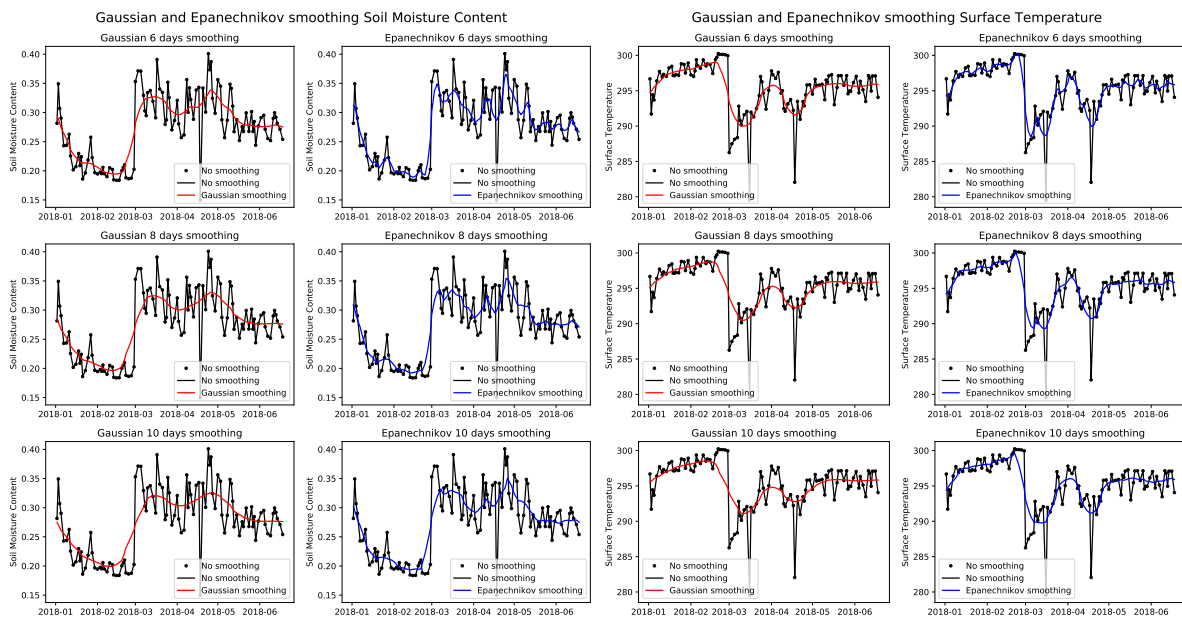


Figure D.1: Gaussian and Epanechnikov smoothing of soil moisture, for 6 days, 8 days and 10 days.

Figure D.2: Gaussian and Epanechnikov smoothing of surface temperature, for 6 days, 8 days and 10 days.

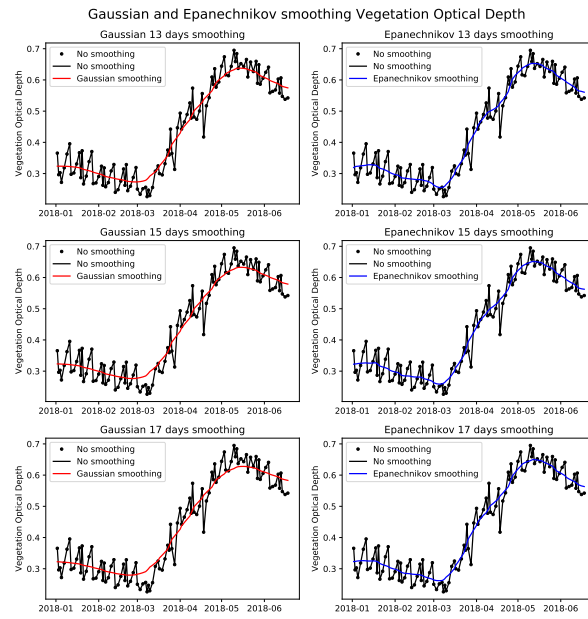


Figure D.3: Gaussian and Epanechnikov smoothing of vegetation optical depth, for 6 days, 8 days and 10 days.

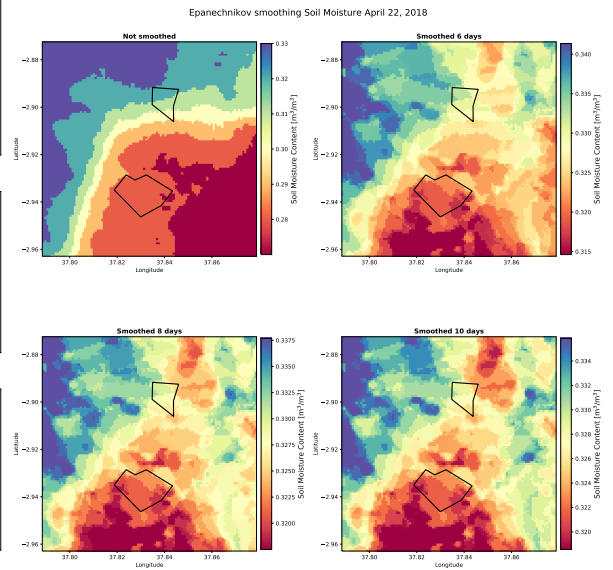


Figure D.4: Epanechnikov smoothing of soil moisture for a smoothing window of 0, 6, 8 and 10 days.

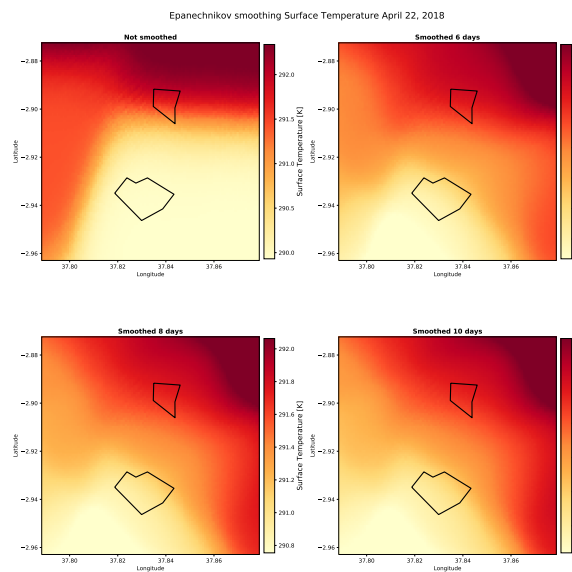


Figure D.5: Epanechnikov smoothing of surface temperature for a smoothing window of 0, 6, 8 and 10 days.

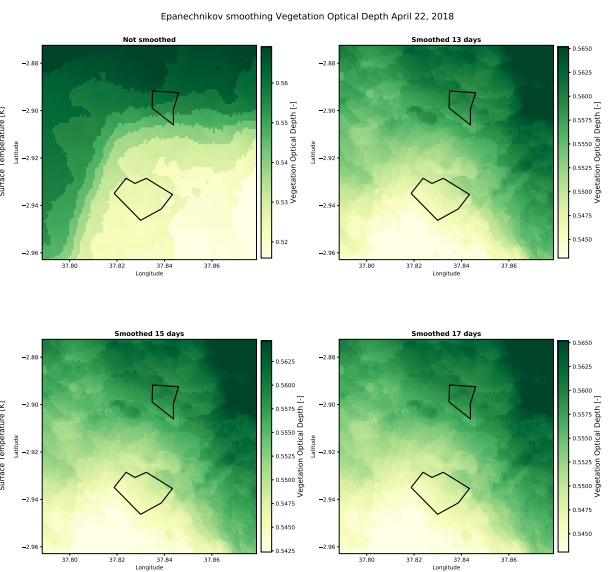
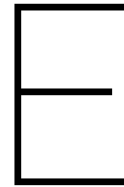


Figure D.6: Epanechnikov smoothing of soil moisture for a smoothing window of 0, 13, 15 and 17 days.



Results of raw brightness temperature data

E.1. Raw brightness temperature time series

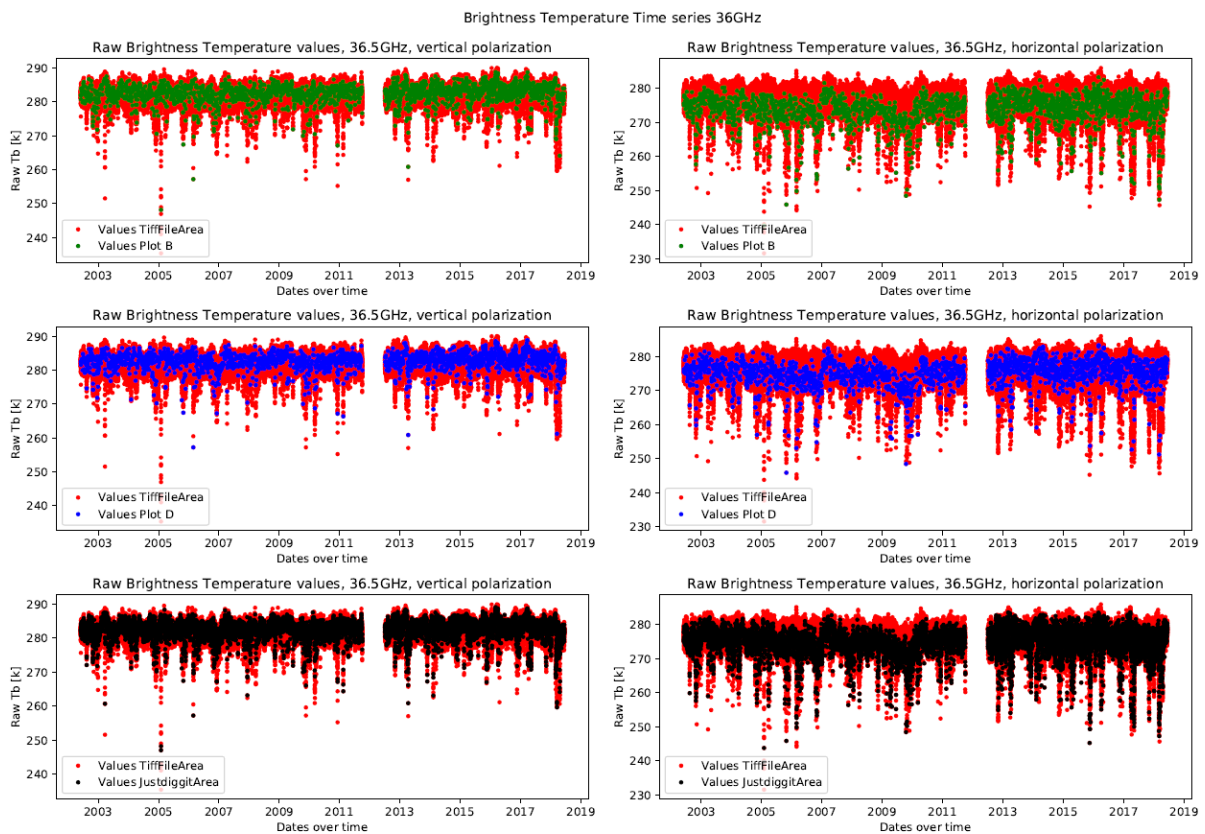


Figure E.1: Time series of Raw Brightness Temperatures at 36GHz, for Justdiggit Area, Plot B and Plot D

E.2. Raw brightness temperature anomalies

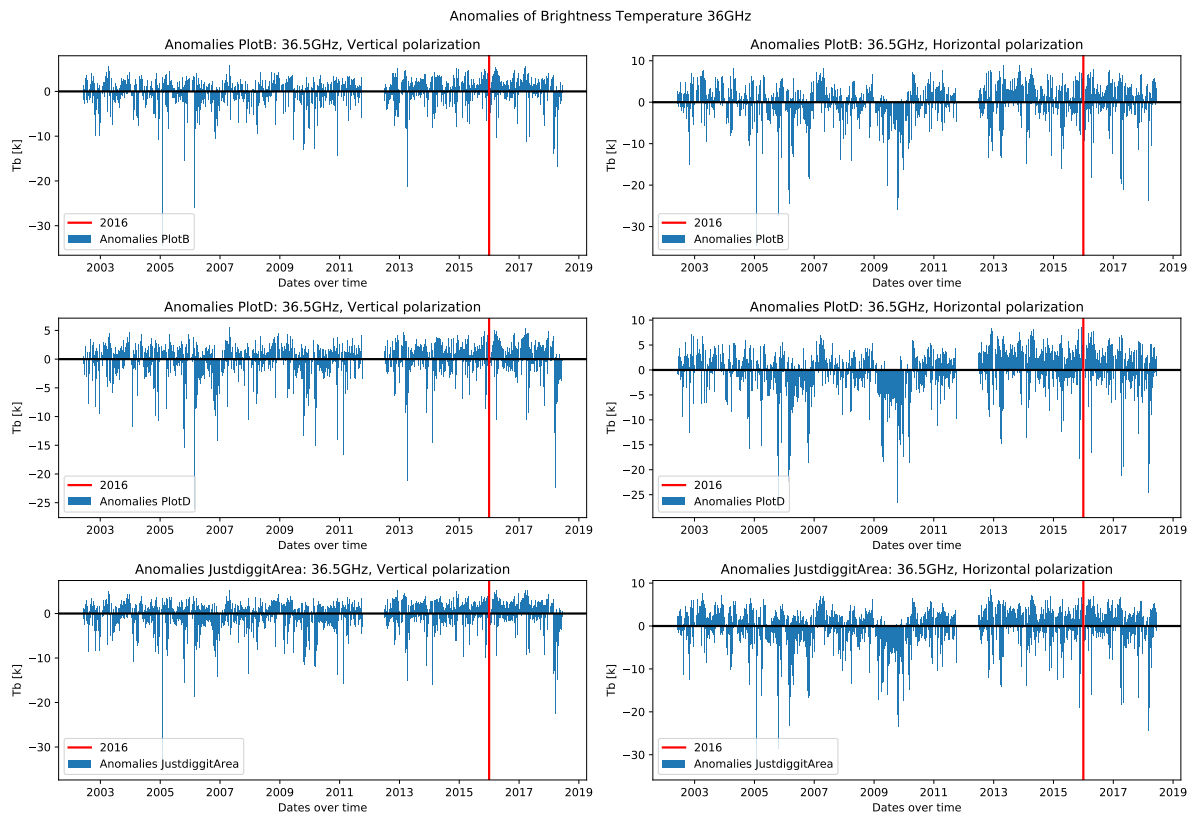


Figure E.2: Anomalies of Raw Brightness Temperatures for Justdiggit Area, Plot B and Plot D. The red line indicates the start of the 2016, in when the Justdiggit projects were implemented.

E.3. Raw brightness temperature error plots

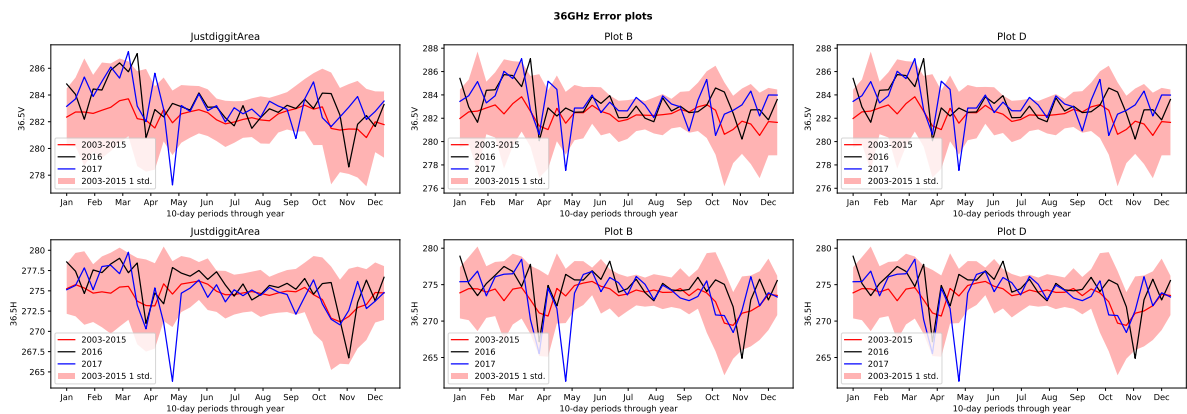


Figure E.3: Error plots of Raw Brightness Temperatures for Justdiggit Area, Plot B and Plot D, with individual years 2016 and 2017. In terms of rainfall, 2016 represents a regular year, while 2017 was an exceptional dry year according to TRMM data of NASA.

E.4. Microwave Polarization Difference Index

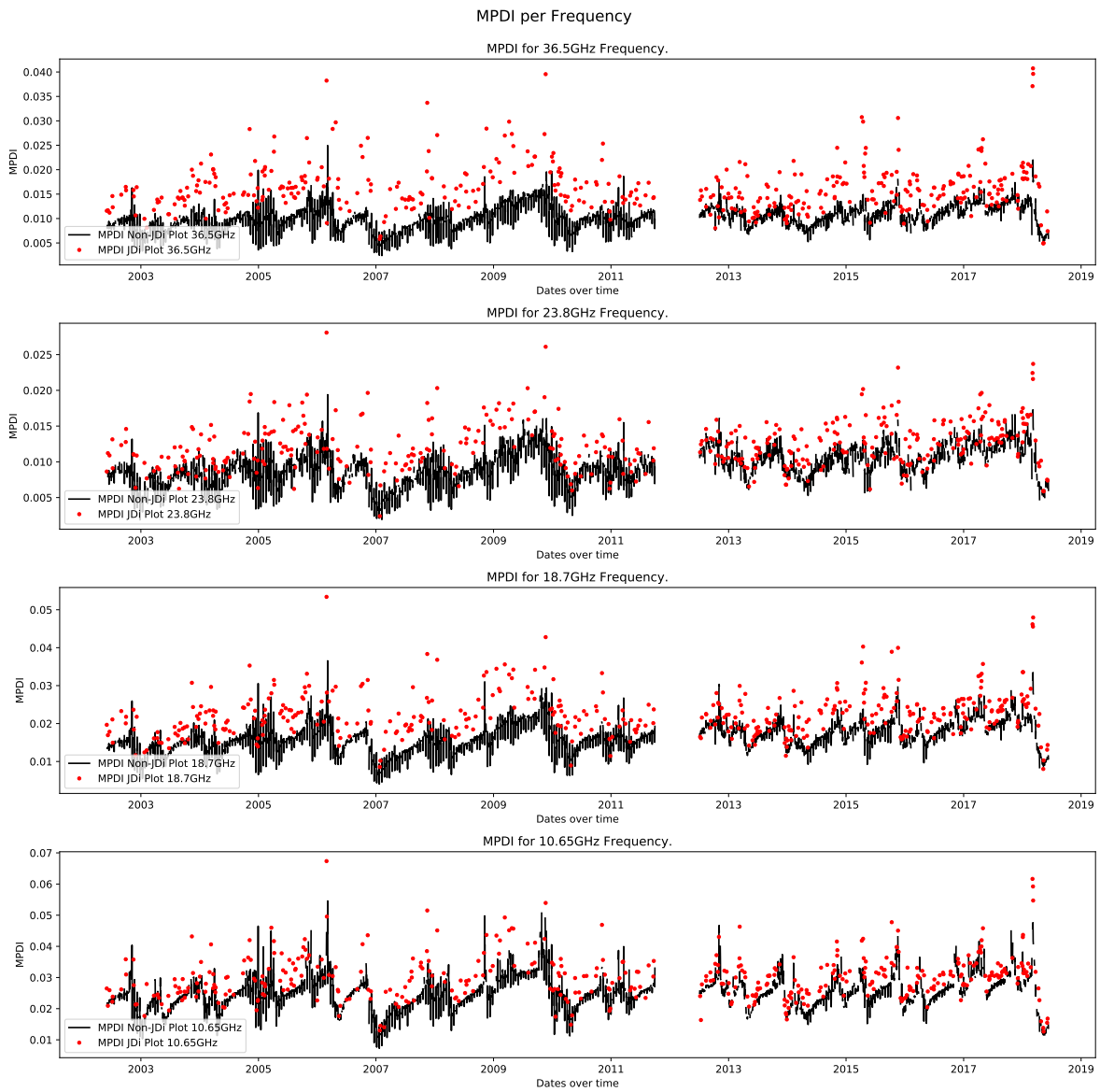


Figure E.4: MPDI for Justdigitt Area and Plot B, for 36.5GHz, 23.7GHz, 18.7GHz and 10.65GHz. As shown, the AMSRE-period shows a larger variability in MPDI than the AMSR2-period, for all frequencies.

